A COMPARISON OF THE STRUCTURE AND FLOW CHARACTERISTICS OF THE UPPER TROPOSPHERE AND STRATOSPHERE OF THE NORTHERN AND SOUTHERN HEMISPHERES

BY

ROBERT F. ADLER

Atmospheric Science
PAPER NO.
216

US ISSN 0067-0340

DEPARTMENT OF ATMOSPHERIC SCIENCE
COLORADO STATE UNIVERSITY
FORT COLLINS, COLORADO

A COMPARISON OF THE STRUCTURE AND FLOW CHARACTERISTICS OF THE UPPER TROPOSPHERE AND STRATOSPHERE OF THE NORTHERN AND SOUTHERN HEMISPHERES

by

Robert F. Adler

This report was prepared with support from the National Aeronautics and Space Administration (Grant NGR 06-002-098) and the Atomic Energy Commission (Contract No. AT(11-1)-1340). Principal Investigator: E. R. Reiter

Atmospheric Science Paper No. 216

Department of Atmospheric Science
Colorado State University
Fort Collins, Colorado
April 1974

ABSTRACT OF DISSERTATION

A COMPARISON OF THE STRUCTURE AND FLOW CHARACTERISTICS OF THE UPPER TROPOSPHERE AND STRATOSPHERE OF THE NORTHERN AND SOUTHERN HEMISPHERES

The general circulations of the Northern and Southern Hemispheres are compared with regard to the upper troposphere and stratosphere using atmospheric structure obtained from satellite, multi-channel radiance data. Specifically, the data are from the Satellite Infrared Spectrometer (SIRS) instrument aboard the Nimbus 3 spacecraft. The inter-hemispheric comparisons are based on two months of data (one summer month and one winter month) in each hemisphere.

The mean meridional circulation of the Southern Hemisphere stratosphere in winter is studied using zonally-averaged vertical motion fields calculated by a heat budget technique. The mean pattern for July 1969 shows two main cells with the polar night jet stream associated with an indirect cell. There are shown to be significant variations in the horizontal eddy heat flux and vertical motion patterns in the Southern Hemisphere in relation to the presence or absence of a minor midwinter warming.

Horizontal eddy heat fluxes in the upper troposphere of both hemispheres are examined and in mid-latitudes found to be approximately equal in magnitude when averaged over the summer and winter month. The Southern Hemisphere mid-latitude eddy heat flux is also shown to have significant longitudinal variations, apparently associated with the location of the southern continents.

The relative importance of standing and transient eddies in both hemispheres is investigated. The results confirm that, in general, standing eddies are less important in the Southern Hemisphere. This

distinction is true for the temperature structure as reflected in the eddy available potential energy (AE), the eddy kinetic energy (KE) and the mid-latitude eddy heat flux. The distribution with latitude of the relative importance of standing and transient eddies is also studied.

The zonal mean temperature and geopotential height gradients in the upper troposphere between 20° and 80° latitude are confirmed to be larger in the Southern Hemisphere in both the winter and summer, the inter-hemispheric difference being much greater in summer. Comparisons between the hemispheres of zonal and eddy available potential energy (AZ and AE) and zonal and eddy kinetic energy (KZ and KE) indicate that the ratios of AZ to AE and KZ to KE are larger in the Southern Hemisphere.

In relation to the disparity in the breakdown climatologies of the Arctic and Antarctic stratospheric polar vortices, the structure of the two vortices is shown to be different so that a previously-derived instability criterion tends to be met in the Northern Hemisphere, but not in the Southern Hemisphere, during midwinter. In the Southern Hemisphere, the structure varies between midwinter and spring so that the vortex tends to meet the instability criterion in spring when the vortex normally breaks down.

Robert Frederick Adler
Department of Atmospheric Science
Colorado State University
Fort Collins, Colorado 80521
April, 1974

ACKNOWLEDGEMENTS

The author wishes to thank his graduate committee: Dr. Elmar R. Reiter, Dr. Thomas H. Vonder Haar, Dr. Alan K. Betts and Dr. Duane C. Boes. During the early part of this study Chris Kendall assisted in the data compilation. The computer programming necessary for this investigation was very ably performed by Alice Fields. The manuscript was typed by Deborah Smith. Kathy Adler assisted in the editing and proofreading.

The research contained in this report was supported mainly by the National Aeronautics and Space Administration under Grant NGR 06-002-098. Additional support was received from the Atomic Energy Commission under Contract No. AT(11-1)-1340.

TABLE OF CONTENTS

TABLE OF CONTENTS - Continued

LIST OF TABLES

LIST OF FIGURES

LIST OF FIGURES - Continued

LIST OF FIGURES - Continued

LIST OF SYMBOLS

A	available potential energy
a	earth's radius
AE	eddy available potential energy
AZ	zonal available potential energy
c_1, c_2	constants in Planck's Law
c_3, c_4	constants in temperature - Planck function approximation
c_p	specific heat at constant pressure
D	geopotential thickness
$F(\phi_1)$	northward flux of energy across latitude ϕ_1
f	Coriolis parameter
g	acceleration of gravity
K	kinetic energy
k	wave number
KE	eddy kinetic energy
KZ	zonal kinetic energy
N	radiance
P	potential vorticity
p	pressure
R	gas constant or percentage of AE contained in standing eddies
R_N	net radiation at top of the atmosphere

s	sample standard deviation
T	temperature
t	time
u	zonal wind speed
$\mathbf{V}_p$	horizontal wind vector on constant pressure surface
v	meridional wind speed
W	Planck function
w	vertical component of motion, $= \frac{dz}{dt}$
z	geopotential height
α_0	constant in regression equations
α_i	coefficients in regression equations, i = 1, 8
ζ_θ	relative vorticity on an isentropic surface
θ	potential temperature
λ	longitude
μ	mean
σ	static stability, $= -\frac{g}{R}\frac{p}{\theta}\frac{\partial\theta}{\partial p}$; or standard deviation
τ	transmittance
ϕ	latitude
ω	vertical component of motion in pressure coordinates, $= \frac{dp}{dt}$

CHAPTER 1

PURPOSE AND STRUCTURE OF DISSERTATION

The primary objective of this study is to investigate and compare particular aspects of the general circulations of the Northern and Southern Hemispheres, especially with regard to upper tropospheric and stratospheric layers. The study is based on atmospheric structure in both hemispheres derived from satellite, multi-channel radiance data. The satellite data provide information on atmospheric structure in both hemispheres with equal, or nearly equal, time and space resolutions, thus providing an excellent basis for inter-hemispheric comparisons.

The major topics explored in this study include:

a. atmospheric structure as reflected in the quantities zonal and eddy available potential energy, and zonal and eddy kinetic energy;

b. upper tropospheric horizontal eddy heat flux and its spatial distribution;

c. the relative importance of standing and transient eddies;

d. the structure of, and the mean meridional circulation in, the winter stratospheric polar vortices.

Previous observational studies of the Southern Hemisphere general circulation have been handicapped by a lack of horizontal resolution and by a relative lack of data in the upper troposphere and stratosphere. Data from the International Geophysical Year (IGY) in

1957-1958 form the basis for most previous studies. Approximately 70 radiosonde stations in the Southern Hemisphere formed the IGY upper-air network. This is essentially the same network that exists at present. In the Northern Hemisphere approximately 500 upper-air stations report regularly. Despite an effort to place radiosonde stations in data-sparse regions over Southern Hemisphere oceans, the IGY data set has very large gaps in its coverage. A post-analyses of the IGY data produced daily surface and 500 mb analyses which also have been used in a number of general circulation studies. Above 500 mb there are no post-analysis maps available and the quantity of upper-air data decreases with height, especially above 100 mb. However, some investigations of the stratosphere in the Southern Hemisphere have been carried out using satellite radiance information to infer atmospheric structure.

The present investigation is based on atmospheric structure derived from the Satellite Infrared Spectrometer (SIRS) instrument aboard the Nimbus 3 spacecraft. Temperature information is obtained using linear regression equations based on a comparison of satellite radiances and radiosonde data for the specific months and areas considered in this study. Daily analyses are produced using twenty-four hours of satellite data. This daily data set has an adequate spatial distribution for hemispheric analysis of patterns of the sizes important in the large-scale energy and transport phenomena of the general circulation. Because of factors discussed in a following chapter, the technique used to obtain atmospheric structure from the SIRS radiances is at its best in the upper troposphere and stratosphere. The satellite data, therefore, provide information concerning atmospheric structure

with adequate spatial resolution, with equal resolution in the two hemispheres and with the best results to be expected in the upper troposphere and stratosphere. Although there are limitations, the satellite radiance data have the potential to provide a great deal of information concerning the comparison of the circulations of the Northern and Southern Hemispheres. To check the validity of computations made with the SIRS-based structure, a second set of calculations is carried out in the Northern Hemisphere using National Meteorological Center (NMC) gridded data. Although some comparisons between the hemispheres are made of quantities based on structure through the depth of the atmosphere, they are generally restricted to tropospheric layers above 500 mb, and the stratosphere. One summer month and one winter month are used in each hemisphere.

For reasons discussed in Chapter 5 the structure obtained from the SIRS data tends to underestimate gradients. Mean meridional gradients are incorrectly estimated only slightly. However, variations in the east-west direction and the variance around a latitude circle of a variable, are significantly underestimated. Consequently, the satellite data would seem most appropriate for comparing mean meridional gradients. However, these gradients can be, and have been, accurately estimated from monthly mean or even climatological data in a number of studies for both hemispheres. Terms which involve longitudinal gradients calculated on a daily basis are much more difficult to estimate from the limited radiosonde network of the Southern Hemisphere. Therefore, although there is a systematic underestimation of east-west gradients, the satellite data gives the time and space coverage so that a great deal of information about the eddy terms can be obtained.

Because of the underestimation, absolute magnitudes will not be as important as relative values in this study.

Chapter 2 of this dissertation summarizes previous studies of the Southern Hemisphere's general circulation and investigations of inter-hemispheric comparisons. Chapter 3 describes the satellite system, the technique used to obtain atmospheric structure from the satellite radiance data and the limitations of the method.

Chapter 4 contains the results of the inter-hemispheric comparisons in the troposphere. Values are presented for the zonal and eddy components of available potential energy (A) and kinetic energy (K), with the emphasis being on the contributions of upper tropospheric layers to the vertically integrated total. The eddy flux of sensible heat in the upper troposphere is also discussed. Spatial variations and the relative contributions of standing and transient eddies are examined.

Differences between the hemispheres with regard to the winter stratosphere are investigated in Chapter 5. The relation of vortex structure to breakdown characteristics for the two hemispheres is discussed and calculations of the mean meridional circulation in the polar stratosphere of the Northern and Southern Hemispheres are presented. Variations in wave characteristics and in the mean meridional circulation in the Southern Hemisphere are examined in relation to the presence or absence of a minor midwinter warming.

A summary of the study is given in Chapter 6.

CHAPTER 2

REVIEW OF LITERATURE ON SOUTHERN HEMISPHERE GENERAL CIRCULATION AND DIFFERENCES BETWEEN THE HEMISPHERES

2.1 Introduction

Previous general circulation studies of the Northern and Southern Hemispheres reveal significant differences between them. This is not unexpected since there are great contrasts in their physical features. A good description of the meteorologically pertinent physical characteristics of the Southern Hemisphere is given by Taljaard (1972a). Basically, three main factors contribute to the dissimilarity. First, a much smaller proportion of the Southern Hemisphere is covered by land. This is especially true of the middle latitudes. Between 40°S and 60°S, less than 5% of the area is covered by land; in the same latitudes of the Northern Hemisphere, the percentage is approximately 50%. Therefore, while around latitude circles of the mid-latitudes of the Northern Hemisphere there is a large land-sea contrast, in southern mid-latitudes ocean exists almost exclusively. Near the equator (less than 15° latitude), the percentage of land is approximately the same in the two hemispheres. Only in polar regions (greater than about 70° latitude) does the percentage of land in the Southern Hemisphere become significantly greater than in the Northern Hemisphere. This contrast in percentages at high latitudes reflects, of course, the presence of the Antarctic continent in the south polar region. This large, domed

land mass at the pole is the second main factor in the difference between the hemispheres. The third is the orography. The only mountain range in the Southern Hemisphere, which compares to those of the Northern Hemisphere, is the Andes Range of South America which runs south from the equator along almost the entire length of the west coast of the continent. Its highest portions are north of approximately 35°S, and the range as a whole, and especially its southern portion, is relatively narrow. South Africa is a plateau averaging about 1000-2000 meters, while Australia is a low plateau averaging below 500 meters in elevation. As a result, the Southern Hemisphere, with the exception of the Andes Range, does not possess orographic barriers of the number and lateral extent of those of the Northern Hemisphere.

2.2 Radiation budget

Observations of the earth's radiation budget from satellites and calculations of the budget from radiation models both reveal significant contrasts between the Northern and Southern Hemispheres. However, budget parameters averaged over each hemisphere and over the year show no obvious differences between the hemispheres. Vonder Haar and Suomi (1971) summarize satellite measurements showing that the Northern and Southern Hemispheres have almost the same annual average albedo (30%) and emitted infrared radiation. But, while on a season-by-season basis the emitted infrared radiation values compare favorably in the two hemispheres, the albedo values do not. High albedos occur in the Northern Hemisphere in winter and spring and in the Southern Hemisphere in summer and fall. A very low albedo (23%) is observed for the Southern Hemisphere winter. This low seasonal value is related to the

high percentage of ocean coverage of the sunlit portion of the hemisphere during the polar night.

More important to the general circulation than hemispheric values of radiation budget components are the latitudinal variations of these parameters. Vonder Haar and Suomi (1971), Vonder Haar (1972) and Raschke, Vonder Haar, Bandeen and Pasternak (1973) discuss pole-to-pole latitudinal profiles of radiation budget parameters as observed from satellites. Newell, Vincent, Dopplick, Ferruzza and Kidson (1970) compare satellite observations of net radiation as a function of latitude with various computations from radiation models on a seasonal basis. Sasamori, London and Hoyt (1972) compare their radiation model calculations for the Southern Hemisphere with satellite observations. In general, the observations compare favorably with the calculations, especially in regard to north-south gradients.

The mean annual pole-to-pole profile of net radiation R_N from satellite observations is given in Figure 2.1. On an annual basis, assuming no storage in the planetary system, the net radiation distribution is related to the northward transport of energy by the atmosphere and ocean by

$$F(\phi_1) = 2\pi a^2 \int_{-\pi/2}^{\phi_1} R_N(\phi) \cos\phi \, d\phi \qquad 2.1$$

where $F(\phi_1)$ is the northward transport or flux of energy across latitude ϕ_1, R_N is the net radiation, and a is the earth's radius. The net radiation gradient is a sort of forcing function for the circulation of the atmosphere and ocean, although it is, because of its high dependency on clouds and thermal structure, not independent of the circulation.

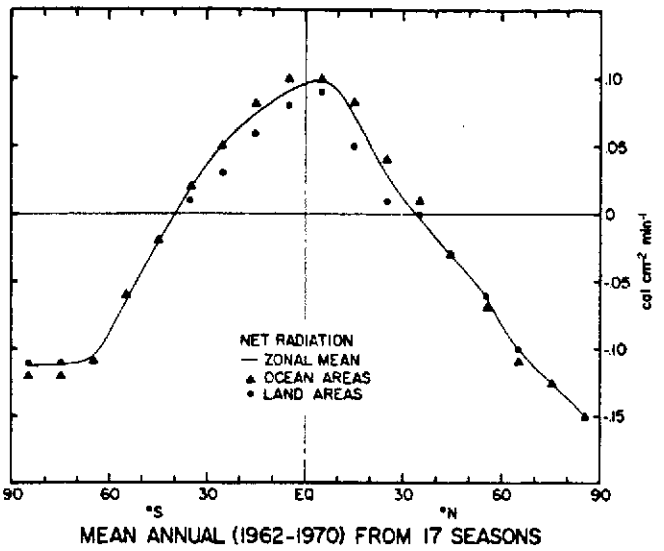

Fig. 2.1 Mean annual, satellite-based net radiation distribution (from Vonder Haar, 1972).

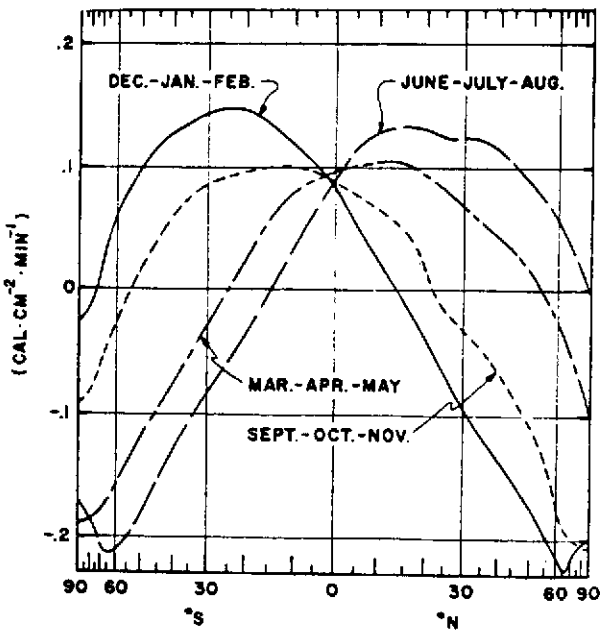

Fig. 2.2 Mean seasonal values of the meridional profiles of net radiation obtained from satellite measurements (from Vonder Haar and Suomi, 1971).

From Figure 2.1 it is obvious that the equator-to-pole gradient of R_N is larger in the Northern Hemisphere than in the Southern Hemisphere (Vonder Haar and Suomi, 1971). However, the equator-to-pole difference in net radiation may be misleading with regards to possible relations to the general circulation. That is, a stronger equator-to-pole net radiation difference does not necessarily mean that that hemisphere's general circulation is stronger in terms of mid-latitude energy fluxes. A better parameter perhaps is the hemispheric maximum of the required energy flux itself. This maximum will occur at the latitude of $R_N = 0$. Calculations of the energy transport from net radiation considerations by Vonder Haar and Suomi (1971) and Newton (1972) indicate that the maximum in the two hemispheres is nearly identical, with the Southern Hemisphere having a slightly higher value. These similar values indicate that, on an annual balance, the circulation of the Southern Hemisphere must carry as much, or slightly more, energy poleward at the latitude of maximum transport. The energy flux is divided between the atmospheric circulation and the ocean circulation. Although calculations of the ocean contribution are uncertain, Sellers (1965) concludes that the percentage of the energy transport carried out by the oceans is greater in the Northern than in the Southern Hemisphere. From the estimates of total transport from the satellite net radiation measurements, it then follows that the atmosphere of the Southern Hemisphere must transport more energy polewards than its counterpart north of the equator. This conclusion is heavily dependent upon the evaluations of the ocean transport in the two hemispheres. As shown by Vonder Haar (1972) and Vonder Haar and Oort (1973), there are significant discrepancies between the ocean fluxes given by Sellers (1965) and

the ocean contribution calculated as a residual of measured atmospheric transport and satellite-measured net radiation.

The annually-averaged storage term is usually neglected, even though there is a lack of good estimates of it. On a seasonal basis, however, the storage is probably larger and not negligible. Therefore, season-by-season, the net radiation is not balanced by the divergence of energy flux. However, the seasonal net radiation gradients (Figure 2.2) are still important as a forcing for the general circulation. During the winter in both hemispheres, there is a reversal of the gradient near the poles. The reversal is more pronounced in the Southern Hemisphere and shows up in the annual mean curve as the flat part of the curve near the South Pole in Figure 2.1. The net radiation gradients between high and low latitudes for winter are nearly the same for the two hemispheres. There is, however, a large variation between the hemispheres in the summer mean gradient. The equator-to-pole difference is only slightly larger in the Southern Hemisphere; however, it appears that the equator-to-pole gradient underestimates the hemispheric dissimilarity. While the value of the net radiation is nearly equal at the equator, in the latitude band 10°-40° there are substantially higher values of R_N in the Southern Hemisphere. These higher values in the low latitudes, coupled with the lower values at higher latitudes (>70°) in the Southern Hemisphere, indicate a much greater latitudinal forcing in the Southern Hemisphere summer than in the Northern Hemisphere summer. It is also interesting to note that there is a major difference in the radiation budgets of the two polar regions in summer. While there is a negative net radiation poleward of about 70°S, in the Northern Hemisphere the net radiation is positive at all

latitudes, except zero at the pole. This disparity results largely from an inequality in albedo between the two regions.

Longitudinal variations of components of the radiation budget may also be important to the atmospheric circulation. The geographical distributions of various budget components and the net radiation as observed from satellites are discussed by Vonder Haar and Suomi (1971) and Vonder Haar (1972). The mean annual pattern for the net radiation shows pronounced longitudinal fluctuations in the tropics, and a nearly zonal pattern in middle and high latitudes of each hemisphere. A comparison of the patterns at 15°N and 15°S shows longitudinal features of larger amplitude in the Southern Hemisphere (Vonder Haar and Suomi, 1971). No such hemispheric difference can be detected at higher latitudes. Vonder Haar (1972) displays figures which seem to indicate that the Northern Hemisphere has a greater inter-annual variability in the longitudinal distribution of albedo and longwave radiation than the Southern Hemisphere.

2.3 Mean tropospheric temperature structure and flow fields

The recent publication of the Southern Hemisphere, upper-air climatology by Taljaard, van Loon, Crutcher and Jenne (1969) enables a comparison to be made for various levels with a Northern Hemisphere climatology such as that of Crutcher and Meserve (1970). The temperature, height and wind climatologies of the Southern Hemisphere are discussed in detail by van Loon (1972a, b, c) and zonal mean cross-sections from pole-to-pole are discussed by Lorenz (1967), Newell et al. (1970) and van Loon (1972c).

The cross-sections of temperature and zonal wind show significant variations between the hemispheres. On a mean annual basis, the pole-to-equator temperature gradient at 500 mb is larger in the Southern Hemisphere. This is also the case for the summer and winter seasons individually with the distinction between the hemispheres being small in winter and large in summer. This seasonal variation in hemispheric differences is also prevalent in the latitudinal distribution of net radiation (see Section 2.2). The distributions of net radiation and temperature are, of course, interdependent.

Zonal mean geostrophic wind is related to latitudinal temperature gradient by the thermal wind relation. It follows that the maximum in the mean westerlies should be larger in the Southern Hemisphere on an annual average, with the difference much larger in the summer. The summer contrast is striking, with the Southern Hemisphere westerlies having a mean maximum speed about 50% higher than that found north of the equator. The difference in winter is less, with maximum speeds almost the same.

Zonal cross-sections, however, do not reveal some of the most important inter-hemispheric dissimilarities. Crutcher and Meserve (1970) are the most recent source for Northern Hemisphere, upper-air climatic maps. Comparison of the Northern Hemisphere 500 mb and 200 mb mean height fields of January and July with the Southern Hemisphere maps of Taljaard et al. (1969) for July and January respectively, reveal sharp differences with regard to zonal variations. The mean patterns in both seasons are much more zonal in the Southern Hemisphere. In the Northern Hemisphere a three-wave pattern is evident, especially in winter. The lack of large standing waves apparently reflects the lack

of geographic and orographic forcing in the Southern Hemisphere. However, the more zonal Southern Hemisphere patterns are not altogether symmetric about the pole. The distributions of 500 mb and 200 mb heights at 60°S for both January and July indicate that the polar vortex is not centered on the pole but offset towards about 50°E, towards Madagascar. This placement is related to a mean jet position at about 45°-50°S, centered at about 50°E, as evident on the geostrophic wind climatologies of van Loon, Taljaard, Jenne and Crutcher (1971). This is the major jet stream in the summer (January). In winter (July) the mean wind maps for 500 mb and 200 mb show two major wind maxima. One is at the aforementioned position at about 50°E. The other location at 500 mb is to the east of Australia at 180°E, at latitude 26°S. At 200 mb the wind maximum has lengthened and cuts across the eastern part of the Indian Ocean, across southern Australia at about 30°S, and across the western Pacific Ocean. The highest analyzed isotach is for 50 m sec^{-1}. In summer (January) a weak maximum is also evident at 200 mb across eastern Australia and the western Pacific Ocean at about 30°S. The same feature is not distinctly evident on the mean map for 500 mb. Therefore, while the Southern Hemisphere mean tropospheric flow is more zonal than that in the Northern Hemisphere, there are important zonal variations.

2.4 Energy and momentum budgets

The energy cycle of the Southern Hemisphere, and the components thereof, have not been studied in as much detail as those of the Northern Hemisphere. Descriptions of the atmospheric energy cycle have therefore been based mainly on Northern Hemisphere studies such as

Oort (1964). However, some studies with a global scope have been conducted. Determination of the poleward transport of energy by the atmosphere and ocean combined on an annual basis has been accomplished using satellite net radiation data (see Section 2.2) or model computations of the radiative budget of the planetary system. Some flux computations have been carried out in the Southern Hemisphere using IGY data.

Newton (1972) gives a comprehensive discussion of the Southern Hemisphere general circulation in relation to global energy and momentum budgets. A consistent description of atmospheric and oceanic fluxes is arrived at by using absolute angular momentum, water and energy balance requirements along with flux computations where available. The momentum budget results discussed by Newton (from Newton, 1971) for both the annual case and the individual seasons indicate a number of differences between the two hemispheres. The Southern Hemisphere's tropics and mid-latitudes are, respectively, a greater surface source and sink of momentum for the atmosphere than the same areas of the Northern Hemisphere on an annual basis. The Southern Hemisphere also has, on an annual average, a greater poleward flux of momentum across 30° latitude. In addition, the momentum flux undergoes a much weaker annual variation in the Southern Hemisphere than in the Northern Hemisphere. However, maximum fluxes occur during winter both above and below the equator.

Newton's discussion of the annual energy balance is based on the latitudinal distribution of net radiation values. These consist of a combination of calculated and satellite-observed values. The total energy flux is divided into the latent heat flux, and the oceanic and atmospheric fluxes of potential heat which is defined as the sum of the

enthalpy and the potential energy. The latent heat fluxes were determined by precipitation-evaporation budget calculations. The flux curves determined by Newton are given in Figure 2.3. The oceanic component is based on an adjustment of the flux curve of Sellers (1965). Newton's modification decreases Sellers' estimate of the poleward transport by the ocean in the Southern Hemisphere, and increases the poleward transport by the ocean in the Northern Hemisphere. With the total energy transport (both the ocean and atmosphere) being nearly equal in the two hemispheres, the energy transport by the Southern Hemisphere atmospheric circulation must be greater than that of its northern counterpart.

In the tropics (0-30°) the poleward potential heat transport by the atmosphere is much greater south than north of the equator. The latent heat flux in the southern tropics is also greater, but is directed equatorward in both hemispheres. In mid-latitudes the potential heat flux and the latent heat flux are nearly equal in the two hemispheres. A breakdown of the atmospheric potential heat flux into toroidal and eddy components shows that in the tropics the variation between the hemispheres shown in Figure 2.3 is in the toroidal component. Thus, on an annual basis, the Southern Hemisphere has a much stronger Hadley cell in low latitudes. This stronger mean meridional circulation also accounts for the difference between the tropics of the two hemispheres with regard to the equatorward latent heat flux. In mid-latitudes the eddy component of the energy transport dominates and is approximately of the same magnitude in both hemispheres, according to Newton.

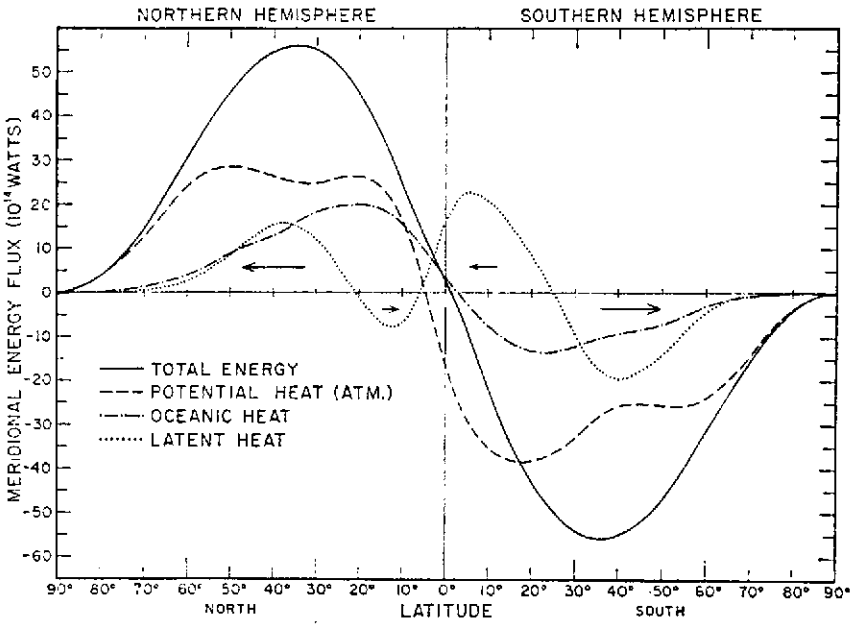

Fig. 2.3 Annual mean meridional flux of total energy for the earth-atmosphere system, and its apportionment between oceanic flux and atmospheric flux of potential heat and latent heat (from Newton, 1972).

Newell et al. (1970) also discuss the global energy budget of the atmosphere, and make global and hemispheric estimates of the components of the energy cycle in the troposphere (100-1000 mb) for the four seasons. The four basic components to the atmospheric energy cycle, zonal and eddy available potential energy (AZ and AE) and zonal and eddy kinetic energy (KZ and KE), are calculated where possible. In addition, conversion rates, generation rates and dissipation rates are calculated. The AE and KE computations are severely hindered by the lack of data giving longitudinal variations on a day-to-day basis. The values for AZ and KZ indicate that for respective seasons, the Southern Hemisphere always has the larger values, the greatest difference between the hemispheres being during the summer. The quantities AZ and KZ are computed from climatological cross-sections. The energy conversion from AZ to AE is calculated using climatological values of temperature. During the winter months in each hemisphere, the AZ to AE conversion rates are of the same approximate magnitude; during the summer, the Southern Hemisphere conversion rate is much larger. The AE to KE conversion rate is not estimated in the Newell et al. study.

2.5 Standing and transient eddies

One of the major observed differences between the general circulations of the two hemispheres is the relative importance of standing and transient eddy motions. In the Northern Hemisphere, standing waves are evident in upper-air climatologies with mean troughs east of the Asian and North American continents and a weaker third trough in eastern Europe. No such strong stationary wave pattern is evident in the Southern Hemisphere climatologies, although the flow is not completely

symmetric about the pole (see Section 2.3). Van Loon and Jenne (1972) do show the presence of standing waves 1, 2, and 3 in the Southern Hemisphere, but the amplitudes of wave numbers 2 and 3 are much less than the same ones in the Northern Hemisphere.

The relative lack of a standing eddy component of motion in the Southern Hemisphere is also evident in calculations of heat and momentum transport and in calculations of eddy kinetic energy. Obasi (1963) and Kao, Jenne and Sagendorf (1971a) indicate that the transient eddies account for almost all of the poleward transport of momentum in the Southern Hemisphere. In addition, Obasi (1965) points out that what standing eddies there are in the Southern Hemisphere extract energy from the mean flow, unlike the standing eddies in the Northern Hemisphere which supply energy to the mean flow. Analyses of meridional eddy heat transport by Robinson (1970), Newton (1972) and Kao, Jenne and Sagendorf (1971b) in the Southern Hemisphere again reveal the overwhelming importance of the transient waves. On the other hand, Oort (1971) states that, in the Northern Hemisphere, the standing eddies transport half of the sensible heat during the winter months.

Kao, Jenne and Sagendorf (1970) investigate the spectral properties of Southern Hemisphere eddy kinetic energy at 500 mb. Wave number spectra for both the total motion and for the stationary waves are given. A similar study (Kao and Wendell, 1970) gives the Northern Hemisphere version. For both the zonal velocity and the meridional velocity, the standing waves contribute less to the total eddy kinetic energy in the Southern Hemisphere than they do in the Northern Hemisphere. This difference is larger for the meridional velocity.

A comparison of spectra of kinetic energy for the Northern and Southern Hemispheres reveals another interesting hemispheric variation. The magnitudes of the zonal and meridional components relative to each other are different in the two hemispheres. Wooldridge and Reiter (1970), using relative separation velocities obtained from GHOST balloon pairs, indicate a much larger ratio of meridional to zonal spectral density at synoptic-scale wavelengths in the Southern Hemisphere than is found in the Northern Hemisphere for similar lagrangian studies. A comparison of the wave number spectra of Kao and Wendell (1970) for the Northern Hemisphere and Kao, Jenne and Sagendorf (1970) for the Southern Hemisphere also indicates a dissimilarity in the spectral densities of zonal and meridional flow. In the Northern Hemisphere, the spectral density of u is larger than that of v at the synoptic scale (~ wave number 6), while in the Southern Hemisphere, the spectral density of v is larger.

Although the studies just discussed emphasize the relative lack of standing eddies in the Southern Hemisphere, there are features in the cloudiness and precipitation climatologies (see van Loon, 1972d) which indicate some sort of geographic anchoring. In the western South Pacific Ocean, there is a narrow band of mean cloudiness and mean precipitation running from the northwest to the southeast from a point at about 10°S, 180°W to 35°S, 150°W. The band is evident in both winter and summer, but is more obvious in summer. A second cloud band, similarly oriented, occurs east of South America; however, this band is not as distinct as the Pacific Ocean one. No similar cloud area exists in the Indian Ocean.

The reason for the existence and location of these bands is uncertain. The cloudy region in the Pacific Ocean is coincident with a maximum in cyclone frequency (Taljaard, 1972b). Although the equatorward limit of the clouds is associated with the inter-tropical convergence zone and tropical cyclones, farther south the band is associated with frontal troughs and extratropical low pressure centers. In the Atlantic Ocean, the cyclone frequency maximum parallels, but is just south of, the cloud belt. The cause of this preference in cyclone tracks is unclear.

The mean upper-level wind fields (van Loon, 1972c) show middle and upper troposphere wind speed maxima in the region of the Pacific Ocean cloud band. The axis of the jet stream is located at about 28°S. In January the maximum is delineated best at 200 mb as an extension eastward from Australia of relatively high wind speeds with a peak of about 23 m sec^{-1}. In these longitudes there are actually two peaks, the other being farther poleward at about 50°S. In July at 200 mb there is a large jet stream center at 28°S centered over Australia and extending eastward with the speeds decreasing eastward. At 500 mb a maximum in the westerlies is located east of Australia at 28°S, 180°W. Therefore, in both seasons, there are upper-level features of importance occurring in association with the Pacific Ocean cloud band.

The upper-level support for the Atlantic Ocean cloud band is indistinct, possibly because of a lack of upper-air data over the region. There are, however, indications on some of the isotach analyses that the band is located in the left-rear quadrant of a jet stream isotach maximum, which, in the Southern Hemisphere, should show upper-level divergence through vorticity considerations.

In the summer (January), the Pacific Ocean cloud band extends southeastward from the inter-tropical convergence zone (ITCZ). Across the Indian Ocean and to the northeast of Australia to 180°W, the ITCZ is located at approximately 10°S. East of about 140°W eastward to the Indian Ocean, the mean position of the ITCZ in summer is on the equator. Consequently, at the northern end of the cloud band, there is low-level convergence at the ITCZ. The southerly location of the ITCZ across the Indian Ocean and the western Pacific Ocean and the existence of a mean wind speed maximum in the middle and upper troposphere probably provide the conditions for cyclone development in the region of the cloud band.

The extension of the ITCZ southward across the eastern half of the hemisphere in January is related to the strong northerly, low-level flow coming across the equator from the Asian winter monsoon. The upper-level flow in the Southern Hemisphere may also be affected by monsoon conditions on the other side of the equator. Therefore, in trying to find complete explanations for Southern Hemisphere climatological features, one must consider the global atmosphere as a whole.

2.6 Stratosphere

The stratospheres of the Northern and Southern Hemispheres are quite alike during the summer months and quite dissimilar during the winter. The circulation during summer in both hemispheres is dominated by a warm anticyclone centered over the polar regions. In the Southern Hemisphere, the center of the anticyclone is slightly off the pole towards 150°W (Labitzke and van Loon, 1972). The isotherms are nearly concentric around the pole. The Northern Hemisphere in July shows basically the same type of height and temperature patterns with the

anticyclone centered very close to the pole (Craig, 1965). The temperatures in the Southern Hemisphere at 30 mb are higher than those in the Northern Hemisphere poleward of about 30°, and colder equatorward of that latitude, indicating a stronger meridional temperature gradient in the Southern Hemisphere (Labitzke and van Loon, 1972). The 30 mb heights in the polar region are, however, lower in the Southern Hemisphere because of a much colder troposphere. At 50 mb the height gradients indicate that stronger mean easterlies are present in the Northern Hemisphere. However, because the meridional temperature gradient is larger in the Southern Hemisphere, the easterlies increase with height faster there. Although Muench (1968) shows evidence of large-scale disturbances in the Northern Hemisphere summer stratosphere, both hemispheres are considered synoptically inactive at these heights relative to occurrences during the winter.

From summer to winter in both hemispheres, temperature gradients in high latitudes reverse, westerlies take the place of easterlies, and the polar-night vortex is formed. Climatologically, the Southern Hemisphere vortex has lower temperatures and lower heights. The southern vortex is also more symetric about the pole than its Northern Hemisphere counterpart. The climatic 50 mb height and temperature fields for the Northern Hemisphere (Craig, 1965) show pronounced wave numbers 2 and 3, while the flow at that level in the Southern Hemisphere is almost completely zonal at high latitudes.

The major reason for the difference in the winter stratospheric climatologies is that the wintertime polar vortices of the Northern and Southern Hemispheres exhibit contrasting breakdown climatologies. In most years, the Northern Hemisphere vortex breaks down completely in

midwinter. Often the vortex never becomes re-established. A detailed summary of events during Northern Hemisphere breakdowns is given by Reiter (1969a). The Antarctic vortex, on the other hand, has not been observed to undergo the complete, midwinter breakdown typical of the Arctic vortex, although midwinter minor warmings have been observed (Labitzke and van Loon, 1972). The final, complete collapse of the Antarctic vortex does not occur until spring.

This difference in breakdown characteristics between the two hemispheres has not been completely explained. Case studies in the Northern Hemisphere have shown that the main source of energy for the breakdowns is an eddy flux of energy from the troposphere (Julian and Labitzke, 1965 and Matsuno, 1971). The waves which are important in the vertical flux into the stratosphere are the very long, slowly moving or stationary waves. In the Northern Hemisphere during the winter, stationary wave numbers 2 and 3 are prominent in the climatological fields of the upper troposphere. These stationary waves are associated with the distribution of geography and orography in the Northern Hemisphere. In the Southern Hemisphere mid-latitudes, the land-sea variation is essentially nonexistent, and the orographic barriers are minor compared to those in the Northern Hemisphere. The effect of this rather uniform surface is apparently a relative lack of standing eddies which may result in a lack of upward propagation of energy from the troposphere to the stratosphere in the Southern Hemisphere. Since this vertical flux of energy has been identified as the major source of energy for the Northern Hemisphere breakdowns, the lack of standing waves in the Southern Hemisphere may be related to the lack of midwinter breakdowns in the Southern Hemisphere.

A number of studies (Reed, Wolfe and Nishimoto, 1963; Mahlman, 1966; Julian and Labitzke, 1965; Vincent, 1968) have shown that the mean meridional circulation in the lower half of the stratosphere in the Northern Hemisphere winter has a two-celled structure with rising motion in low latitudes and over the pole and sinking motion in mid-latitudes. This zonally-averaged vertical motion pattern exists before, during and after midwinter breakdowns of the polar vortex (Mahlman, 1966). In the Southern Hemisphere the mean meridional circulation is practically unknown. Rubin and Weyant (1963) do indicate a sinking motion over the pole below 75 mb. Also Reiter (1969a, 1971), on the basis of ozone measurements over Antarctica, postulates a general sinking motion over the pole in the stratosphere. This descent over the polar region would tend to compensate for decreasing temperature due to the large radiative loss during the polar night.

Some previous studies of Southern Hemisphere stratospheric circulation have used atmospheric structure inferred from satellite radiances. Nordberg, McCulloch, Foshee and Bandeen (1966), Julian (1967) and Shen, Nicholas and Belmont (1968) use 15 micron radiation data to interpret Southern Hemisphere stratospheric temperature patterns. Fritz (1970) and Fritz and Soules (1970) examine stratospheric temperature variations in the Southern Hemisphere using 15 micron radiances from the SIRS experiment. Smith, Woolf and Jacob (1970) and Miller, Finger and Gelman (1970) use 30 mb temperature and/or height information derived from SIRS data to study wintertime stratospheric patterns in the Southern Hemisphere.

CHAPTER 3

METHOD USED TO OBTAIN ATMOSPHERIC STRUCTURE FROM NIMBUS 3 SIRS DATA

3.1 Satellite system

The primary data used in this study are from the Satellite Infrared Spectrometer (SIRS) experiment aboard the Nimbus 3 spacecraft. The satellite orbit is essentially circular at 600 nautical miles above the surface, is sun synchronous with a local noon equator crossing, and has an inclination of 100° which results in the orbital track never being poleward of latitude 80°. Successive orbits are 26° of longitude apart at the equator, and the period of the orbit is 107 minutes.

The SIRS instrument measures the infrared radiation from the earth in eight spectral bandpasses, ranging from 11 to 15 microns (899 to 669 cm^{-1}). The eight channels are thus in a spectral interval where the atmospheric absorption varies from near 0% in the atmospheric "window" at 11 microns to near 100% at 15 microns in the CO_2 absorption band. This change in absorption with wavelength is the basis for obtaining temperature information as a function of height from the SIRS radiances. The field of view of the instrument is 11.5° on a side, which results in a view of the surface of 120 nautical miles on a side. A detailed description of the SIRS instrument is given by Wark, Hilleary, Lienesch and Clark (1969).

A number of techniques to obtain atmospheric thermal structure from multi-channel, satellite radiance data have been developed and used. They are reviewed by Fleming and Smith (1972). The methods can be separated into two categories: matrix inversion and iteration. Although some require no prior knowledge of atmospheric thermal structure, most are based on additional information given by atmospheric temperature and radiance statistics. The simplest statistical-based scheme is a regression technique, in which near simultaneous satellite radiance observations and radiosonde observations are compared to develop regression equations, with atmospheric temperature as the dependent variable, and radiances as the independent variables. This type of procedure applied to Nimbus 3 data is discussed by Smith, Woolf, and Jacob (1970). The method used to obtain the thermal structure for the present study is similar to the regression technique of Smith, Woolf and Jacob (1970), but uses the geopotential height difference between pressure levels as the dependent variable.

3.2 Physical basis for thickness - radiance regression technique

The thickness D between pressure surfaces in the atmosphere is proportional to a weighted mean temperature in the layer, as given by equation 3.1.

$$D = z_2 - z_1 = \frac{R}{g} \int_{p_2}^{p_1} T \, d\ln p \qquad 3.1$$

The radiance observed by a satellite in a particular channel is also a function of a weighted mean temperature through a layer. Equation 3.2 is the infrared radiative transfer equation. N_i is the radiance observed in the i^{th} channel by the satellite instrument, W_i is the Planck function defined in equation 3.3, τ_i is the i^{th} channel

transmittance function, and the subscript s represents surface conditions.

$$N_i = \frac{1}{\pi}\int_o^{p_s} W_i \frac{d\tau_i}{d\ln p}\, d\ln p + \frac{1}{\pi} W_i(T_s)\left[1 - \int_o^{p_s} \frac{d\tau_i}{d\ln p}\, d\ln p\right] \qquad 3.2$$

$$W_i = \frac{c_1 k_i^3}{e^{(c_2 k_i/T)} - 1} \qquad 3.3$$

In equation 3.3, k_i is the wave number. The term $\frac{d\tau_i}{d\ln p}$ is the weighting function for the i^{th} channel. The weighting functions for the eight SIRS channels are shown in Figure 3.1. Channels near the middle of the 15 micron absorption band have maxima at high altitudes, while channels out on the wing of the absorption band have peaks at lower altitudes. Channel 1 ($899 cm^{-1}$) is in the atmospheric "window."

For the moment, assume a cloudless atmosphere and neglect the second term on the righthand side of equation 3.2, the surface contribution term. This term would be identically zero when dealing with channels 4 through 8 where the surface elevation is small. The term can also be considered known because T_s could be calculated using channel 1 ($899 cm^{-1}$), and $W_i(T_s)$ could then be computed using equation 3.3. With the surface contribution term neglected, equation 3.2 becomes

$$N_i = \frac{1}{\pi}\int_o^{p_s} W_i \frac{d\tau_i}{d\ln p}\, d\ln p \qquad 3.4$$

The Planck function W_i can be closely approximated by a linear function of temperature over a limited range of temperature when dealing with the 11-15 micron portion of the spectrum. For example, over a 40°K

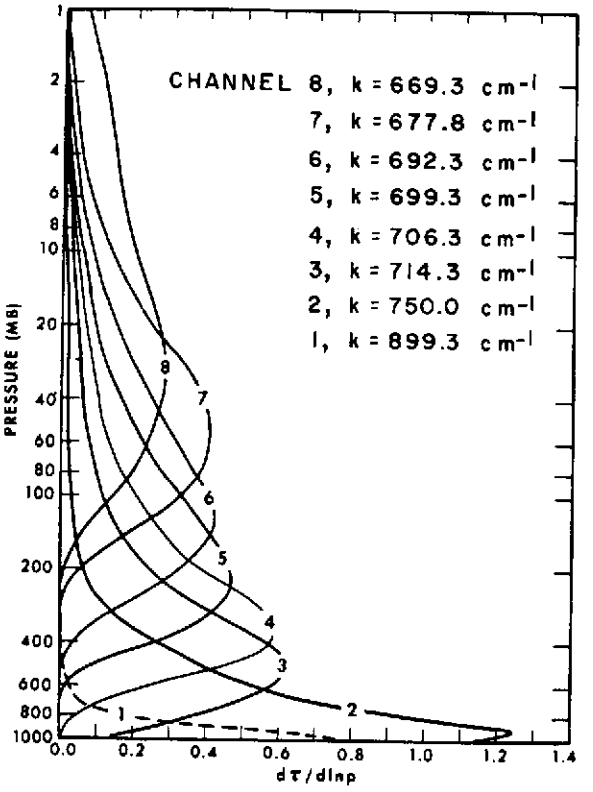

Fig. 3.1 Derivative of transmittance with respect to the logarithm of pressure. These functions approximately describe the relative sensitivity of the eight SIRS radiance observations to temperature variations in various altitude layers of the atmosphere (from Smith, Woolf and Jacob, 1970).

temperature range from 214°K to 254°K, a linear fit would reproduce Planck function values within 3% for the wavelength range from 13.4 micron ($750cm^{-1}$) to 15.0 micron ($670cm^{-1}$). Therefore,

$$W_i \cong c_3 + c_4 T \tag{3.5}$$

Substituting equation 3.5 into equation 3.4, one obtains

$$N_i \cong \frac{1}{\pi} c_3 \int_o^{p_s} \frac{d\tau_i}{d\ln p} d\ln p + \frac{1}{\pi} c_4 \int_o^{p_s} T \frac{d\tau_i}{d\ln p} d\ln p \tag{3.6}$$

The first term on the right side of equation 3.6 is known, and subtracting it from N_i results in

$$N_i' = \frac{1}{\pi} c_4 \int_o^{p_s} T \frac{d\tau_i}{d\ln p} d\ln p \tag{3.7}$$

where $N_i' \cong N_i - \frac{1}{\pi} c_3 \int_o^{p_s} \frac{d\tau_i}{d\ln p} d\ln p$. If $\frac{d\tau_i}{d\ln p}$ were a rectangular function as shown in Figure 3.2, equation 3.7 would reduce to

$$N_i' = \frac{1}{\pi} c_4 \int_{p_1}^{p_2} T \, d\ln p \tag{3.8}$$

In other words, the N_i' would be proportional to a weighted, layer-mean temperature between two pressure levels, which in turn is proportional to the thickness D of the layer. Unfortunately, a glance at Figure 3.1 shows that the weighting functions are not rectangular. However, it is also evident from an inspection of Figure 3.1 that a linear combination of the weighting functions could be made that is "more rectangular" than any individual weighting function. Thus, a linear combination of radiances would be more closely proportional to the layer mean

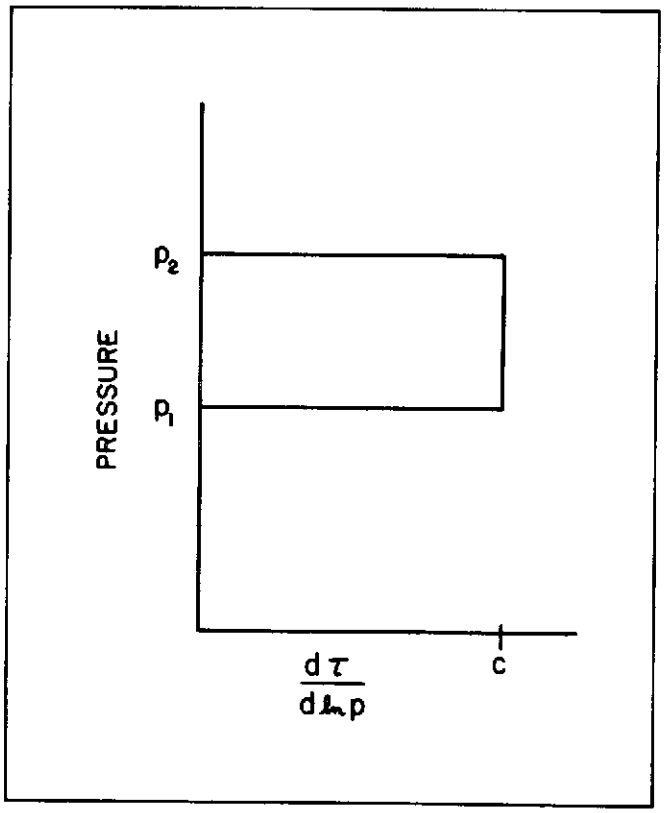

Fig. 3.2 Idealized weighting function.

temperature or thickness than an individual radiance. Fleming (1972) discusses a mathematical technique to determine the optimum linear combination of radiances. In the present study, the linear combination is determined through a step-wise regression technique.

3.3 Thickness regression method

From the discussion in the previous section, one would expect a high correlation between the thickness D and a linear combination of channel radiances. To determine the coefficients of the linear combination, a step-wise, least-squared error, multiple regression technique is used. The regression equation is

$$D = \alpha_0 + \alpha_1 N_1 + \alpha_2 N_2 + \text{---} + \alpha_8 N_8 \ , \qquad 3.9$$

where D is the thickness and N_1 through N_8 are the satellite radiances in the eight channels. The dependent variables in the regression procedure are the thicknesses for the following layers: 100-700 mb, 700-500 mb, 500-300 mb, 300-200 mb, 200-100 mb, 100-50 mb, 50-30 mb, and 30-10 mb. The independent variables are the radiances of the eight SIRS channels. Separate regression equations are determined for each layer, for each of the latitude zones 20-40°, 40-60°, and 60-80° in both hemispheres and for each month studied. The division by latitude is required because the relationship between thickness and radiance derived in Section 3.2 is based on the Planck function being approximately linear with respect to temperature. This approximation is only valid over a limited temperature range; therefore, the data is divided into latitude zones to restrict the temperature variation in each data group.

The equations in Section 3.2 are for a cloud-free atmosphere. The regression technique is based on a comparison of thickness information

and cloud-free radiance data. When the derived regression equations are applied to other radiance data, only cloud-free data are used. To eliminate cloud-contaminated data from the comparison data set and from the application of the regression equations, a simple, objective "cloud check" procedure based solely on the satellite radiance information is used. The SIRS channels with weighting function peaks in the low troposphere (channels 1 through 3) are the ones most affected by the presence of clouds. Channels with weighting function peaks in the stratosphere (channels 7 and 8) are only rarely affected by the presence of tropospheric clouds. The radiance in the atmospheric window (channel 1, k = 899 cm^{-1}) in the absence of clouds is related to the surface temperature through equation 3.3. In the presence of an overcast, the channel 1 radiance is a function of cloud-top temperature, which is lower than the surface temperature. Therefore, channel 1 radiances much below normal would indicate the presence of clouds; however, the radiance at this wavelength is highly variable even in the absence of clouds because of its dependence on the surface temperature. Large changes occur along satellite tracks in the presence of sharp changes in surface characteristics such as land-sea boundaries. Also, large diurnal changes are present in the window radiance because of large changes in land surface temperature. Channels 2 and 3 are also affected by clouds, but are not so severely affected by surface characteristics as channel 1. Therefore, they are used for the "cloud check."

SIRS radiance data is eliminated as being cloud-contaminated when the observed radiance in both channels 2 and 3 is below critical magnitudes. The criteria for both channels were determined by a comparison

of SIRS data and satellite video data and are a function of latitude and season. The latitude profiles of the critical values for each season are given in Figures 3.3 and 3.4. Any data with both channel 2 and 3 radiances below the critical levels shown in Figures 3.3 and 3.4 are eliminated as cloud-contaminated. The units of radiance along the ordinate in the figures are ergs cm^{-2} sec^{-1} $steradian^{-1}$ $(cm^{-1})^{-1}$, abbreviated as (ergs/). The "cloud check" procedure is simple and certainly not foolproof. Some slightly cloud-contaminated data may still find its way into the final data set. The procedure outlined above removes, on the average, about 15% of the original data points.

and 3 radiances below the critical levels shown in Figures 3.3 and 3.4 are eliminated as cloud-contaminated. The units of radiance along the ordinate in the figures are ergs cm^{-2} sec^{-1} $steradian^{-1}$ $(cm^{-1})^{-1}$, abbreviated as (ergs/). The "cloud check" procedure is simple and certainly not foolproof. Some slightly cloud-contaminated data may still find its way into the final data set. The procedure outlined above removes, on the average, about 15% of the original data points.

To obtain the regression coefficients, comparison sets of radiance and thickness data are developed. The observations are near-simultaneous and at, or close to, the same geographic position. Somewhat different techniques are used for the Northern and Southern Hemispheres. In the Northern Hemisphere, for the layer 100 to 1000 mb, the SIRS radiance data is matched with the National Meteorological Center (NMC) gridded data. For satellite data occurring within three hours of NMC map time, the NMC grid point data are linearly interpolated to the satellite track position. For the layers above 100 mb, station data are matched with the satellite radiance information. The station location

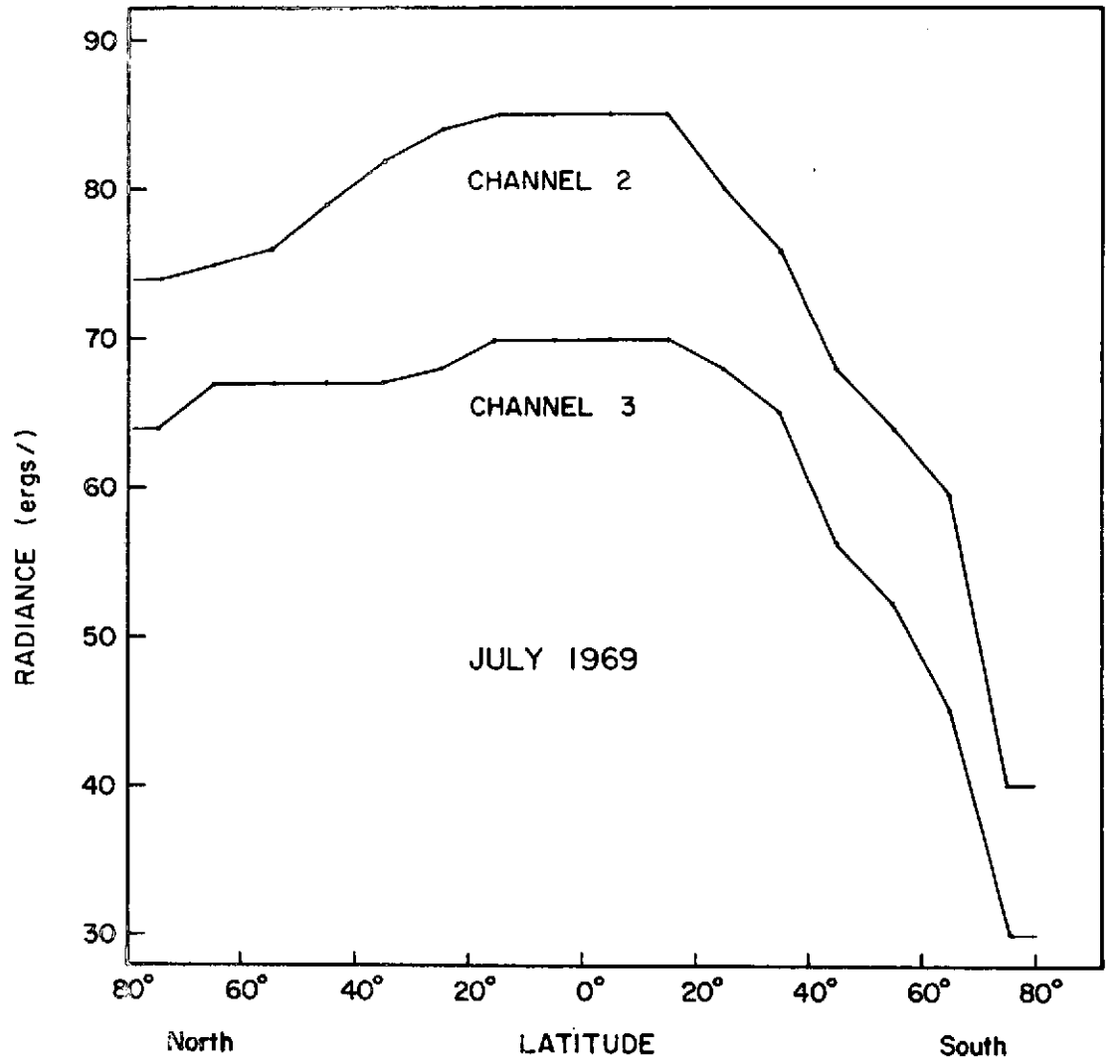

Fig. 3.3 The distribution with latitude of critical values of channels 2 and 3 for the cloud check procedure for July 1969.

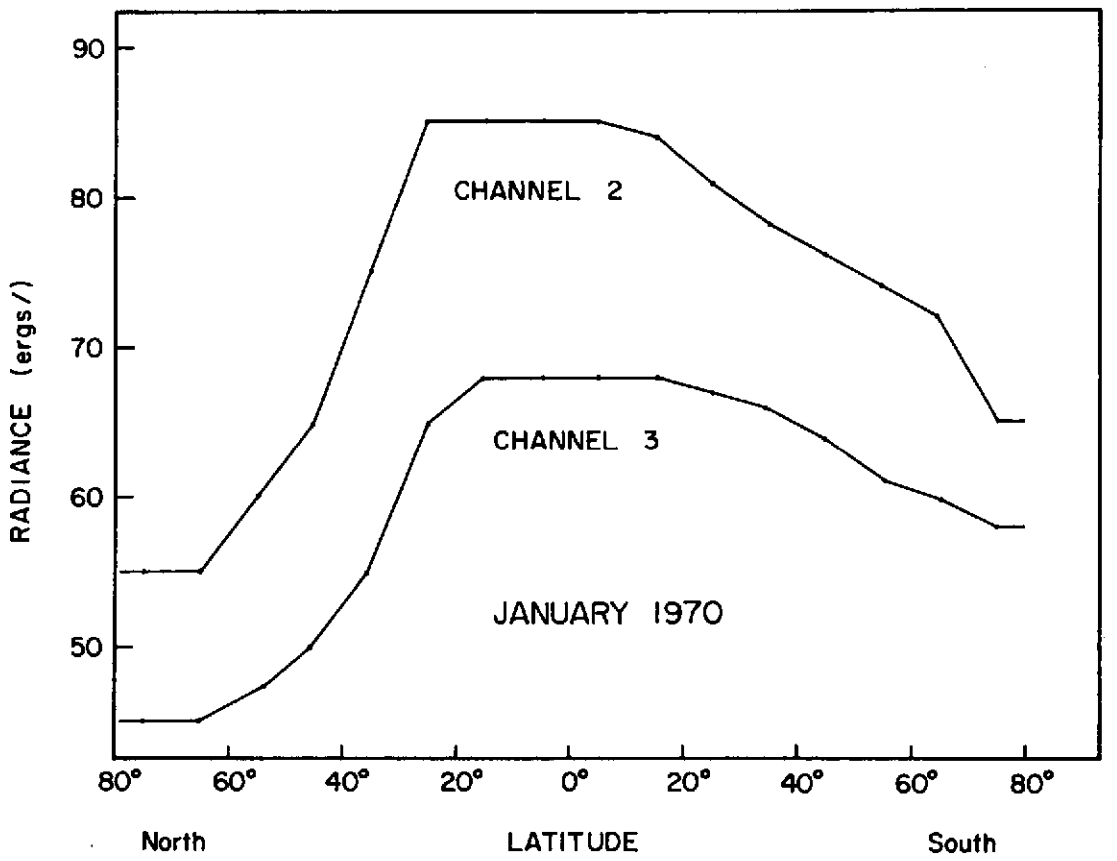

Fig. 3.4 The distribution with latitude of critical values of channels 2 and 3 for the cloud check procedure for January 1970.

must be within 180 nautical miles of the satellite position, and the satellite time must be within three hours of the station observation time.

In the Southern Hemisphere, a different technique is used. Station data are matched with satellite radiances for all levels. Because of the relative lack of stations in the Southern Hemisphere and the need for a sufficient number of data points for the regression analysis, the match up restrictions are somewhat relaxed from those in the Northern Hemisphere. For each 24-hour period surrounding the 0000 GMT and 1200 GMT radiosonde times, radiance information is placed into a five degree latitude by five degree longitude grid for the latitudes 20°S to 80°S. The radiance fields are analyzed and the radiances in each of the eight channels are linearly interpolated from the grid locations to the stations. The match-up is restricted to times and locations when there are original satellite data within a geographic box 600 nautical miles on a side surrounding the station. This method is used for all levels. In the Southern Hemisphere no regression equations are developed for the 10-30 mb layer, because of a lack of radiosonde data at that altitude. The Northern Hemisphere regression equations for this layer and for the respective season are used to complete the Southern Hemisphere temperature structure.

The choice of the regression equations to be used in computing thicknesses is based on certain statistical and practical criteria. The step-wise, least-squared error, multiple regression technique uses an F test to determine if additional independent variables should be introduced into the particular regression under consideration. In

addition, the number of independent variables is restricted to a maximum of four. Most of the regression equations have three independent variables; however, a few have less than three.

3.4 Regression statistics

The regression equation coefficients for thickness used in this study are given in the Appendix along with the percentage of variance explained and the standard error of estimate (approximately equal to root mean square error) for each of the regression equations. The standard errors for each of the eight layers are given in Table 3.1 for each hemisphere and season. These statistics are for the three latitude bands combined (area weighted), and for the dependent data on which the regression equations are based. The errors are largest in the lowest layers because not quite all cloud-contaminated radiance information is removed by the "cloud check" procedure. In order to be absolutely sure that no cloud-contaminated data are entering the system, one would have to eliminate a large portion of the satellite radiances, allowing only the small remaining portion to be available for computations. As a result the "cloud check" parameters are set so that most cloud-contaminated data are omitted, but some borderline cases are accepted; hence the larger errors are in the lowest layer.

In general, the standard errors of estimate in Table 3.1 are comparable to those in other studies using a regression method. Smith, Woolf and Jacob (1970) show errors ranging from 1.0°C to 2.6°C for a May-June period using data from the same SIRS instrument. These values are similar to those in the first column of Table 3.1. Ohring (1972)

	N. H July 69	N. H January 70	S. H July 69	S. H January 70
10-30 mb	1.3° C	2.1° C		
30-50 mb	1.4	3.0	1.7° C	1.8° C
50-100 mb	1.6	2.3	1.7	2.2
100-200 mb	1.9	2.0	1.9	2.4
200-300 mb	1.9	2.4	2.3	1.9
300-500 mb	2.0	2.8	2.3	2.0
500-700 mb	2.0	3.5	2.8	2.1
700-1000 mb	2.6	5.2	3.2	3.1

Table 3.1. Hemispheric standard errors of estimate for thickness regression equations

obtains errors of between 2°C and 3°C using radiances from the Nimbus 3 Infrared Interferometer Spectrometer (IRIS) and a step-wise regression technique.

In the Northern Hemisphere, standard errors are generally larger in the winter month. This difference is associated with the tighter gradients and more rapid movement of systems in the winter. Smith, Woolf and Jacob (1970) also observed an increase in standard error from summer to fall. Because of the larger errors, the regression results for January 1970 are examined in more detail for the 100-1000 mb layer. The January data is divided into three subsets: 1-6 January, 14-19 January, and 26-31 January. Regression equations are derived for the subset of 1-6 January and are applied to the two independent sets. Separate equations are used for each of the latitude bands discussed in the last section. Root mean square errors are given in Table 3.2. The errors for the independent data are larger than those for the dependent

group, but there is, in general, less of a change between the two independent sets. Thus, the regression equations appear stable. When the three sets of data are combined and new regression equations determined, the errors associated with the combined data drop to near the 1-6 January set values. The above was done with regression equations restricted to a maximum of three independent variables or channels.

	Dependent 1-6 January 1970	Independent 14-19 January 1970	Independent 26-31 January 1970	3 sets combined
100-200 mb	1.9° C	2.2° C	2.6° C	2.1° C
200-300 mb	2.4	2.8	2.8	2.5
300-500 mb	2.7	3.0	3.1	2.8
500-700 mb	3.8	4.8	5.1	3.8
700-1000 mb	5.2	7.2	6.6	5.7

Table 3.2. Root mean square errors for regression coefficients stability test

3.5 Limitations of method

The satellite-derived thickness fields used in this study are computed by applying the regression equations to radiance data (eight channels) at 5° latitude by 5° longitude grid locations. The data are processed and placed into the latitude-longitude grid system in the following way. Each set of eight observations of radiance (there are approximately 3000 sets for each hemisphere between 20° and 80° latitude for each 24 hours) is first checked for blatant errors and then for the presence of clouds as discussed in Section 3.3. If there are obvious errors or the data are determined to be cloud-contaminated, the set of observations is excluded. These two checks eliminate about 20% of the

data. Each accepted set of radiances is positioned at the nearest 5° by 5° grid location. Multiple sets of data at a particular location are averaged. For each 24 hour period an average of 400 of the 936 possible locations contain original data. The remainder of the locations are filled in by linear interpolation with a greater weight placed on the east-west direction. Geopotential height information is obtained by adding the thicknesses to a 1000 mb height field. This results in height data at the following levels: 700 mb, 500 mb, 300 mb, 200 mb, 100 mb, 50 mb, 30 mb, and 10 mb. In the Northern Hemisphere NMC 1000 mb height fields are used. In the Southern Hemisphere 1000 mb height analyses are obtained by converting daily surface pressure analyses of the Commonwealth Bureau of Meteorology, Australia. The Southern Hemisphere surface pressure analyses are nearly hemispheric in scope, but where they are blank the field is filled in subjectively by a combination of extrapolation and climatology.

The thickness and height fields produced in this study from the SIRS data have certain limitations and possible biases. Because only "cloud-free" data are used in the satellite-based analyses, there is a bias of clear areas over cloudy areas which could produce a bias in the thickness of height fields if cloudiness is correlated with temperature and/or height. This correlation is certainly true in the low layers where low pressure centers are accompanied by areas of cloudiness. In the upper troposphere however, the correlation is much less. Although the failure to determine atmospheric structure in cloudy areas means that atmospheric eddies are not defined perfectly, the data on either side of cloudy areas are usually sufficient for adequate analysis.

In the following chapters, comparisons are made of general circulation parameters calculated in the Northern and Southern Hemispheres from SIRS-based atmospheric structure. In the Northern Hemisphere, calculations made with SIRS-based structure and ones made with NMC fields are compared. These comparisons reveal a systematic difference between the two sets of computations. Gradients in the NMC fields are underestimated in the SIRS-based fields. The amount is, in general, small with regard to meridional gradients and substantial with regard to longitudinal gradients. For example, the mean temperature gradient between 20°N and 80°N in the troposphere tends to be underestimated by about 10%. On the other hand, the variance of temperature around a latitude circle in the upper troposphere is underestimated by about 50%, indicating that the amplitude of eddies is evaluated incorrectly by about 30%, since the variance involves squares of deviations.

The underestimation of meridional gradients is minimal because separate regression equations are used for each of the three latitude bands. The variance of temperature around latitude circles is underestimated because of a number of factors. First, some features, usually small, are not detected by the satellite-based structure. This is a relatively minor effect and is closely related to the distribution of satellite data. More important is the general result that the SIRS-based thickness fields tend to be "smoother" than the NMC fields which is partially due to the way the usable radiance data is distributed in space for a 24-hour period. Although a particular feature may be detected by the satellite data, the lack of a pass directly over the center of the feature results in an underestimation of the amplitude.

In addition, 24 hours of information are combined to produce the daily fields from which the SIRS-based calculations are made. These calculations are compared to conventional data fields (NMC) at a particular time (1200 GMT). If the NMC fields were first averaged over 24 hours, the calculated values of temperature variance would than be less because the averaging would reduce the amplitudes of moving waves. The regression technique also tends to aid in producing smoother fields than the NMC fields. The thickness-radiance regression equations work very well near the mean thickness for that latitude band, but tend to underestimate deviations from the mean, producing slightly "smoothed-out" fields.

In addition to the effects discussed above which apply at all levels, in the lowest layers the distribution of satellite data, the slight smoothing of the radiance data and the effect of eliminating cloud-contaminated data combine to produce temperature fields which do not indicate the large east-west gradients that are present. The two calculations of the temperature variance agree best at higher elevations. This is partly due to the decreasing effect of possible cloud effects, but more importantly due to the change in the character of the dominant waves with height. In the troposphere smaller, transient waves contribute significantly to the temperature variance; in the stratosphere larger, quasi-stationary, or slowly moving, waves dominate. The large waves in the stratosphere are much more easily detected and more accurately depicted because of the time and space distributions of the satellite data.

Because of the limitations of the SIRS-based structure described in this section, the emphasis of this study is not on the absolute magnitude of quantities in each hemisphere, but on relative magnitudes and on parameters well estimated from the satellite-derived data fields.

CHAPTER 4

COMPARISONS BETWEEN THE HEMISPHERES IN THE TROPOSPHERE

4.1 Available potential and kinetic energies

4.1.1 Formulae and notation

The comparison between hemispheres in this section will be made within the context of calculations of available potential and kinetic energies. The concept of available potential energy (A) and its role in the atmosphere's energy cycle have been discussed by Lorenz (1955, 1967), Dutton and Johnson (1967) and Reiter (1969). The formulations for A and its components, the zonal available potential energy (AZ) and eddy available potential energy (AE), are essentially the same among the various authors. The so-called exact formula shows A to be a function of the variance of pressure on isentropic surfaces. An approximate formula for A (or AZ and AE) involving the variance of temperature on constant pressure surfaces is often used in calculations of available potential energy and is also adopted in this study.

The notation used in this study closely follows that of Reiter (1969a, 1969b). Brackets represent an average over the coordinate given by the subscript. Parentheses indicate deviations from the mean. For example,

$$X = [X]_\lambda + (X)_\lambda \qquad 4.1$$

where λ is longitude. The term $(X)_\lambda$ is the deviation of X from the

zonal average, $[X]_\lambda$. An average over both latitude and longitude is defined as

$$[X]_{\lambda,\phi} = \frac{1}{1 - \sin\phi_s} \int_{\phi_s}^{\pi/2} [X]_\lambda \cos\phi \, d\phi, \tag{4.2}$$

so that $[X]_{\lambda,\phi}$ is an area-weighted mean. In equation 4.2, ϕ_s is the latitude confining the integration. If the integration covers the globe, $\phi_s = -\pi/2$. The expression

$$([X]_\lambda)_\phi = [X]_\lambda - [X]_{\lambda,\phi} \tag{4.3}$$

defines the deviation of a zonally-averaged parameter from an average over both latitude and longitude. For a more detailed description of this notation the reader is referred to Reiter (1969b).

With this notation the computational formulas for AZ and AE, respectively, are

$$AZ = \int_o^{p_s} \frac{[([T]_\lambda)_\phi^2]_{\lambda,\phi}}{2[\sigma]_{\lambda,\phi}} \, dp, \tag{4.4}$$

$$AE = \int_o^{p_s} \frac{[(T)_\lambda^2]_{\lambda,\phi}}{2[\sigma]_{\lambda,\phi}} \, dp, \tag{4.5}$$

where p_s is the surface pressure. The term $[\sigma]_{\lambda,\phi}$ is the mean static stability given by

$$[\sigma]_{\lambda,\phi} = [T(\frac{g}{c_p} + \frac{\partial T}{\partial z})]_{\lambda,\phi} = [-\frac{g}{R}\frac{p}{\theta}\frac{\partial\theta}{\partial p}]_{\lambda,\phi} . \tag{4.6}$$

In the calculations presented here, the temperature T in equations 4.4 and 4.5 is determined from the thickness between constant pressure

surfaces. Strictly speaking, the thickness is proportional to the virtual temperature, not just the temperature. However, in all calculations made in this study, no distinction is made between the two. The integrations of equations 4.4 and 4.5 are approximated by a summing over layers in the vertical. The static stability $[\sigma]_{\lambda,\phi}$ is obtained using calculated mean temperatures at the upper and lower edges of the particular layer. For example, $[\sigma]_{\lambda,\phi}$ for the 300-500 mb layer is calculated using hemispheric averaged 300 mb and 500 mb temperatures. In the satellite-based calculations, these temperatures are obtained using regression equations derived in addition to those for thickness. The calculations are contained area-wise by latitudes 20° and 80° in each hemisphere. Vertically the integration is from the surface to as high as 10 mb.

The total kinetic energy (K) of the atmosphere is usually divided into two components, zonal kinetic energy (KZ) and eddy kinetic energy (KE), the formulas for which are given in equations 4.7 and 4.8 respectively.

$$KZ = \int_{o}^{p_s} \frac{[[u]_\lambda^2 + [v]_\lambda^2]_{\lambda,\phi}}{2g}\, dp \qquad 4.7$$

$$KE = \int_{o}^{p_s} \frac{[(u)_\lambda^2 + (v)_\lambda^2]_{\lambda,\phi}}{2g}\, dp \qquad 4.8$$

The resulting units are in terms of energy per unit area. The geostrophic approximation is used to calculate the winds above in the present study. The term $[v]_\lambda$ cannot be evaluated because it is identically zero under the geostrophic assumption. However, $[v]_\lambda$ is at

least one order of magnitude less than $[u]_\lambda$. Therefore, $[u]_\lambda^2 >> [v]_\lambda^2$ and KZ can be accurately calculated knowing just the mean zonal flow.

4.1.2 Mean meridional gradients

The zonal available potential energy (AZ) is a function of the variance of zonally-averaged temperature about $[T]_{\lambda,\phi}$, the area-weighted temperature usually calculated on a global or hemispheric basis. AZ is therefore very dependent on the mean meridional temperature gradient. Figure 4.1 shows the monthly mean, layer-mean temperature in the 300-500 mb layer in both hemispheres for January and July. For the Northern Hemisphere (parts a and b), three curves are shown: climatology (based on data from Oort and Rasmusson, 1971), and two curves based on NMC analyses and SIRS-based analyses respectively. For the Southern Hemisphere (parts c and d), there is a climatological curve (based on data from Taljaard, van Loon, Crutcher and Jenne, 1969) and the SIRS-based curve. All temperatures are computed from thicknesses. The climate curves are based on climatological 300 mb and 500 mb heights.

The diagrams of Figure 4.1 display the differences between the hemispheres already noted in Section 2.3. In both seasons shown, the mean temperature gradient between 20° and 80° latitude is larger in the Southern Hemisphere. The inter-hemispheric difference is largest in the summer. In winter (Figure 4.1a and c) the gradient from 20° to 45° latitude is about the same with the climatological curves actually showing a sharper drop-off with latitude in the Northern Hemisphere. Poleward of 45° however, there is a much larger mean gradient present in the Southern Hemisphere. In summer (Figure 4.1b and d), in addition to the obvious variation in mean gradient, there is a very distinct

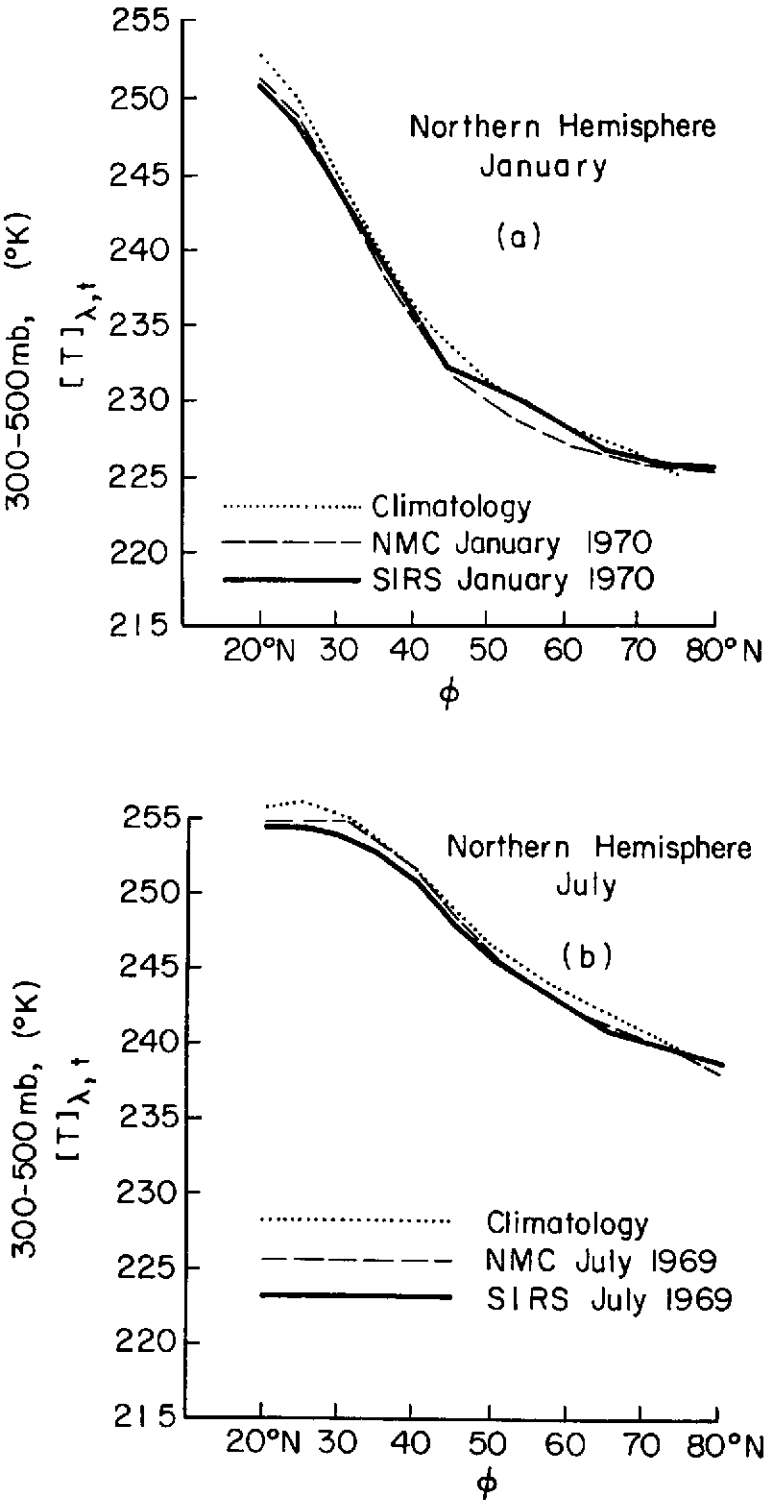

Fig. 4.1 Mean meridional temperature gradients in the upper troposphere (300-500 mb) in the Northern and Southern Hemispheres for January and July.

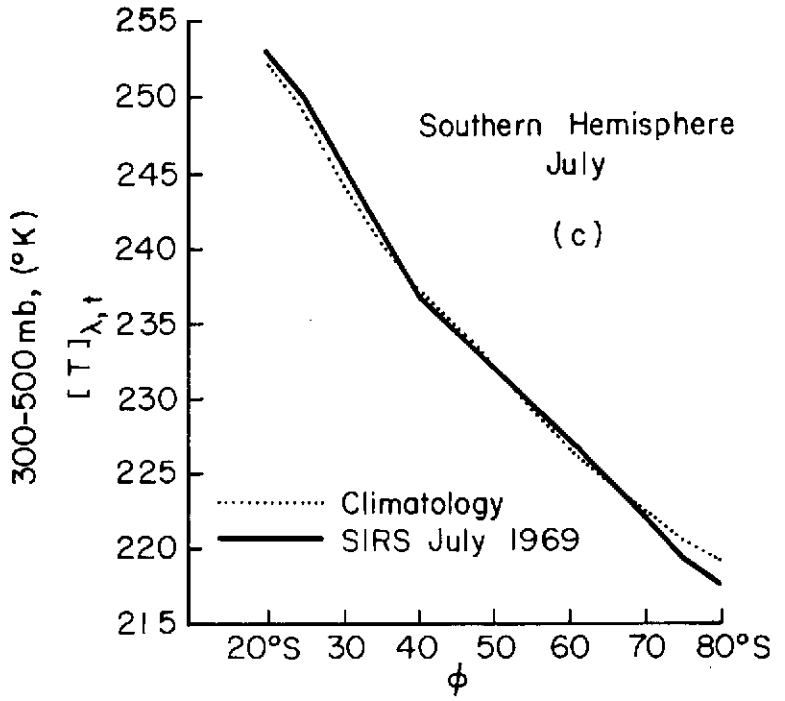

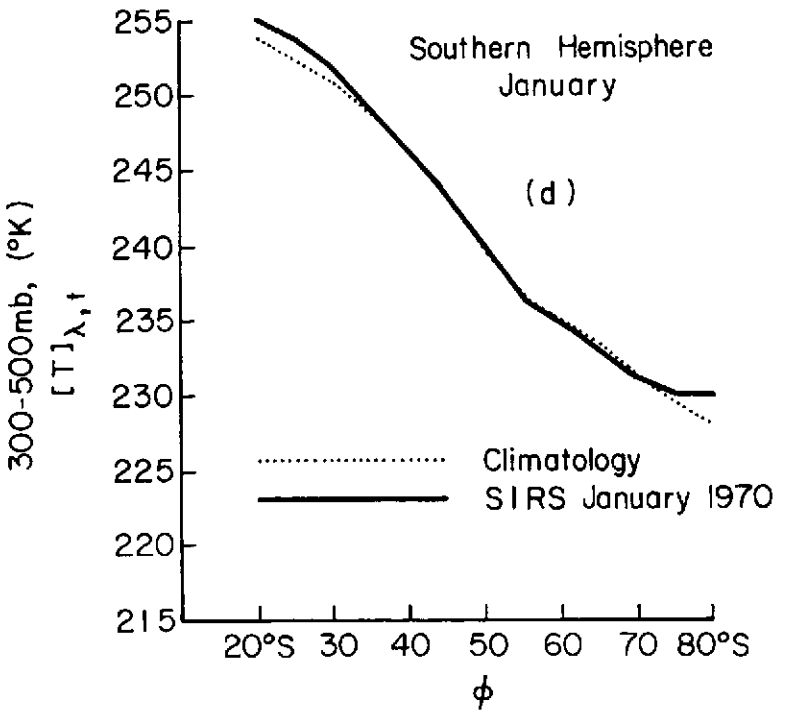

Fig. 4.1 Continued.

difference in low latitudes (between 20° and 30° latitude). In the Northern Hemisphere, there is little or no decrease in temperature between 20°N and 30°N; in the Southern Hemisphere there is a sharp decrease. This variation is probably related to the much stronger summer monsoon regime in the Northern Hemisphere.

The SIRS-based curves in Figure 4.1 in general agree well with the NMC-based curves (in the Northern Hemisphere) and climatology. One significant difference occurs in Figure 4.1a between 50°N and 60°N. The maximum deviation between the SIRS-based temperature and the NMC temperature is 1.5°K and is located at 55°N. At other latitudes, the NMC and SIRS curves closely agree. A similar difference does not show up in the Northern Hemisphere July (Figure 4.1b) diagram. In addition, neither of the Southern Hemisphere SIRS curves show an abrupt change of temperature gradient as is evident at 55°N in Figure 4.1a. The probable reason for the overestimation of the temperature at 55°N by the SIRS-based technique is related to the distribution of satellite data in January 1970 in the Northern Hemisphere. That month in the Northern Hemisphere has substantially (~ 25%) fewer original satellite data points than the other three data samples examined. In addition, the distribution of data with respect to longitude is uneven, with a relative lack of data in two regions of longitude, the primary one being over the western Pacific Ocean. This results in a greater underestimation of the amplitude of a temperature trough than the amplitude of the accompanying temperature ridge. Therefore, an overestimation of the zonally-averaged temperature occurs.

The zonal kinetic energy (KZ) is closely tied to zonally-averaged geopotential height distributions through the geostrophic wind relation.

Figure 4.2 shows various comparisons of the height distribution at 200 mb. The comparison in Figure 4.2a of NMC and SIRS curves reveals a substantial difference between the two curves in the latitude zone 50°-60°N, with the SIRS values of $[z]_\lambda$ being larger by up to 95 m at 55°N. This overestimation of the geopotential height is related to the overestimation of tropospheric temperature at the same latitudes as discussed in the last paragraph. None of the SIRS curves in Figures 4.2b-d indicate a similar effect.

In general, the latitude distributions of $[z]_\lambda$ in Figure 4.2 display the same inter-hemispheric differences and seasonal variations that were evident in the upper tropospheric temperature distributions seen in Figure 4.1. For the winter month (Figures 4.2a and c), the main difference occurs poleward of 45° latitude. At 75° latitude, the Southern Hemisphere climatological height is 350 meters lower than that in the Northern Hemisphere. In summer the difference at 75° latitude increases to almost 600 meters. For both months in the Southern Hemisphere, the SIRS-based curves of 200 mb $[z]_\lambda$ lie very close to the climatological curves. This agreement indicates that, at least in regard to mean zonal features, the months used in this study for the Southern Hemisphere are not atypical.

Figure 4.3 shows the mean geostrophic zonal flow at 200 mb as a function of latitude in the Southern Hemisphere. The SIRS and climate curves, calculated from the geopotential height distributions in Figure 4.2, agree fairly well. The jet stream moves poleward from July to January and the peak wind speed is larger in July. Although at 500 mb the peak wind is higher in January (summer) than in July (winter)

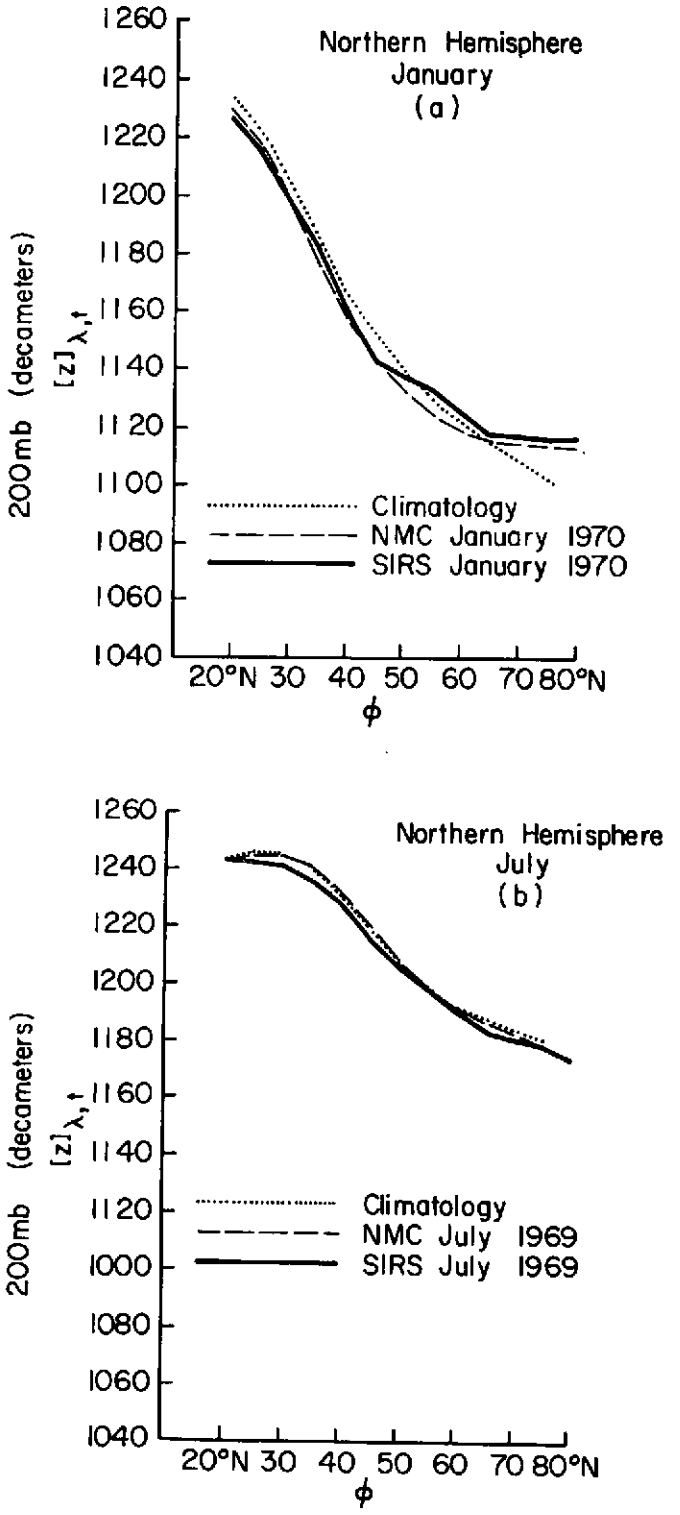

Fig. 4.2 Mean meridional geopotential height gradients at 200 mb in the Northern and Southern Hemispheres for January and July.

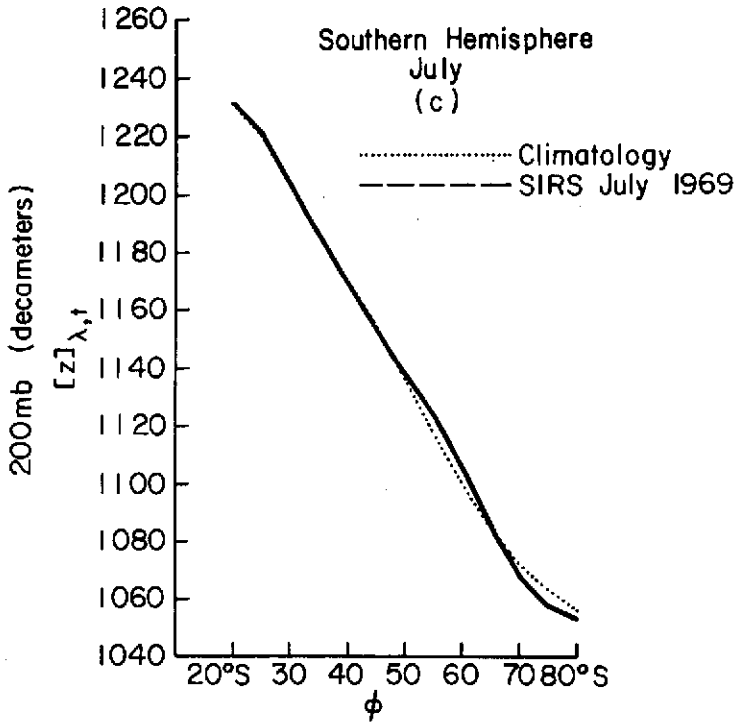

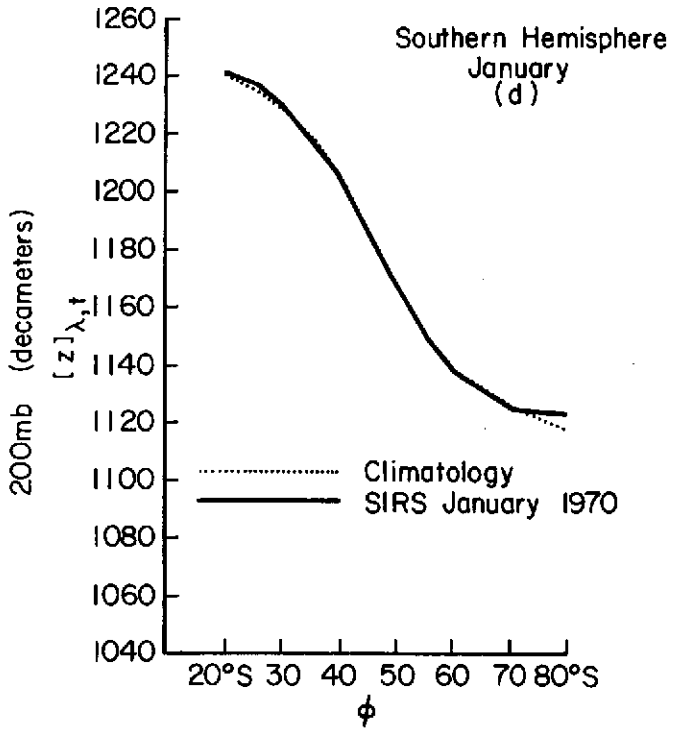

Fig. 4.2 Continued.

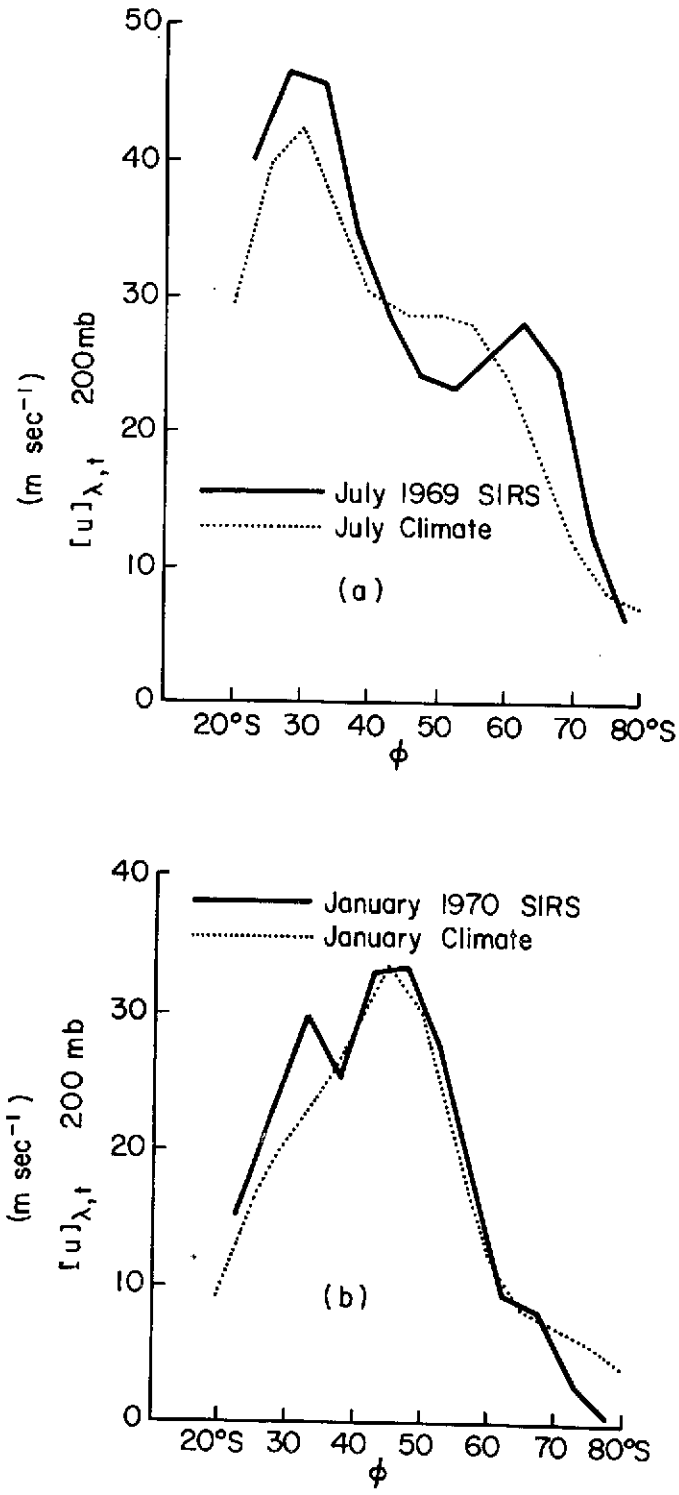

Fig. 4.3 Distribution with latitude of zonal mean geostrophic wind at 200 mb in the Southern Hemisphere for July and January.

(van Loon, Taljaard, Jenne and Crutcher, 1971), the opposite is true at higher levels such as 300 mb and 200 mb, as seen in Figure 4.3.

4.1.3 Results of available potential and kinetic energy comparisons

The results of the computation of AZ are given in the first two lines of Table 4.1. Calculations are made on a daily basis, then averaged over the month. The contributions to the total AZ from the 100-1000 mb layer, AZ(100-1000 mb), and the 300-500 mb layer, AZ(300-500 mb) are shown. Calculations for the Northern Hemisphere are presented using both the NMC fields and the SIRS-derived structure. The results of the AZ computations indicate the same hemispheric differences that were indicated in Figure 4.1. The summer disparity is very striking, with the Southern Hemisphere having twice the AZ(100-1000 mb) as does the Northern Hemisphere. The AZ(300-500 mb) results are presented for comparison with the meridional temperature gradients of Figure 4.1.

	WINTER			SUMMER		
	January 1970	January 1970	July 1969	July 1969	July 1969	January 1970
	NMC N.H.	SIRS N.H.	SIRS S.H.	NMC N.H.	SIRS N.H.	SIRS S.H.
AZ(100-1000 mb)	41.2	38.4	43.7	16.3	15.5	34.9
AZ(300-500 mb)	10.9	10.0	16.0	4.5	4.6	9.1
AE(100-1000 mb)	11.1	4.0	3.2	6.6	1.5	2.0
AE(300-500 mb)	2.0	0.7	1.0	1.8	0.6	0.6

Table 4.1. Zonal and eddy available potential energy in the Northern and Southern Hemispheres for a winter and a summer month. All values are in units of 10^5 joules m^{-2}.

Newell et al. (1970) present calculations of components of the atmosphere's energy cycle in both hemispheres. The calculations of the zonal components are based on climatological data. The results of the present study in terms of AZ(100-1000 mb) confirm, at least qualitatively, the hemispheric differences noted in the Newell study. The results are difficult to compare quantitatively because of differences in the computational technique. The calculations by Newell et al. cover the area 0°-90° latitude compared to the 20°-80° latitude span used in this study. In general, Newell's values for AZ(100-1000 mb) are larger.

Evaluation of the time-mean zonal available potential energy can be made quite accurately from monthly mean, or even climatological temperature fields. For example, calculations of AZ(100-1000 mb) for July 1969 and January 1970 made on a daily basis from the NMC data fields, then averaged over the month, are only one percent larger than the same quantity calculated from the monthly-mean data fields. Quite the opposite is true for eddy terms, such as the eddy available potential energy. Estimations of AE made from monthly-mean temperature fields represent only the contribution of standing eddies. To obtain accurate estimates of AE, the computations must be made on a daily basis.

The last two lines of Table 4.1 contain the results of the AE evaluations. Unlike the AZ calculations, those for AE indicate a large underestimation of the eddy term by the SIRS-based calculations. The reasons for this underestimation are discussed in Chapter 3 (Section 3.5). Because of the large underestimation, inter-hemispheric comparisons are difficult. Although the results for the 100-1000 mb layer are also presented, this author considers the computations for the 300-500 mb layer more reliable for comparisons. The 300-500 mb layer

is the highest that is still basically part of the troposphere. Therefore, it should still exhibit the characteristics of the troposphere and yet be relatively free (compared to lower layers) of cloud-contamination problems. Very tentative conclusions based on AE(300-500 mb) are that, at least in the upper troposphere, in winter the Southern Hemisphere has greater AE than the Northern Hemisphere, and in summer the two hemispheres have approximately equal quantities of AE.

In winter AE(100-1000 mb) is calculated to be larger in the Northern Hemisphere, while AE(300-500 mb) is larger in the Southern Hemisphere. This variation with height in the hemispheric difference is probably true. At low levels the greater land-sea contrast in the Northern Hemisphere produces greater east-west gradients of temperature than over the relatively homogeneous Southern Hemisphere. Based on computations in this study, in winter AE(700-1000 mb) in the Northern Hemisphere is more than twice as large as that for the Southern Hemisphere.

The computed KZ and KE for both hemispheres and months are given in Table 4.2. The values for KZ(75-1000 mb) and KE(75-1000 mb) are computed from height fields from 100 mb to 700 mb. KZ(150-250 mb) and KE(150-250 mb) are based on just the 200 mb heights. In both seasons the KZ values are larger in the Southern Hemisphere, especially in the summer. The KE values in Table 4.2 show little, if any, hemispheric difference, at least for the values for 200 mb (last line in table). At 200 mb, although the KZ is greater in the Southern Hemisphere in both seasons, the KE is approximately the same. This indicates, tentatively, that the ratio of KZ to KE in the Southern Hemisphere is greater than

that in the Northern Hemisphere. This is probably true for both seasons, but especially true in summer.

	WINTER			SUMMER		
	January 1970	January 1970	July 1969	July 1969	July 1969	January 1970
	NMC N.H.	SIRS N.H.	SIRS S.H.	NMC N.H.	SIRS N.H.	SIRS S.H.
KZ(75-1000 mb)	18.2	14.2	17.4	2.9	2.5	10.3
KZ(150-250 mb)	5.3	4.2	5.2	0.9	0.8	2.6
KE(75-1000 mb)	10.0	6.0	4.9	5.1	3.6	3.5
KE(150-250 mb)	1.8	0.9	0.9	1.2	0.6	0.7

Table 4.2. Zonal and eddy kinetic energy in the Northern and Southern Hemispheres for a winter and a summer month. All values are in units of 10^5 joules m^{-2}.

4.1.4 Standing and transient eddy contributions

The eddy available potential energy (AE) can be thought of as consisting of the energy in standing eddies plus the energy in transient eddies. The percentage of AE contained in standing or stationary eddies is given in Table 4.3. The energy of the standing eddies is computed from the mean temperature structure for the month. Unlike the values for AE in Table 4.1, the percentages in the SIRS and NMC columns in Table 4.3 for the Northern Hemisphere are very much alike. Thus, at least with regard to AE, it appears that the underestimation by the SIRS-based calculations is essentially the same with regard to both standing and transient waves.

The percentages for the Southern Hemisphere in Table 4.3 are substantially lower than those for the Northern Hemisphere. The

inter-hemispheric difference is largest in summer with the Southern Hemisphere percentages being about one half the Northern Hemisphere values. In winter in the Northern Hemisphere, there is a significant contrast between the percentages for AE(100-1000 mb) and those for AE(300-500 mb). The higher percentages for the 100-1000 mb layer occur because of the contribution from the lowest layer (700-1000 mb). The land-sea contrast produces a large percentage (60%) of standing to total AE in that layer. No such difference in the percentages between AE(100-1000 mb) and AE(300-500 mb) is obvious in the Southern Hemisphere in either season, or in the Northern Hemisphere in summer.

	WINTER			SUMMER		
	January 1970	January 1970	July 1969	July 1969	July 1969	January 1970
	NMC N.H.	SIRS N.H.	SIRS S.H.	NMC N.H.	SIRS N.H.	SIRS S.H.
AE(100-1000 mb)	52%	55%	34%	58%	55%	25%
AE(300-500 mb)	40%	42%	31%	54%	58%	23%

Table 4.3. Percentage of eddy available potential energy (AE) contained in standing eddies.

The percentages in Table 4.3 seem to indicate that standing eddies are more dominant relative to transient eddies in the Northern Hemisphere than in the Southern Hemisphere. This conclusion agrees with observations by other authors (see Section 2.5). However, since the present study is based on only one month of data for each season, the reliability of this result will be examined closer. The analysis will focus on the winter comparison of AE(300-500 mb), where the smallest inter-hemispheric

difference occurs. It will be shown that there is a high probability that the difference in statistics is due to an actual difference between the hemispheres rather than to sampling limitations.

To evaluate the probability outlined above, many years of calculations of the percentages in Table 4.3 would be welcome. Such statistics do not exist. However, Ellis (1974) has calculated various general circulation parameters including AE(200-850 mb) for nine years (1963-1971). These statistics are examined in order to estimate the variances of the percentages in Table 4.3. For the AE(200-850 mb) parameter for nine Januarys, the values of Ellis show a sample mean of 8.78×10^5 joules m^{-2} and a standard deviation (s) of 0.79×10^5 joules m^{-2}. The ratio of standard deviation s to the mean is .09. It is assumed that this ratio of .09 holds for AE(300-500 mb) as well; therefore, the standard deviation of this parameter is estimated to be 0.06×10^5 and 0.09×10^5 joules m^{-2} for the Northern and Southern Hemispheres, respectively. In this exercise values of AE(300-500 mb) to two decimal places are used (the values in Table 4.1 are rounded-off to one place).

The term of interest here, however, is the ratio of AE(300-500 mb) due to standing eddies to the total AE(300-500 mb). This ratio multiplied by 100 is identified by R. That is,

$$R = \frac{AE(\text{standing eddies})}{AE(\text{total})} \times 100, \qquad 4.9$$

or

$$R = \frac{AE(\text{standing eddies})}{AE(\text{standing eddies}) + AE(\text{transient eddies})} \times 100. \qquad 4.10$$

In the following paragraph let X represent the AE(standing eddies) and Y represent AE(total). Therefore,

$$R = \frac{X}{Y} \times 100. \qquad 4.11$$

Differentiating equation 4.11 gives

$$dR = \left(\frac{dX}{Y} - \frac{X}{Y^2}\, dY\right) \times 100. \qquad 4.12$$

To estimate the standard deviation of R, σ_R, the differentials in equation 4.12 are replaced by finite differences corresponding to the standard deviations of the variables.

$$\sigma_R \cong \left| \frac{\sigma_x}{Y} - \frac{X}{Y^2}\, \sigma_y \right| \times 100 \qquad 4.13$$

Here X and Y represent typical values or means. It is assumed that deviations in X and Y are always of the same sign. All the variables on the right side of equation 4.13 are known except σ_x. Equation 4.13 will be solved with $\sigma_x = 0$ and with

$$\frac{\sigma_x}{X} = 0.5\, \frac{\sigma_y}{Y}\,. \qquad 4.14$$

Using the values in Table 4.4, σ_R is calculated in both hemispheres to be 3 is $\sigma_x = 0$ and 2 if σ_x is given by equation 4.14. Henceforth, the value of $\sigma_R = 2.5$ is used.

It is assumed that the distribution being sampled from is Normal with an unknown mean μ and standard deviation $\sigma_R = 2.5$. The highest probability that the respective Northern and Southern Hemisphere values of R (42 and 31) came from the same distribution occurs if μ is halfway

between the two values 42 and 31; i.e., $\mu = 36.5$. The two values, 42 and 31 are then both more than 2σ away from $\mu = 36.5$. Accordingly, the probability that the two hemispheres are actually alike despite the differences in the percentages in Table 4.3 is low. Conversely, the probability is high that there is an actual disparity between the hemispheres.

	N. H.	S. H.
X	$.26 \times 10^5$	$.31 \times 10^5$
Y	$.67 \times 10^5$	1.01×10^5
σ_y	$.06 \times 10^5$	$.09 \times 10^5$
σ_x(by eq. 4.14)	$.01 \times 10^5$	$.01 \times 10^5$
$\sigma_R(\sigma_x = 0)$	3	3
$\sigma_R(\sigma_x$ by eq. 4.14)	2	2

Table 4.4. Values used in estimation of σ_R.

Table 4.5 shows the percentage of KE attributable to standing eddies. These values indicate the same hemispheric differences as are observed in the values for AE in Table 4.2. The percentages based on the 200 mb level (last line of Table 4.5) show that the Southern Hemisphere percentages at tropopause level are less than those in the Northern Hemisphere. The Northern Hemisphere values are about the same in the two months, while in the Southern Hemisphere the summer values are lower. The same sort of trends are noted in the percentages for AE given in Table 4.3. The reason for this difference in seasonal variation of standing eddy importance in the two hemispheres lies with the relative strength of the summer monsoon in each hemisphere. The

presence of a very strong summer monsoon circulation in the Northern Hemisphere maintains, or even increases, the percentages shown in Tables 4.3 and 4.5. In the Southern Hemisphere, the summer monsoon circulation is much weaker, and the area-averaged percentages in the tables decrease from winter to summer.

	WINTER			SUMMER		
	January 1970	January 1970	July 1969	July 1969	July 1969	January 1970
	NMC N.H.	SIRS N.H.	SIRS S.H.	NMC N.H.	SIRS N.H.	SIRS S.H.
KE(75-1000 mb)	31%	33%	23%	28%	34%	17%
KE(150-250 mb)	32%	31%	24%	30%	31%	18%

Table 4.5. Percentage of eddy kinetic energy contained in standing eddies.

4.2 Temperature variance and eddy kinetic energy as a function of latitude

4.2.1 Temperature variance

The contribution to eddy available potential energy from a specific layer, e.g. AE(300-500 mb), is a function of the variance of the temperature around latitude circles weighted by $\cos\phi$. This variance as a function of latitude in the 300-500 mb layer is shown in Figure 4.4. In the Northern Hemisphere, curves are shown for both the NMC-based and SIRS-based calculations. There is a definite lack of agreement between

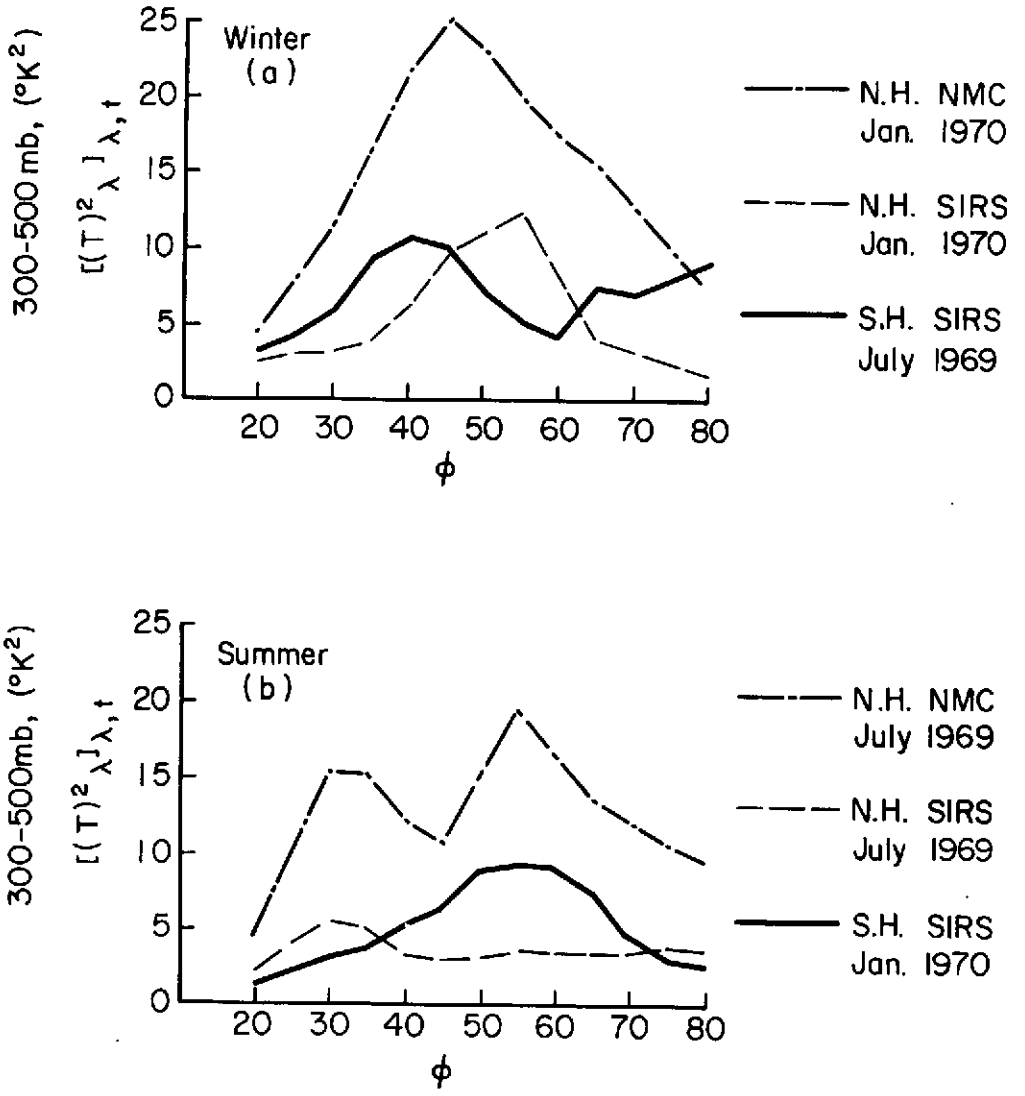

Fig. 4.4 Variance of temperature around latitude circles for the layer 300-500 mb in both hemispheres; (a) winter, (b) summer.

the NMC and SIRS curves beyond the typical underestimation. In winter in the Northern Hemisphere, the SIRS curve indicates the maximum variance at 55°N, while the NMC data indicates the peak at 45°N. The Southern Hemisphere temperature variance pattern in winter is quite different from that in the Northern Hemisphere. The variance appears to peak at a lower latitude in the Southern Hemisphere, but the reliability of this conclusion is questionable in view of the difference between the NMC and SIRS curves for the Northern Hemisphere. However, the Southern Hemisphere curve shows a secondary maximum in high latitudes not evident at all on the Northern Hemisphere curves. This high-latitude maximum is no doubt related to presence of the Antarctic continent. The relative contribution of standing and transient eddies in this maximum will be discussed in a following paragraph.

The curves for summer (Figure 4.4b) show that the SIRS distribution does not adequately describe the features shown in the NMC curve for the Northern Hemisphere. The NMC curve shows two maxima, one at about 30°N and another at 55°N while the SIRS curve indicates the low latitude maximum, but not the peak at 55°N. The Southern Hemisphere curve shows only one maximum, at 55°S. The low latitude maximum in the Northern Hemisphere is related to the summer monsoon over Asia, and the maximum at 55°N is associated with migratory and stationary waves in the main belt of strong westerlies which has moved poleward from winter to summer. In the Southern Hemisphere in summer there is no temperature variance peak in low latitudes according to the SIRS-derived data.

The 300-500 mb layer has been singled out in this section because it is the highest layer of the eight thickness layers obtained from the

satellite data that still reflects tropospheric temperature characteristics. The agreement between NMC and SIRS-based calculations increases with height. For example, Figure 4.5 shows the mean temperature variance in the 200-300 mb layer. Agreement between NMC and SIRS curves in the Northern Hemisphere is substantially better than in the 300-500 mb layer just below. However, the variances in this upper layer, especially in high latitudes, are beginning to reflect occurrences in the stratosphere instead of in the troposphere.

The ratio of standing eddy temperature variance to total variance as a function of latitude indicates the latitudinal variability of the relative importance of standing and transient eddies. The distribution of this parameter for the 300-500 mb layer is given in Figure 4.6. Although there is rather poor agreement between the NMC and SIRS temperature variance curves in Figure 4.4, there is excellent agreement with regard to the ratio in Figure 4.6. The percentages in the second row of Table 4.3 in Section 4.1.4 are essentially area or cosine-weighted averages of the ratio in Figure 4.6. In both seasons there are significant differences between the hemispheres. In winter both hemispheres show a relatively high value at 20° latitude, where the total variance is small, and a relative minimum at 25° or 30° latitude. Poleward of that latitude, the patterns are quite different. North of 30°N, there is a single maximum in mid-latitudes (50°-55°N), while the Southern Hemisphere shows a double maximum with a peak at 40°S and a general area of high values at, and south of, 65°S. The areas of maximum relative contribution by standing eddies coincide generally with the maxima of

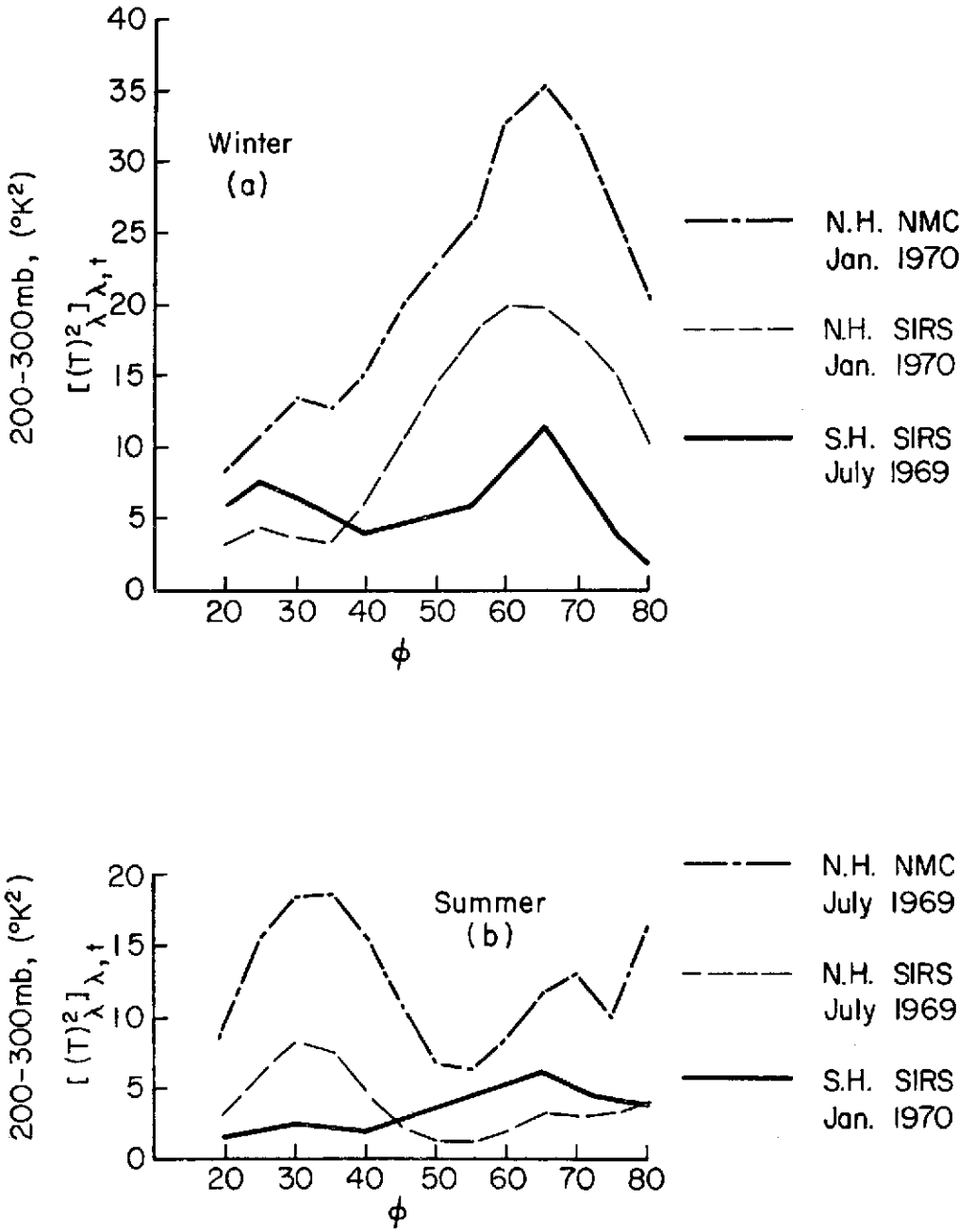

Fig. 4.5 Variance of temperature around latitude circles for the layer 200-300 mb in both hemispheres; (a) winter, (b) summer.

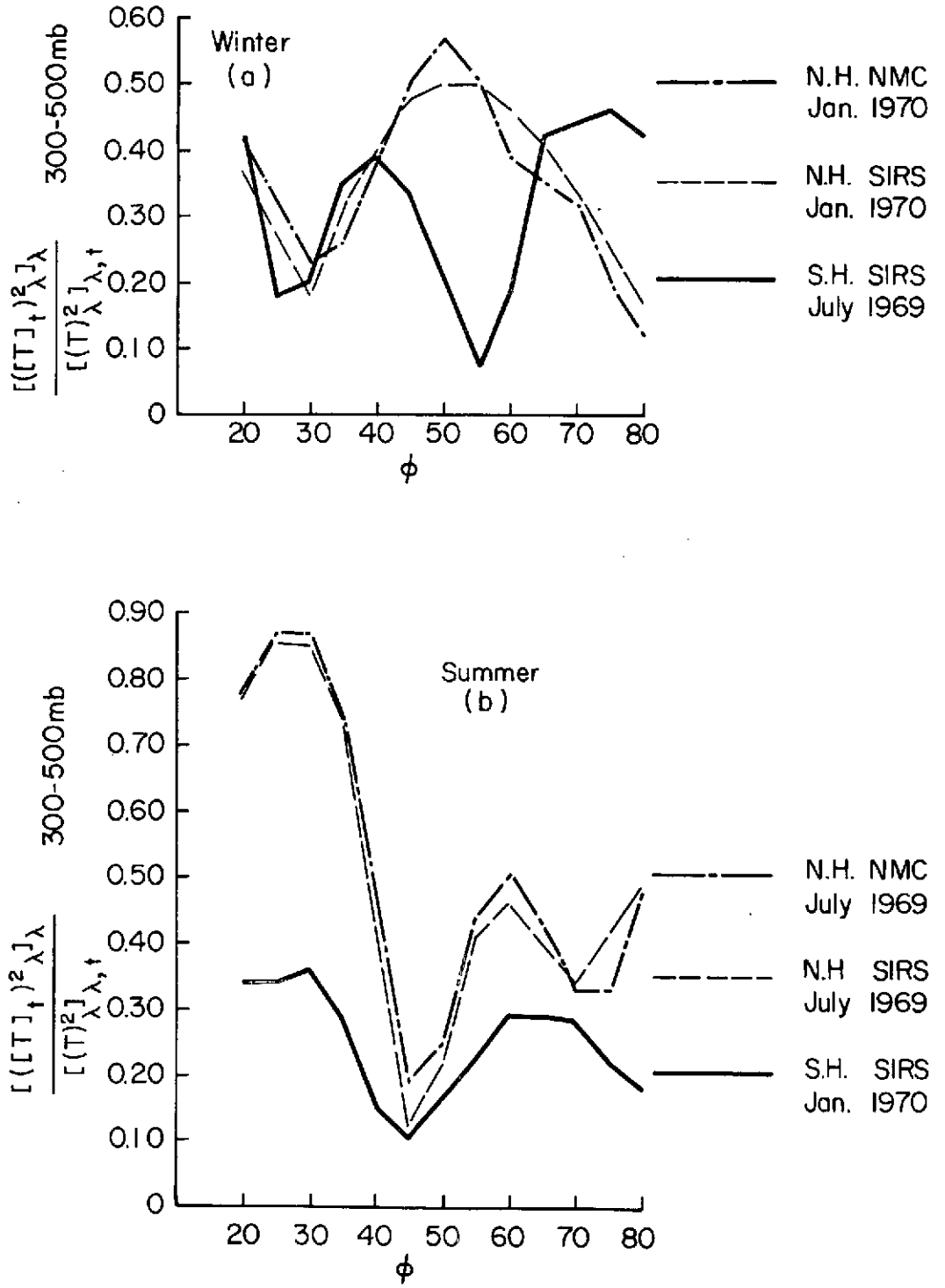

Fig. 4.6 Ratio of temperature variance due to standing eddies to total variance for the layer 300-500 mb; (a) winter, (b) summer.

total variance (Figure 4.4a). That is, large temperature variance is associated with a relatively large percentage contribution by standing eddies.

In summer (Figure 4.6b) the latitudinal distributions in each hemisphere are similar with regard to the location of relative and absolute maxima and minima, but not with regard to magnitudes. At all latitudes the Northern Hemisphere values exceed those of the Southern Hemisphere. There has also been a large change in the patterns from the winter to the summer month. Both hemispheres display an absolute maximum in the region of 25-30° with the Northern Hemisphere values exceeding those of the Southern Hemisphere. This maximum is related, at least in the Northern Hemisphere, to the summer monsoon. In the Southern Hemisphere, the total variance is small (Figure 4.4b) and the percentage contribution of standing eddies is also relatively small. These two facts merely indicate the relative weakness of the Southern Hemisphere summer monsoonal regime. Both hemispheres have a minimum at 45° and relatively high values poleward of about 55°. The Northern Hemisphere values are significantly higher than those in the Southern Hemisphere. These maxima around 60° in Figure 4.6b are associated with the maxima of total variance at 55° in Figure 4.4.

4.2.2 Eddy kinetic energy at 200 mb

The distributions of $[u]_{\lambda,t}$ and, therefore, the zonal kinetic energy are well known in the Southern Hemisphere because they can be calculated accurately from climatological data. However, the distribution in space of eddy kinetic energy, especially at upper tropospheric

and tropopause levels, is not well known. Kao and Jenne and Sagendorf (1970) and van Loon (1972c) use the IGY 500 mb height fields to examine the latitudinal distributions of eddy kinetic energy in the Southern Hemisphere. Both studies show mid-latitude peaks (~ 40-50°S) in summer and winter, similar to what is found in the Northern Hemisphere (see Oort and Rasmusson, 1971) at 500 mb. The distribution of eddy kinetic energy at 200 mb is, however, quite different from that at 500 mb.

Eddy kinetic energy at 200 mb as a function of latitude is shown for winter and summer in Figures 4.7 and 4.8, respectively. The solid curves represent the total eddy kinetic energy, and the dashed curves represent the standing eddy contribution. The difference between the two curves is the transient eddy kinetic energy. Parts a and b of each diagram show the Northern Hemisphere values calculated from NMC data and from the SIRS-based structure, respectively. The NMC curves for winter (Figure 4.7a) indicate one distinctive maximum at 32.5°N for both the total and standing eddy kinetic energy. This agrees well with Oort and Rasmusson (1971), whose tables show a maximum at 35°N. The SIRS curves (Figure 4.7b) also show the maxima at 32.5°N, but, in addition, show secondary maxima at 57.5°N. The appearance of this second peak is totally related to the standing eddy maximum. This erroneous peak in the standing eddy contribution at 57.5°N is probably related to the problems in the distribution of satellite data which produced the errors in the $[z]_{\lambda,t}$ curve at 200 mb (Figure 4.2a) and in the $[T]_{\lambda,t}$ curve for the 300-500 mb layer (Figure 4.1a) in January in the Northern Hemisphere at the same latitude. This data distribution problem does not occur in the other month or the other hemisphere.

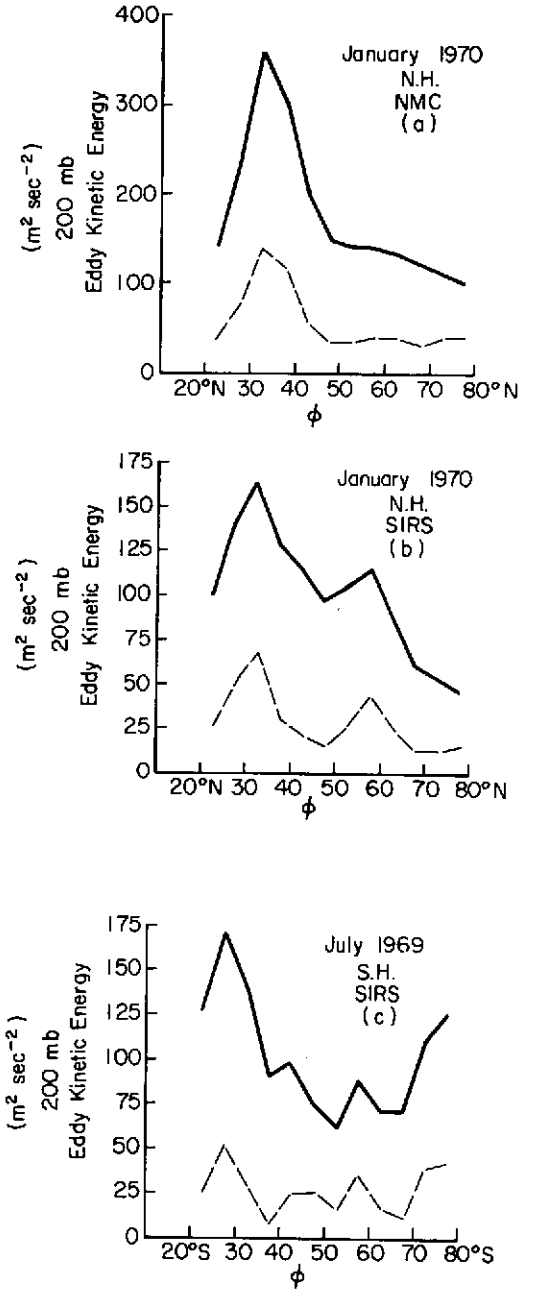

Fig. 4.7 Distribution with latitude of eddy kinetic energy at 200 mb in both hemispheres during winter. Total eddy kinetic energy (solid lines), standing eddy kinetic energy (dashed lines).

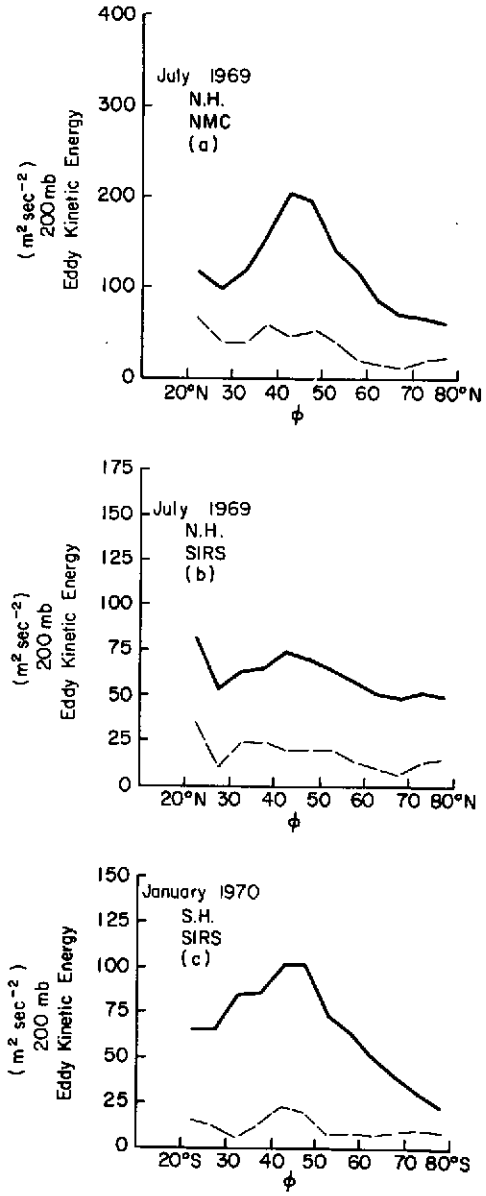

Fig. 4.8 Distribution with latitude of eddy kinetic energy at 200 mb in both hemispheres during summer. Total eddy kinetic energy (solid lines), standing eddy kinetic energy (dashed lines).

The Southern Hemisphere winter (July 1969) curves are shown in Figure 4.7c. The peaks in the total eddy kinetic energy and in the standing eddy contribution occur at 27.5°S, at a slightly lower latitude than those in the Northern Hemisphere. This observed difference may very well just be a function of the small sample. The magnitudes of the peaks in the two hemispheres in winter, as calculated from the satellite-based structure, are nearly the same. The Southern Hemisphere curve also shows a secondary maximum in high latitudes, poleward of 70°S (Figure 4.7c). No similar peak exists in the Northern Hemisphere. This peak in the eddy kinetic energy is composed of maxima in both the standing and transient eddy components and also shows up in calculations for lower layers, including 500 mb. However, the calculations of Kao, Jenne and Sagendorf (1970) do not show this peak in the IGY data at 500 mb, although their computations do not extend farther poleward than 70°S. The magnitude of the high latitude peak in Figure 4.7c may also be larger than what it normally is. The evidence for this are the large values of $[u]_{\lambda,t}$ from 60° to 75°S (Figure 4.3a), relative to the climatological values at that latitude. If the eddy kinetic energy is associated with this jet stream, then the values in Figure 4.7c may be an overestimate of normal conditions. Therefore, the existence under normal conditions of an eddy kinetic energy maximum at high latitudes is undecided.

At the latitude of peak eddy kinetic energy in both hemispheres in winter, the standing eddies contribute significantly. In the Northern Hemisphere at 32.5°N, the standing eddies percentages are 39% and 41% for the NMC and SIRS-based calculations, respectively. At 27.5°S the

percentage as determined from the SIRS-based calculations is 30%. These values are larger than the percentages averaged over the hemisphere, presented in Table 4.5. This means that there is a positive correlation between the eddy kinetic energy and the percentage contribution of standing eddies. At 500 mb, Kao, Jenne and Sagendorf (1970) show the peak eddy kinetic energy to be at about 50°S in winter. The percentage contribution of standing eddies there is 12% according to their calculations. This percentage is much lower than the 30% at 200 mb calculated here. This disparity may be related to the difference in level used, a difference in the latitude location of the peak, or to an underestimation of the standing eddy contribution by Kao et al. However, at 200 mb and 50°S the percentage is still about 30%, using the statistics of the current study. Another reason for the variation could be that, as far as can be determined, Kao's standing eddy contribution is computed from fields averaged over three months rather than the one month used in this study. This reduces the percentage contribution of the standing eddies. However, it seems unlikely that this difference in averaging time could account for all the difference between 30% and 12%. It therefore seems possible that studies based on the IGY data fields have underestimated the role of standing eddies.

The distribution of 200 mb eddy kinetic energy in summer is shown in Figure 4.8. The peak has shifted poleward to about 45° in both hemispheres with the Southern Hemisphere magnitude being substantially larger than the Northern Hemisphere one, as calculated from SIRS-based structure in both hemispheres (Figures 4.8b and c).

4.3 Eddy heat transport

4.3.1 Distribution of eddy heat transport

The computations of eddy heat flux in the 300-500 mb layer reveal significant differences between the hemispheres. The fluxes are calculated using the 300-500 mb thickness information and the 300 mb and 500 mb height fields. Geostrophic wind speeds are used throughout. The 300-500 mb layer represents the upper troposphere. Although the relative contribution of this layer to the vertically integrated eddy heat flux is small, the layer should possess characteristics of the tropospheric eddy flux fields.

Figure 4.9 shows the results of the eddy heat flux computations for the winter month in each hemisphere. The solid lines represent the total eddy flux, $[(v)_\lambda (T)_\lambda]_{\lambda,t}$, and the dashed lines represent just the standing eddy flux, $[([v]_t)_\lambda ([T]_t)_\lambda]_\lambda$. Parts b and c of the figure have different ordinate scales than part a. Figures 4.9a and 4.9b are the result of the Northern Hemisphere computations based on NMC and SIRS-derived data, respectively. Both diagrams show a maximum in mid-latitudes, although not at exactly the same latitude. The underestimation of the total eddy flux is about 50% at the latitudes of the maxima. The curves for the standing eddies also show a miximum in mid-latitudes.

In addition, it is evident from Figures 4.9a and b that the transient eddy flux is underestimated more than the standing eddy flux. This is quite different from the situation in the second section of this chapter where the relative importance of standing and transient eddies in the variance of temperature around latitude circles was well portrayed by the SIRS-based calculations (see Figure 4.6). The reason for this difference lies in the size of the eddies involved. The variance

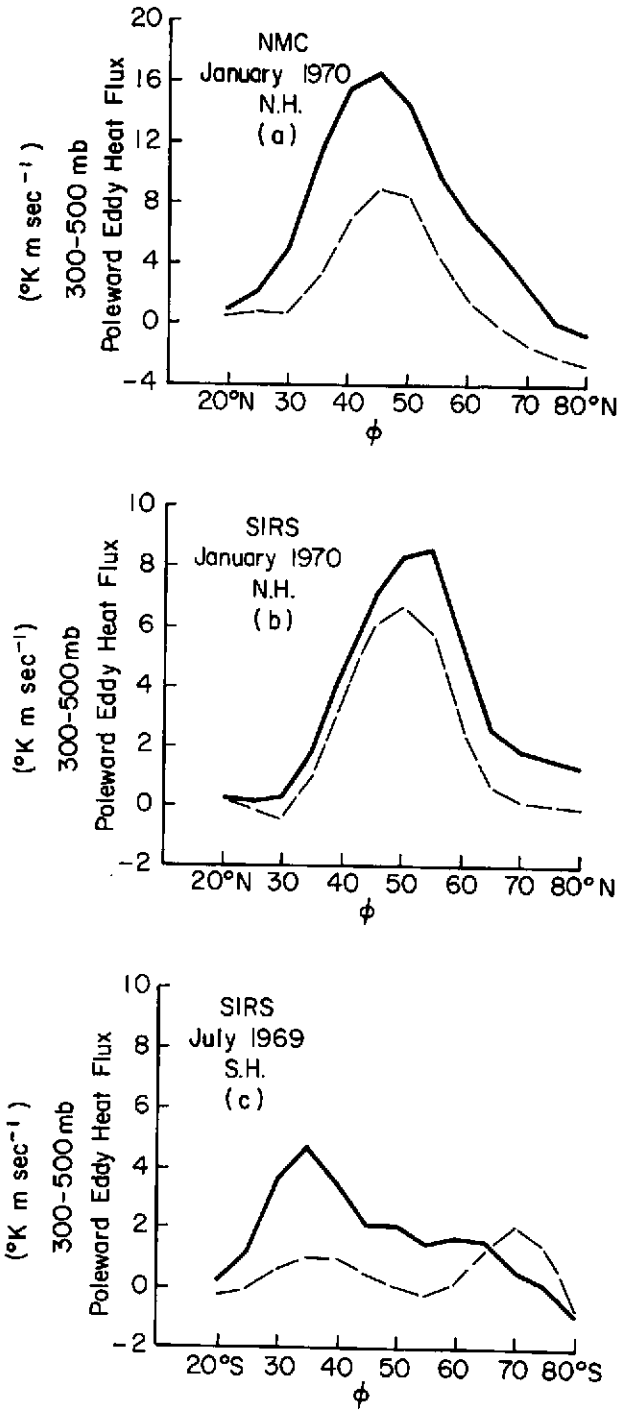

Fig. 4.9 Wintertime, total poleward eddy flux of heat, $\pm [(v)_\lambda (T)_\lambda]_{\lambda,t}$ (solid lines), and poleward eddy flux of heat due to standing eddies, $\pm [([v]_t)_\lambda ([T]_t)_\lambda]_\lambda$ (dashed lines) for the layer 300-500 mb in both hemispheres.

of temperature around latitude circles in the upper troposphere is dominated by large eddies of hemispheric wave numbers 1 through 3 (Saltzman and Fleisher, 1960). The eddy flux of heat in mid-latitudes is dependent for the most part on large, stationary waves (wave number ~ 3) and shorter (wave number ~ 6), transient waves (Kao and Sagendorf, 1970). The shorter, transient waves are not picked up as well by the SIRS-based structure as are the larger, stationary or near-stationary waves. Therefore, the flux due to stationary waves is better estimated by the SIRS-based calculations than that due to transient waves.

There are striking variations between the curves in Figure 4.9 for the Northern and Southern Hemispheres. First, the maximum eddy flux in the Southern Hemisphere (Figure 4.9c) occurs at 35°S, farther equatorward than either calculation in the Northern Hemisphere (Figures 4.9a and b). However, because the SIRS-based calculation in the Northern Hemisphere (Figure 4.9b) does not correctly identify the latitude of maximum flux, any conclusion as to the relative positions of the latitude of maximum flux in the two hemispheres would be premature. This is especially true since the calculation is based on only one month of data. Other calculations which show the seasonal variation of eddy heat flux (Newell, et al., 1970; Kao, Jenne and Sagendorf, 1971) in the Southern Hemisphere indicate a peak at about 50°S in winter.

The standing eddies show two peaks of poleward heat flux in the Southern Hemisphere, one at 35°-40°S and another at 70°S. In mid-latitudes the flux curve has a relative minimum. This distribution generally parallels that of the percentage of temperature variance due to standing eddies given in Figure 4.6a. Poleward of 65°S the heat flux is dominated by the standing eddies. In mid-latitudes the percentage

of the total eddy flux attributable to standing eddies is much less in the Southern Hemisphere than in the Northern Hemisphere. At the latitude of peak eddy flux in each diagram, the percentage due to standing eddies is shown in Table 4.6.

	N.H.		S.H.
	January 1970 NMC	January 1970 SIRS	July 1969 SIRS
Standing Eddy Percentage	54%	67%	24%

Table 4.6. Percentage of eddy flux of heat in the 300-500 mb layer attributable to standing eddies at latitude of peak eddy flux.

The Southern Hemisphere percentage in Table 4.6 is probably somewhat overestimated judging by the Northern Hemisphere NMC and SIRS percentages. Kao, Jenne and Sagendorf (1971) present heat flux statistics for winter, based on analyzed 500 mb height and 500-1000 mb thickness fields from the IGY, which give a percentage of 12% at 30°S. This value is much less than the one calculated in this study. The difference cannot be totally attributed to the overestimation by the SIRS calculation. The resolution of these differences pertaining to the relative importance of standing eddies in the 30°-40°S latitude band must await further study. Kao, Jenne and Sagendorf (1971) do indicate the standing eddy peak at about 30°S with a sharp decrease to 50°S, but do not indicate the high latitude maximum that is evident in Figure 4.9c.

In summer (Figure 4.10) the standing eddies in each hemisphere are less important in mid-latitudes than in winter. The total eddy flux is less in summer in both hemispheres, but the seasonal change is much

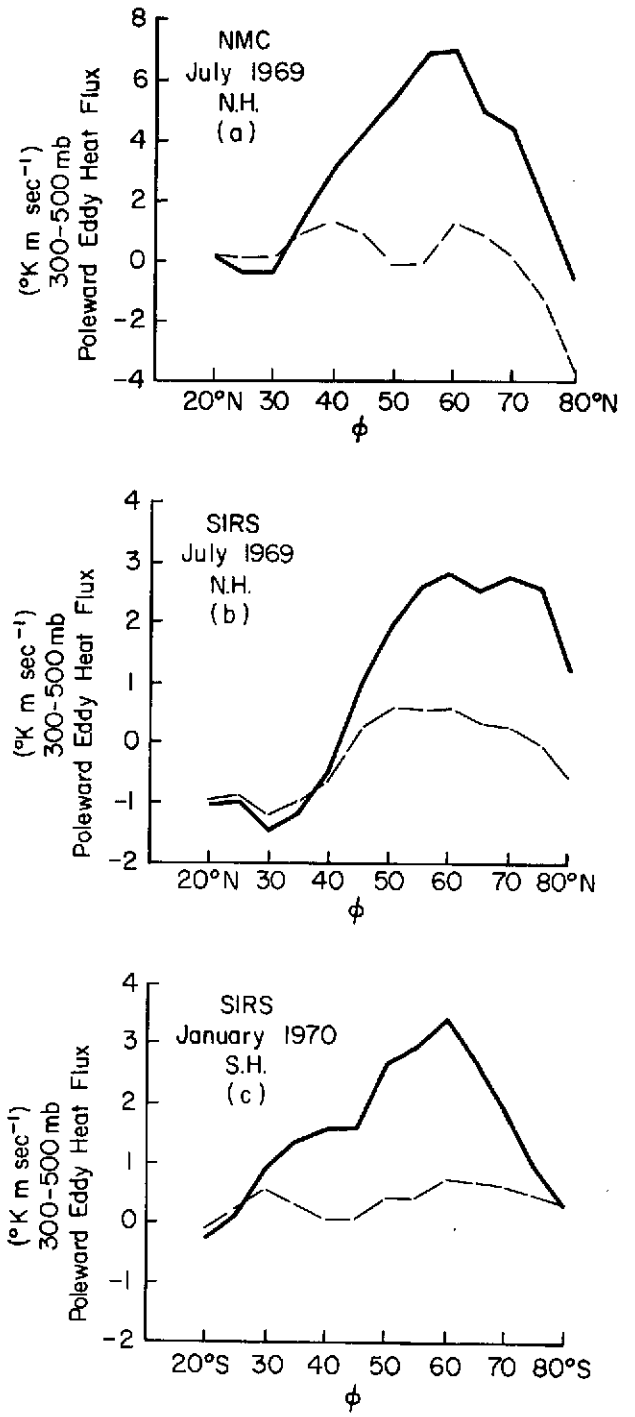

Fig. 4.10 Summertime, total poleward eddy flux of heat, $\pm [(v)_\lambda (T)_\lambda]_{\lambda,t}$ (solid lines), and poleward eddy flux of heat due to standing eddies, $\pm [([v]_t)_\lambda ([T])_\lambda]_\lambda$ (dashed lines) for the layer 300-500 mb in both hemispheres.

larger in the Northern Hemisphere. The latitude of peak eddy flux has moved poleward to about 60° in each hemisphere. The Northern Hemisphere SIRS curve (Figure 4.10b) does not show the sharp drop-off with increasing latitude poleward of 60°N that is evident in the NMC curve (Figure 4.10a). This discrepancy is tied in part to the failure of the SIRS-based calculations to correctly identify the large negative fluxes of the standing eddies north of 70°N.

4.3.2 Mid-latitude magnitude

Robinson (1970) has concluded, on the basis of calculations using primarily IGY station data, that the vertically integrated total eddy flux of heat in mid-latitudes is much greater (by a factor of two) on an annual average in the Northern Hemisphere than in the Southern Hemisphere. At 50° latitude at 400 mb, a similar-sized hemispheric difference is obtained from the tables and charts of Robinson. Newton (1972) concludes that Robinson's Southern Hemisphere mid-latitude fluxes are much too low. Instead he states that the magnitude of the eddy flux of heat at latitude 50° (the approximate latitude of maximum eddy flux) is about the same in both hemispheres. This conclusion is reached as a result of energy budget calculations. The eddy heat flux calculations in the present study offer an opportunity to compare the two hemispheres and possibly determine the relative strengths of the Northern and Southern Hemisphere's eddy fluxes.

The inter-hemispheric comparison is made at latitude 50°, the approximate latitude of the annual maximum. Because of the contrast between the hemispheres in relative strength of standing eddies and the difference in the ability of SIRS-derived structure to determine

correctly the standing and transient eddies, the values in parts b and c of Figures 4.9 and 4.10 cannot be immediately used to establish the comparison. Therefore, the following procedure is adopted. The total eddy flux is divided in each hemisphere and each month into the standing and transient eddy portions. In the Northern Hemisphere the NMC and SIRS-based values are compared. The ratio of NMC to SIRS-based values gives a "correction factor" which when multiplied by the Northern Hemisphere SIRS values results, of course, in the NMC or assumed correct fluxes. The major assumption in this exercise is that the Northern Hemisphere "correction factors" apply in the Southern Hemisphere. Separate factors are determined for standing and transient eddies. For January 1970 in the Northern Hemisphere, the transient and standing eddy "correction factors" are 3.6 and 1.2, respectively. In July the transient eddy factor is 4.1. There is no standing eddy correction term for July because the standing eddy flux at 50°N is negligible. The two transient eddy "correction factors" are averaged, and the mean value of 3.8 is used in the Southern Hemisphere for both months. Applying the derived "correction factors" to the Southern Hemisphere fluxes, adding the standing flux to the transient flux, and averaging over January and July results in the value in the third column of Table 4.7. The adjusted, or corrected, value for the Southern Hemisphere is smaller, but only 14% smaller than the NMC, Northern Hemisphere value. The Southern Hemisphere corrected SIRS value is also approximately twice as large as the annual average value at 400 mb from Robinson (1970). The first entry in the table is from Oort and Rasmusson (1971) at 400 mb. It is smaller than the other two values. This may be because the NMC-based calculations overestimate the flux, or that 1969-1970 was a

period of above average flux. Table 4.7 does indicate, however, that the Southern Hemisphere flux is closer to being equal to the Northern Hemisphere value than to being one half of the Northern Hemisphere value. This conclusion agrees with Newton (1972) and disagrees with Robinson (1970).

	N.H. Climate	N.H. NMC	S.H. SIRS	S.H. ROBINSON
Upper Troposphere Total eddy heat flux	7.0	9.9	8.5	4.1

Table 4.7. Upper troposphere "corrected" total eddy heat flux $[(v)_\lambda (T)_\lambda]_{\lambda,t}$ at 50° latitude averaged over January and July. N.H. climate value from Oort and Rasmusson (1971) at 400 mb. Robinson (1970) S. H. value an annual mean at 400 mb. Units: $^\circ K\ m\ sec^{-1}$.

4.3.3 Longitudinal distributions

The last few paragraphs have dealt mainly with the latitudinal distribution of eddy heat flux. The longitudinal variation at a particular latitude is also important. Haines and Winston (1963) discuss the longitudinal distribution of eddy heat flux in the Northern Hemisphere for the layer 500-850 mb. At 45°N during the winter season (October-March), there are three bands of longitude which contribute greatly to the longitudinally-averaged poleward flux of sensible heat. The three zones, obvious in Figure 4.11, are associated with the location of mean ridge and trough positions (Haines and Winston, 1963). The narrow band located at about 120°E is on the west side of the mean trough off the Asian coast. The peak in the eastern Pacific Ocean is situated on the east side of this trough. The general maximum between 20°W and 100°W is associated with the trough located at the east coast of North

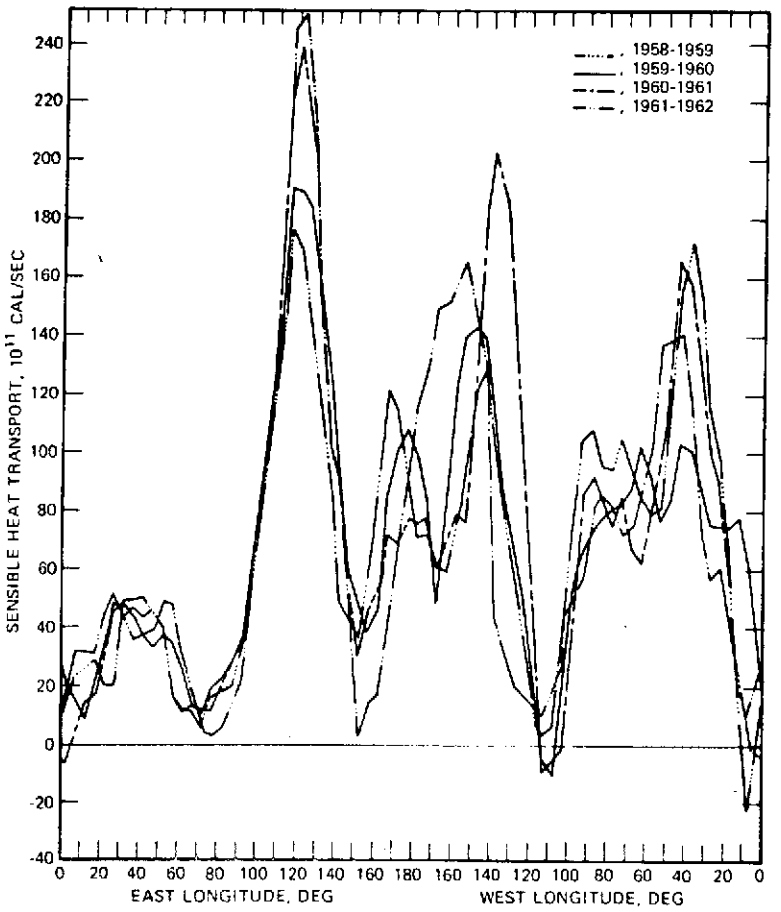

Fig. 4.11 Averages for four consecutive cold seasons (October-March) of contributions in each 5° longitude zone to poleward eddy heat transport across 45°N (from Haines and Winston, 1963).

America, with the peak values at about 40-50°W occurring on the east side of the trough. The relation of the peak locations in Figure 4.11 to the standing eddy pattern in the troposphere does not mean, however, that the fluxes in the figure are totally due to the standing eddies. At 45°N in winter, the eddy heat flux is divided about equally between transient and standing eddies. However, the transient eddies have preferred longitudes of greatest amplitude.

Because the Southern Hemisphere standing eddies are relatively less important, it would be interesting to determine if there are still preferred longitudes of eddy heat flux in the Southern Hemisphere. For this reason calculations of the eddy flux of heat in the 300-500 mb layer for every 10° of longitude were carried out at 45°N and 45°S, at 45°N using both NMC and SIRS-based structure. Figures 4.12a and b show the results for the Northern Hemisphere. In January the NMC curve clearly shows the three areas of poleward heat flux also observed by Haines and Winston (1963) for the lower troposphere. The SIRS curve for January (Figure 4.12a) indicates the strong peak at about 120°E, but only slightly indicates the other two maxima. In summer (Figure 4.12b) the patterns are much weaker (the ordinate scales are different in Figures 4.12a and b) and less cohesive. However, the SIRS curves do indicate the longitudes of large poleward fluxes.

The Northern Hemisphere NMC total flux curve for January 1970 is reproduced in Figure 4.13 as a solid line. Also shown is the flux associated with the standing eddies (calculated from January 1970 mean temperature and height fields). Averaged around the latitude circle, the standing eddies contribute about 50% to the total eddy flux at 45°N (see Figure 4.6a). They obviously play an important role in the

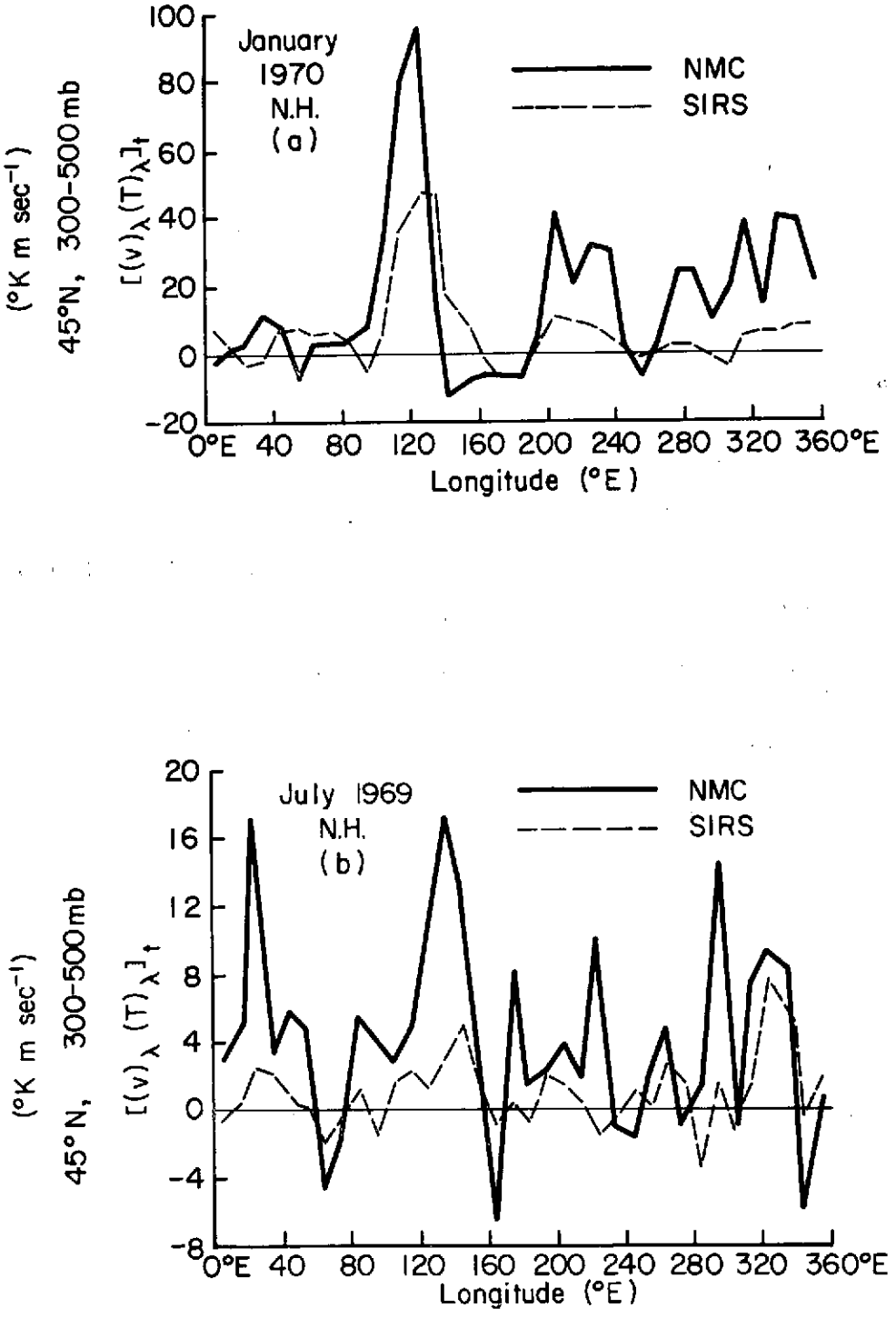

Fig. 4.12 Longitudianl distribution of total eddy heat flux for the layer 300-500 mb, at 45°N in January 1970 and July 1969.

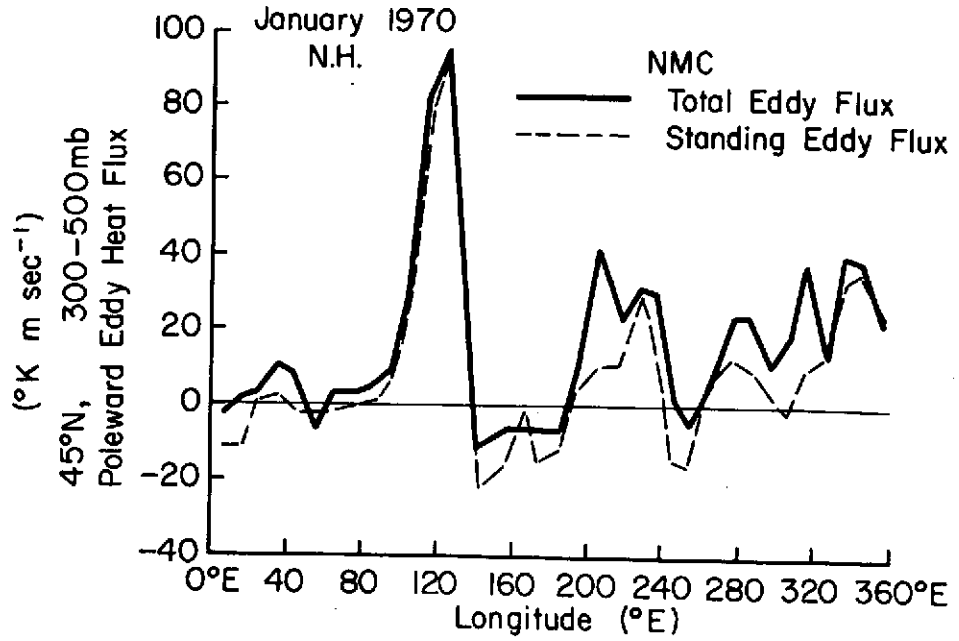

Fig. 4.13 Longitudinal distribution of total eddy heat flux and standing eddy heat flux for the layer 300-500 mb at 45°N in January 1970.

longitudinal variations. The peak eddy flux at 125°E is due almost entirely to standing eddies. The other two regions of large poleward flux show a very pronounced east-to-west variation in the importance of standing eddies. Both regions (one from 200°-240°E, the other between 270° and 360°E) show the standing eddies dominating in the eastern part of the region, and transient waves being relatively more important in the western portion of each region. The contribution by transient eddies is given by the difference between the solid and dashed curves. The same east-to-west variation is present for the region of large flux centered at 120°E, but is not as obvious from the diagram. This east-to-west variation of standing and transient eddy importance reflects the presence of travelling systems amplifying and slowing as they move eastward until they reach maximum amplitude and become stationary.

The longitudinal variations at 45°S calculated from the SIRS-based structure are shown in Figure 4.14 for July 1969 and January 1970. The 45°S latitude circle is land-free, except for where it crosses the Southern tip of South America and New Zealand. In the winter month, July 1969, 22% of the total eddy flux is calculated to have been attributable to stationary eddies. This percentage is probably a slight overestimate, because trnasient eddies are underestimated more than standing eddies (see Section 4.3.1). The calculated percentage for January 1970 is 6%. Both months show longitudinal variations, the winter month showing more organization. In the winter month there are three peaks in the poleward eddy flux: one at 35°E, east of the axis of the African continent; a second at 175°E, just east of New Zealand; and the third from 285°E to 325°E, across and to the east of South America. Peaks in the stationary eddy flux (dashed line in Figure 4.14a) occur

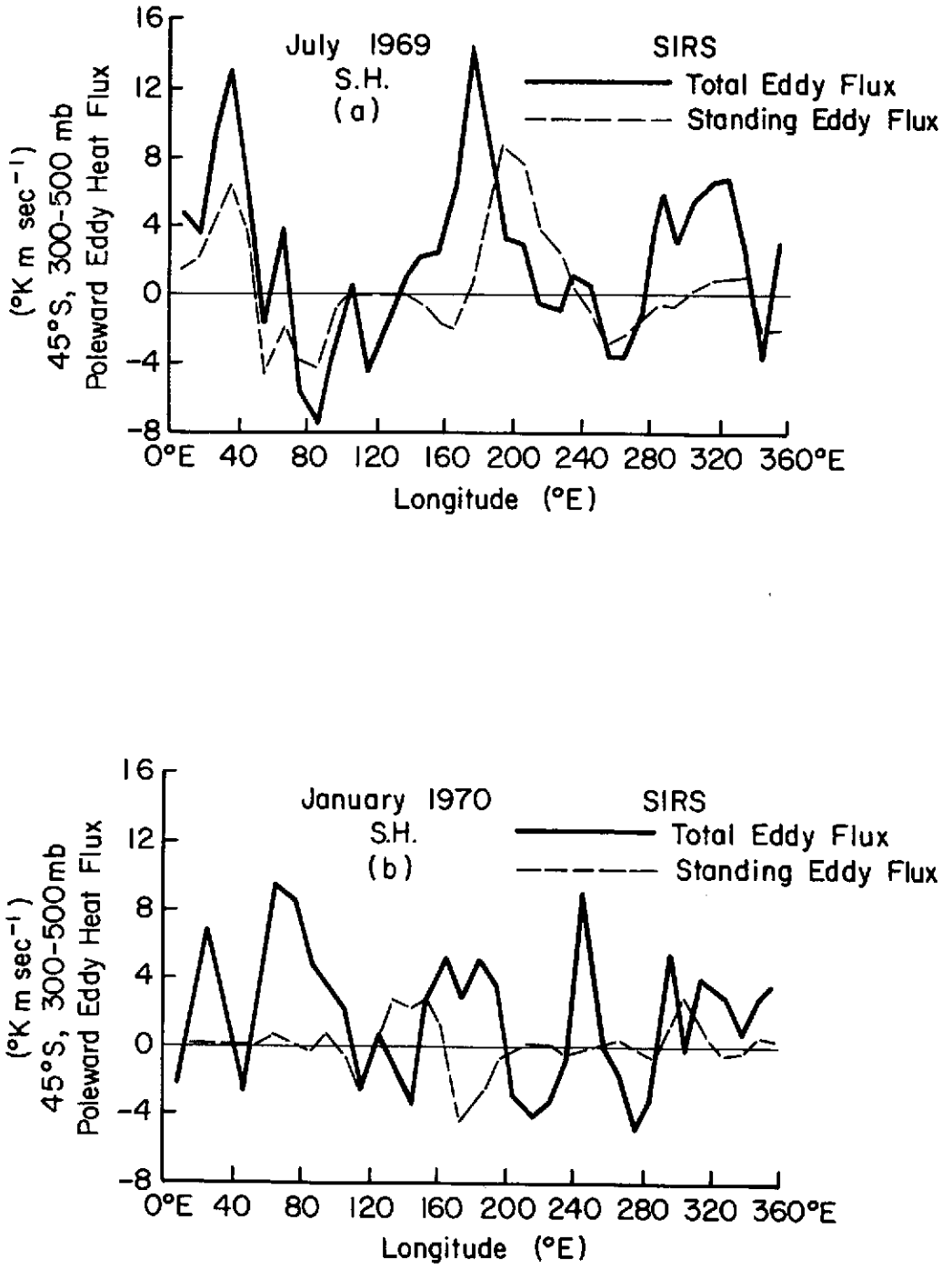

Fig. 4.14 Longitudinal distribution of total eddy heat flux and standing eddy heat flux for the layer 300-500 mb at 45°S in July 1969 and January 1970.

in conjunction with two of the total eddy flux peaks. The South American peak is essentially comprised of just transient eddy flux. The African total eddy flux peak consists of about one half stationary and one half transient eddy flux.

An interesting feature in Figure 4.14a is the displacement of the stationary eddy flux maximum to the east of the total eddy flux peak over New Zealand. The displacement is 20° longitude. Between 185° and 235°E, the stationary eddy flux is greater than the total; therefore, the transient eddy flux is negative.

In summer (Figure 4.14b) the standing eddies are nearly negligible, except at a few longitudes, and the pattern of total eddy flux is more confused. The very narrow peak at 245°E is the result of a very short-lived, but very strong transient system. The other peak areas are in the general locations of their winter counterparts. In the Southern Hemisphere, the peak values in summer are about two-thirds of the winter maximum values. In the Northern Hemisphere, the summer value is only about 18% of the winter value. This again points out the large difference between the hemispheres in seasonal variation.

4.4 Chapter summary

The most significant results in this chapter are those pertaining to the eddy terms. The mean meridional gradients and parameters, such as AZ and KZ, based on them merely confirm previous results based on climatology (Sections 4.1.2 and 4.1.3). It should also be mentioned that the mean meridional gradients calculated from the satellite data are constrained to be similar to the actual ones because separate

regression equations are used for each of three latitude bands in each hemisphere (see Section 3.3).

Calculations presented in this chapter indicate that standing eddies are much less dominant in the Southern Hemisphere than they are in the Northern Hemisphere. This is true for the temperature structure as revealed in the computations of AE (Section 4.1.4), the eddy kinetic energy (Section 4.1.4) and the eddy heat flux (Section 4.3.1). The satellite-based values of the percentage contribution of standing waves to AE and KE are also shown to agree very closely to the NMC-based quantities. With regard to the eddy heat flux the satellite-based percentage is significantly larger than the corresponding NMC value.

The variance of temperature around latitude circles is divided into standing and transient portions in Section 4.2.1. The ratio of standing eddy temperature variance to total variance as a function of latitude describes the latitudinal variation of the relative importance of standing eddies. These statistics show that in winter, in mid-latitudes, standing eddies are much more dominant in the Northern Hemisphere than they are in the Southern Hemisphere. This agrees with the hemispheric-averaged percentages in Table 4.3 in Section 4.1.4. However, in high latitudes (>65°), the reverse is true with the Southern Hemisphere standing eddies making a larger contribution to the total variance than their Northern Hemisphere counterparts. In summer the standing eddy contribution is larger in the Northern Hemisphere at all latitudes, the greatest difference occurring in low latitudes (<40°). At these latitudes in the Northern Hemisphere, the standing eddy contribution is very large and is associated with the presence of the Asian monsoon. The

summer monsoon regime in the Southern Hemisphere is much weaker and the standing eddy contribution in low latitudes is much less.

The magnitude of the mid-latitude eddy heat flux averaged over January and July is shown to be approximately equal in the two hemispheres (Section 4.3.2). This is significantly different from a previous observational study based on IGY data (Robinson, 1970) which concluded that the Southern Hemisphere eddy flux is only one half as large as that in northern mid-latitudes.

The eddy heat flux in southern mid-latitudes is also shown to have significant longitudinal variations (Section 4.3.2). In winter, when the pattern is best defined, there are three peaks of poleward heat flux, apparently associated with the three land areas, Australia, South America, and Africa.

CHAPTER 5

A COMPARISON BETWEEN HEMISPHERES OF THE STRUCTURE OF STRATOSPHERIC POLAR VORTICES

5.1 Relation of vortex structure to breakdown characteristics

5.1.1 Background and theory

In Section 2.6 it was noted that the Northern Hemisphere stratospheric vortex usually breaks down in midwinter, while the Southern Hemisphere vortex does not. A possible explanation for this disparity in breakdown climatologies is a difference in the stability of the vortices in the two hemispheres. Another possibility related to the upward propagation of Rossby waves is discussed in Section 2.6. In this section the stability of the vortices in both hemispheres will be examined. It is shown that the Southern Hemisphere vortex appears to be stable in midwinter, but not in spring when it is observed to break down.

Considering a fluid with both horizontal and vertical shears, Charney and Stern (1962), Pedlosky (1964), and Mahlman (1966) derive essentially identical stability criteria. Charney and Stern (1962) and Mahlman (1966) apply their criteria to the stratospheric polar vortex. As derived in these studies, the necessary condition for instability is that the latitude profile of potential vorticity, $P = (-\frac{\partial\theta}{\partial p})(\zeta_\theta+f)$, must have a relative maximum or minimum. In other words, $\frac{\partial}{\partial\phi}[(-\frac{\partial\theta}{\partial p})(\zeta_\theta+f)]$ must be zero at some point in the latitude profile. In the expression

for the potential vorticity, θ is the potential temperature, p is pressure, ζ_θ is the relative vorticity on an isentropic surface and f is the Coriolis parameter.

Charney and Stern (1962) show latitude profiles of potential vorticity for a case study just before a breakdown of the vortex in the Northern Hemisphere. A relative maximum in P is located just poleward of the jet axis; therefore, the instability criterion is met. The latitude profiles of the components of the potential vorticity, the static stability ($-\frac{\partial\theta}{\partial p}$) and absolute vorticity (ζ_θ+f), indicate that the distribution of static stability is of primary importance in meeting the instability criterion (Mahlman, 1966). While the absolute vorticity shows a continuous increase with increasing latitude, the static stability decreases sharply from the jet axis poleward. If the static stability had remained constant with latitude, the instability criterion would not be met. Thus the distribution of static stability with latitude is the determining factor in the vortex stability criterion. This is fortunate for the present study, because calculations of ζ_θ+f are not available. The vortex structure is examined solely with respect to the static stability.

5.1.2 Some observations of vortex structure

The latitudinal distribution of static stability is quite different in the stratospheric polar vortices of the Northern and Southern Hemispheres. In midwinter, poleward of the axis of the stratospheric jet stream, the stability decreases toward the pole in the Northern Hemisphere. Figure 5.1 shows the distribution with latitude of static stability in the layer 50-100 mb. The solid line indicates the latitude

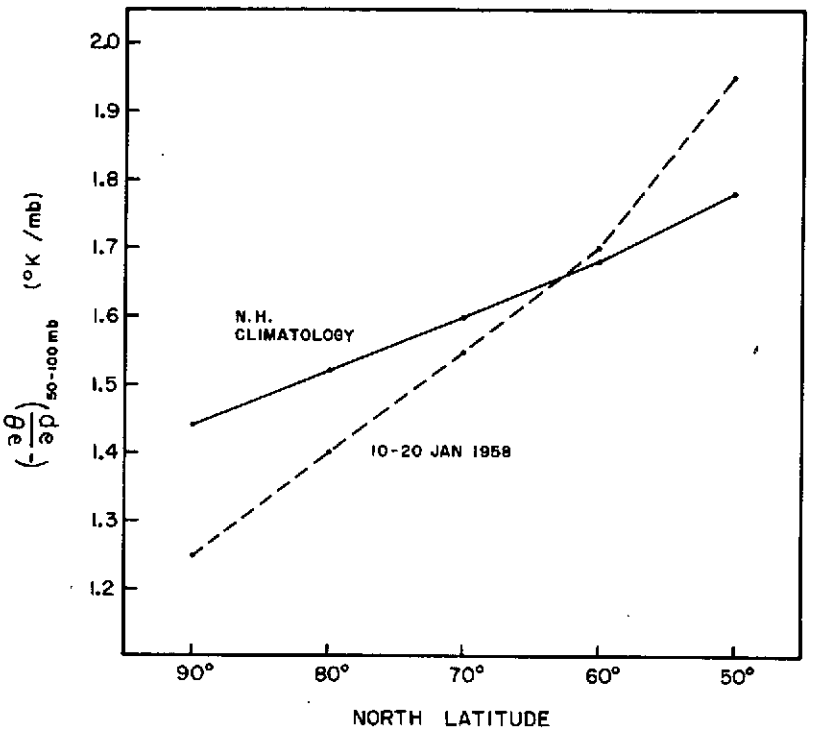

Fig. 5.1 Static stability $(-\frac{\partial\theta}{\partial p})$ in the layer 50-100 mb as a function of latitude in the Northern Hemisphere for January.

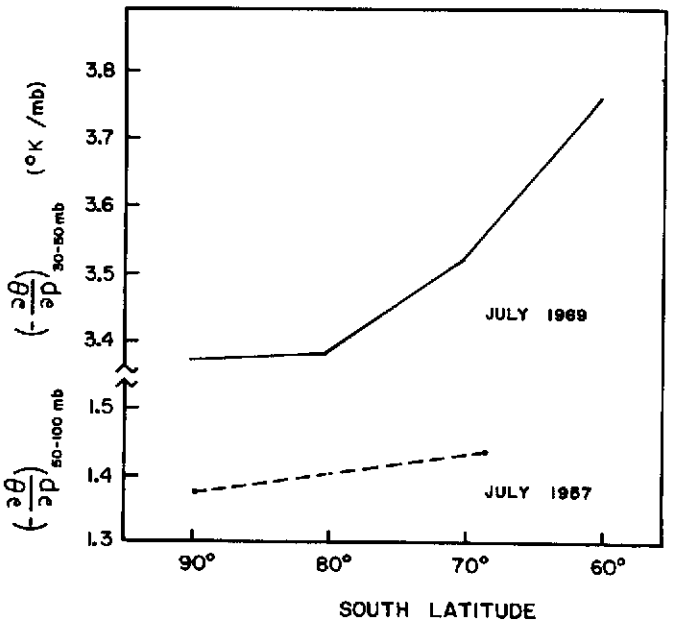

Fig. 5.2 Static stability $(-\frac{\partial\theta}{\partial p})$ in the layers 50-100 mb and 30-50 mb as a function of latitude in the Southern Hemisphere for July.

profile obtained from January mean cross-sections presented by Craig (1965), which are based on four years of data. The decrease of stability with latitude is evident, the value at 90°N being 10% less than that at 70°N. Because vortex breakdowns often occur during January, the January mean thermal structure is not the best example of pre-breakdown conditions. The dashed line in Figure 5.1 displays an example calculated by Mahlman (1966) of the stability profile before the onset of a major breakdown in 1958. A sharp decrease with latitude is again present, with the value of static stability at 90°N being about 19% less than that at 70°N.

The midwinter structure for the Southern Hemisphere is given in Figures 5.2 and 5.3. The dashed line in Figure 5.2 gives conditions in the 50-100 mb layer in July 1957 from station data presented by Taylor (1961). The stability at 90°S is calculated from July 1957 mean temperatures for station Amundsen-Scott. The point plotted at 69°S is an average of conditions at Cape Hallett (72°S, 170°E) and Wilkes (66°S, 111°E). The static stability is nearly constant with latitude with only a 4% decrease from 70°S to 90°S. The profile for July 1969 for the layer 30-50 mb is given by the solid line in Figure 5.2 and is based on temperature maps presented by Labitzke and van Loon (1972). Again from 70°S to 90°S there is a decrease of 4% in stability.

Figure 5.3 shows the latitude profile of hydrostatic stability in the Southern Hemisphere based primarily on temperatures obtained from the SIRS data. The point at 90°S is based on station Amundsen-Scott. The curve in Figure 5.3 is much like the profile given by the solid line in Figure 5.2, with the exception of the increase in static stability from 80°S to 90°S. The lapse rate at 90°S is based on only three days

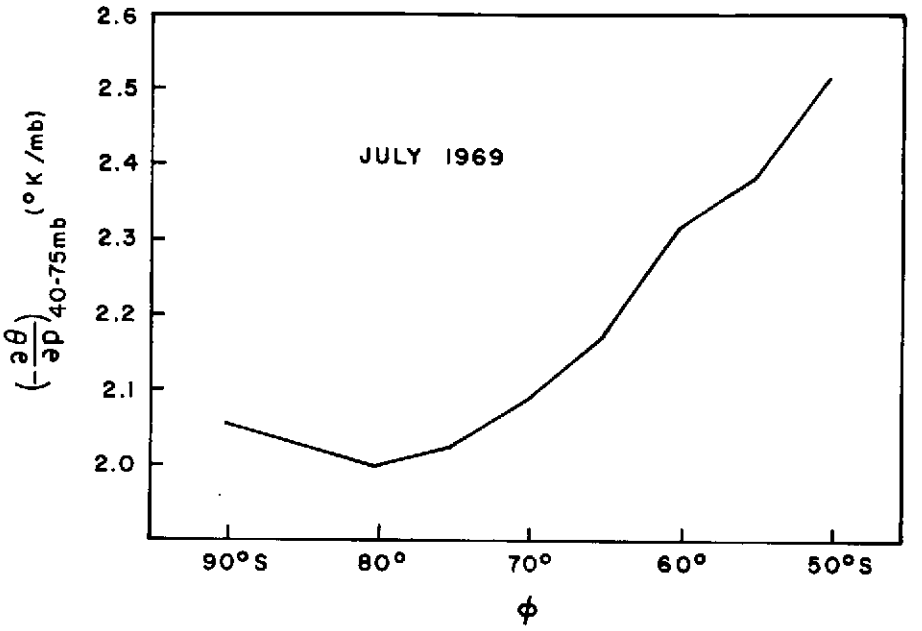

Fig. 5.3 Static stability $(-\frac{\partial\theta}{\partial p})$ in the layer 40-75 mb as a function of latitude in the Southern Hemisphere for July 1969. Values (except at 90°S) determined from SIRS data.

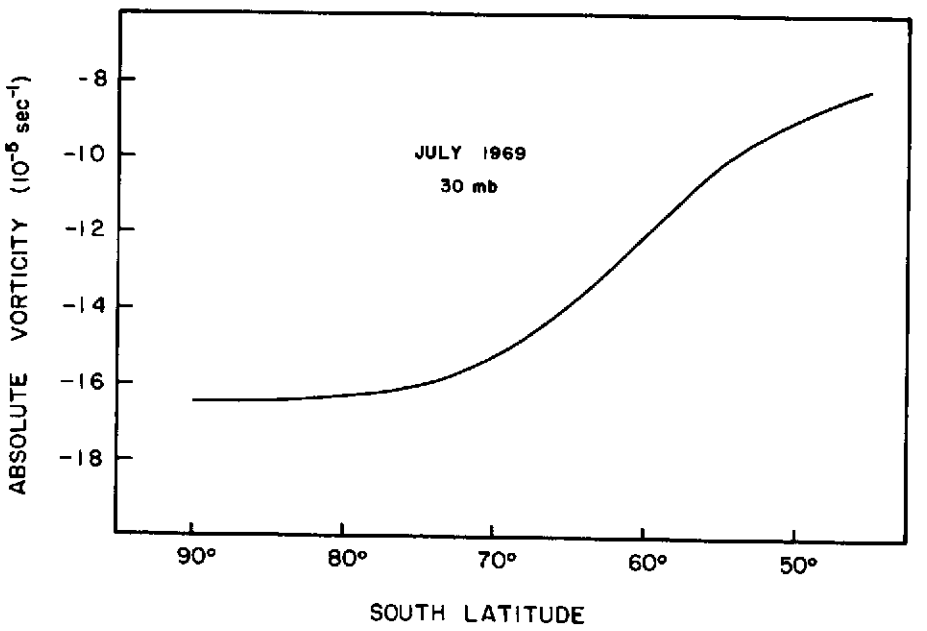

Fig. 5.4 Absolute vorticity as a function of latitude at 30 mb in the Southern Hemisphere for July 1969.

of data at the higher level, therefore it is probably not an accurate measure of the monthly mean. However, it appears that there is no large decrease in high latitudes as there is in the Northern Hemisphere.

The latitude range from 70° to 90° is of the most importance for the following reason. Figure 5.4 gives the latitude profile of absolute vorticity at 30 mb for July 1969 as calculated from the distribution with latitude of zonal wind given by Labitzke and van Loon (1972). While the vorticity on a pressure surface is not the same as the vorticity on an isentropic surface, the author believes that the profile in Figure 5.4 is characteristic of conditions occurring on isentropic surfaces in the mid-stratosphere. The absolute vorticity decreases (becomes larger negative) with latitude, with the maximum rate of decrease occurring at 60°S at the location of the jet axis. Poleward of about 70°S, the absolute vorticity profile flattens, becoming nearly constant with latitude. It is in this latitude range that a sharp decrease of static stability with increasing latitude will produce an extremum in potential vorticity, the criterion for vortex instability. This appears to be the case in the Northern Hemisphere where a sharp decrease in static stability with latitude exists in high latitudes (see Figure 5.1). The Southern Hemisphere, however, does not exhibit the large decrease from 70°S to 90°S (see Figures 5.2 and 5.3). Thus, while the instability criterion is met during midwinter in the Northern Hemisphere (Mahlman, 1966; Charney and Stern, 1962), it will tend not to be met during midwinter in the Southern Hemisphere.

Another indication of the difference in the early winter (before Northern Hemisphere breakdown) thermal structure of the Arctic and Antarctic vortices is given in a comparison of satellite-observed

radiances over the two polar regions, discussed by Labitzke and van Loon (1972). Although the Southern Hemisphere pole is much colder in mid-winter at 30 mb, radiances in SIRS channel 8 (665 cm^{-1}) and in channel A of the Selective Chopper Radiometer (SCR) indicate that the upper stratosphere over the Antarctic is warmer than over the Arctic. Therefore, the static stability would be larger over the South Pole than over the North Pole. At about 50° latitude the 30 mb temperature and the radiances indicate that conditions are much alike in the two hemispheres. Thus, the gradient of static stability ($-\frac{\partial\theta}{\partial p}$) is dissimilar in the two hemispheres.

The variation in static stability distributions between the Northern and Southern Hemispheres in winter is probably related to one of, or a combination of, the following factors: a difference between the hemispheres in the vertical distribution of radiative cooling rates in the polar-night region; a difference in the patterns of eddy heat fluxes; or a difference in mean meridional circulations. The last two factors are investigated in Section 5.2.

The distribution of total radiative heating in the global atmosphere is discussed by Dopplick (1972) on a season-by-season basis. His calculations reveal a large difference between the hemispheres in the magnitude of the total radiative cooling in the polar stratosphere during winter. The total cooling rate is substantially larger in the northern polar region. Dopplick relates this to the much lower Southern Hemisphere temperatures in this region of the lower stratosphere. The cooling rate also increases with height in the polar regions of both hemispheres; therefore, radiation acting alone will result in static stability decreasing with time. The distribution with latitude of this

destabilizing effect also varies between Northern and Southern Hemisphere high latitudes. At 70° and 80° latitude (Dopplick's computations extend to only 80°) the destabilizing effect of radiation is the same in the Northern Hemisphere, while in the Southern Hemisphere it decreases toward the higher latitude. Therefore, the Northern Hemisphere distribution will tend to produce a temperature structure with static stability constant with latitude, while static stability increasing toward the pole would result in southern latitudes. Thus the radiation distribution itself does not seem to produce the structure observed, although the inter-hemispheric difference in the distribution of radiative cooling in association with the other effects may be important in the total explanation of the observed variations in vortex structure.

5.1.3 Winter-to-spring change in the Southern Hemisphere

In spring as the sun returns to high latitudes in the Southern Hemisphere, changes in the stratospheric lapse rate occur in such a way as to produce a larger latitude gradient of static stability. The heating due to the return of the sun and the presence of ozone results in increases in $(-\frac{\partial\theta}{\partial p})$, with greater increases occurring at lower latitudes because of the greater insolation. Figure 5.5 shows the changes in stability in the 50-100 mb layer which take place between June and October, based on monthly mean data from Amundsen-Scott, Cape Hallett and Wilkes stations in 1957. The data for Cape Hallett and Wilkes is again averaged and plotted at latitude 69°S. The change in static stability with latitude is a minimum in July. From July and August to September and October, there is a substantial rise in the static stability at both latitudes and a sharp increase in the slope of

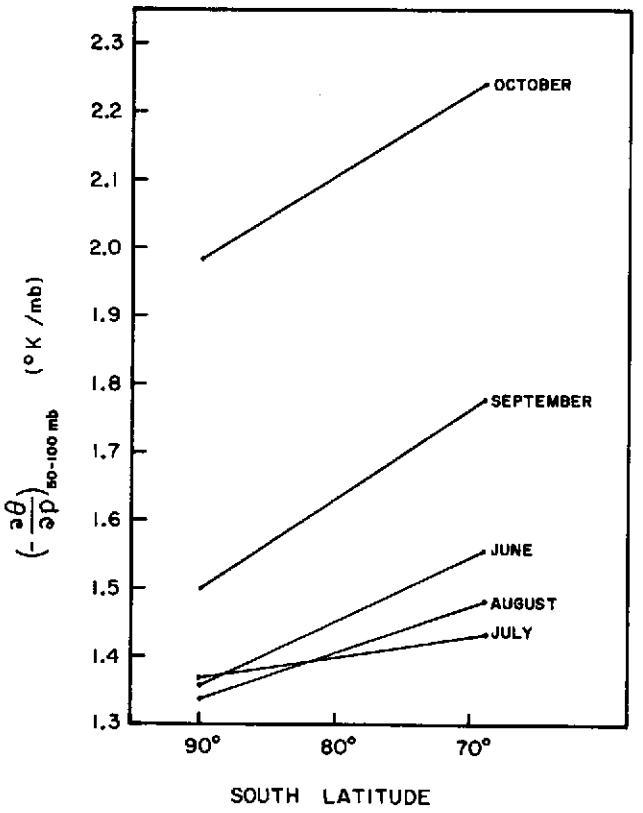

Fig. 5.5 Variation of static stability slope with latitude in the layer 50-100 mb in the Southern Hemisphere from June to October 1957.

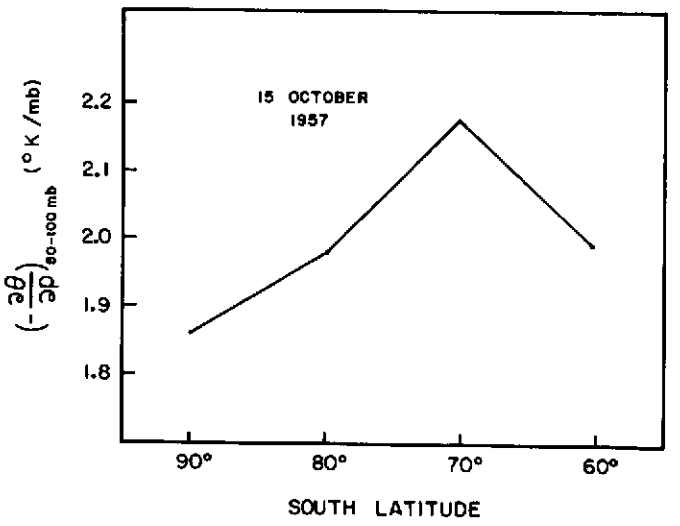

Fig. 5.6 Static stability in the layer 50-100 mb as a function of latitude in the Southern Hemisphere on 15 October 1957.

the profile. In September there is a 15% decrease in static stability between 70°S and 90°S. The increased slope in Figure 5.5 tends to produce a potential vorticity profile which meets the derived instability criterion. Therefore, although in midwinter the flatness of the static stability profile in high latitudes prevents the instability criterion from being met, in spring, when the vortex is observed to break down, a steep slope with latitude develops so that the instability criterion tends to be met. This characteristic is also evident in Figure 5.6 which is produced from a cross-section presented by Palmer and Taylor (1960) for conditions in the Antarctic stratosphere just prior to a vernal breakdown. The decrease with latitude from 70°S to 90°S is again obvious and approximately equal in magnitude to the slope given by Mahlman (1966) for a Northern Hemisphere, midwinter breakdown.

5.1.4 Conclusion

The midwinter stratospheric vortices of the Northern and Southern Hemispheres have been shown to have different structures so that the Northern Hemisphere vortex tends to meet a previously-derived instability criterion, while its southern counterpart does not. This may be the reason for the observed difference in breakdown climatologies of the two hemispheres; but, a complete explanation must take into account the propagation of energy from the troposphere to the stratosphere observed during Northern Hemisphere breakdowns (see Matsuno, 1971). The change from winter to spring in the static stability distribution in the Southern Hemisphere agrees with the observed non-breakdown condition in midwinter and the occurrence of the final collapse of the southern vortex in spring.

5.2 Mean meridional circulation in the wintertime stratosphere

5.2.1 Background

As discussed in Section 2.6, very little is known concerning the mean meridional circulation of the Southern Hemisphere stratosphere. It has been postulated on the basis of surface ozone measurements over Antarctica (see Reiter, 1969, 1971) that there is a general sinking over the pole during winter. The mean meridional motion pattern in the Northern Hemisphere winter has been studied by a number of authors (e.g., Vincent, 1968 and Mahlman, 1966). Their studies all reveal a two-celled structure with rising motion over the pole and in low latitudes, and sinking motion in mid-latitudes. In this section the SIRS-based atmospheric structure in the stratosphere is used to make computations of the zonally-averaged vertical motion fields in both hemispheres during a winter month. In the Northern Hemisphere the calculations are also carried out using conventional data.

5.2.2 Method of calculation

The technique used here to calculate the zonally-averaged vertical motion is similar to that used by Mahlman (1966) for the Northern Hemisphere with conventional data. It is basically a heat budget technique. The total derivative of potential temperature (θ) is expanded to give

$$\frac{d\theta}{dt} = \frac{\partial\theta}{\partial t} + \mathbf{V}_p \cdot \nabla\theta + \omega \frac{\partial\theta}{\partial p} , \qquad 5.1$$

where $\mathbf{V}_p$ is vector horizontal wind on a surface of constant pressure, and ω is the vertical velocity in pressure coordinates. Expansion of the advection term in equation 5.1 gives

$$\frac{d\theta}{dt} = \frac{\partial\theta}{\partial t} + \nabla\cdot\mathbf{v}_p\theta - \theta\nabla\cdot\mathbf{v}_p + \omega\frac{\partial\theta}{\partial p} \quad . \tag{5.2}$$

Rearrangement of the terms gives

$$\left(-\frac{\partial\theta}{\partial p}\right)\omega = \frac{\partial\theta}{\partial t} - \frac{d\theta}{dt} + \nabla\cdot\mathbf{v}_p\theta - \theta\nabla\cdot\mathbf{v}_p \quad , \tag{5.3}$$

Next, equation 5.3 is integrated over the area bounded by two latitudes ϕ_1 and ϕ_2, which in this study are usually 10° apart. This results in

$$\begin{aligned}\int_{\phi_1}^{\phi_2}\left[-\frac{\partial\theta}{\partial p}\omega\right]_\lambda \cos\phi \cancel{d\lambda} = &\int_{\phi_1}^{\phi_2}\left[\frac{\partial\theta}{\partial t}\right]_\lambda \cos\phi\, d\phi + \int_{\phi_1}^{\phi_2}\left[-\frac{d\theta}{dt}\right]_\lambda \cos\phi\, d\phi \\ &+ \frac{1}{a}\left\{\cos\phi_2\,[v_{\phi_2}\theta]_\lambda - \cos\phi_1\,[v_{\phi_1}\theta]_\lambda\right\} \\ &- \int_{\phi_1}^{\phi_2}[\theta\nabla\cdot\mathbf{v}_p]_\lambda \cos\phi\, d\phi \quad ,\end{aligned} \tag{5.4}$$

where a is the Earth's radius and $[\ ]_\lambda$ implies averaging around a latitude circle. The notation used here is explained in detail in Chapter 4 (Section 4.1.1).

The averaged quantities in the last two terms of equation 5.4 are expanded to give

$$[v\theta]_\lambda = [v]_\lambda[\theta]_\lambda + [(v)_\lambda(\theta)_\lambda]_\lambda \tag{5.5}$$

$$[\theta\nabla\cdot\mathbf{v}_p]_\lambda = [\theta]_\lambda[\nabla\cdot\mathbf{v}_p]_\lambda + [(\theta)_\lambda\ (\nabla\cdot\mathbf{v}_p)_\lambda]_\lambda \tag{5.6}$$

where

$$[\theta]_\lambda[\nabla\cdot\mathbf{v}_p]_\lambda = \frac{1}{2\pi}[\theta]_\lambda\int_0^{2\pi}\nabla\cdot\mathbf{v}_p d\lambda \quad . \tag{5.7}$$

Substituting equations 5.5 and 5.6 into equation 5.4, and using equation 5.7 results in

$$\int_{\phi_1}^{\phi_2}\left[-\frac{\partial\theta}{\partial p}\,\omega\right]_\lambda \cos\phi\, d\phi = \int_{\phi_1}^{\phi_2}\left[\frac{\partial\theta}{\partial t}\right]_\lambda \cos\phi\, d\phi + \int_{\phi_1}^{\phi_2}\left[-\frac{d\theta}{dt}\right] \cos\phi\, d\phi$$

$$+ \frac{1}{a}\left\{\cos\phi_2\ [(v_{\phi_2})_\lambda(\theta)_\lambda]_\lambda - \cos\phi_1\ [(v_{\phi_1})_\lambda(\theta)_\lambda]_\lambda\right\}$$

$$+ \frac{1}{a}\left\{\cos\phi_2\ [v_{\phi_2}][\theta]_\lambda - \cos\phi_1\ \ [v_{\phi_1}]_\lambda[\theta]_\lambda\right\} \qquad 5.8$$

$$- \frac{1}{2\pi}\int_{\phi_1}^{\phi_2}[\theta]_\lambda \int_0^{2\pi}\nabla\cdot\mathbf{V}_p \cos\phi\, d\lambda\, d\phi$$

$$- \int_{\phi_1}^{\phi_2}[(\theta)_\lambda(\nabla\cdot\mathbf{V}_p)_\lambda]_\lambda \cos\phi\, d\phi$$

In equation 5.8, the second and third lines represent the effect of the divergence of the eddy flux and of the mean motion flux, respectively. The fourth and fifth lines represent the effect of divergence.

The last term in equation 5.8 involves the correlation of θ and $\nabla\cdot\mathbf{V}_p$. It is assumed small and, therefore, neglected. The second-to-last term in equation 5.8 is well approximated by

$$-\frac{1}{2\pi}\int_{\phi_1}^{\phi_2}[\theta]_\lambda \int_0^{2\pi}\nabla\cdot\mathbf{V}_p \cos\phi\, d\phi\, d\lambda \cong -\frac{1}{2\pi}[\theta]_{\lambda,\phi}\int_{\phi_1}^{\phi_2}\int_0^{2\pi}\nabla\cdot\mathbf{V}_p \cos\phi\, d\phi\, d\lambda, \qquad 5.9$$

where $[\theta]_{\lambda,\phi}$ is the average potential temperature for the area between ϕ_1 and ϕ_2. The right side of equation 5.9 is integrated to obtain

$$-\frac{1}{2\pi}[\theta]_{\lambda,\phi}\int_{\phi_1}^{\phi_2}\int_{o}^{2\pi}\nabla\cdot\mathbf{V}_p\cos\phi\,d\phi\,d\lambda = -\frac{1}{a}[\theta]_{\lambda,\phi}\left\{\cos\phi_2[v_{\phi_2}]_\lambda-\cos\phi_1[v_{\phi_1}]_\lambda\right\} \tag{5.10}$$

Using the right side of equation 5.10 to replace the second-to-last term gives

$$\begin{aligned}\int_{\phi_1}^{\phi_2}\left[-\frac{\partial\theta}{\partial p}\omega\right]_\lambda\cos\phi\,d\phi = {} & \int_{\phi_1}^{\phi_2}\left[\frac{\partial\theta}{\partial t}\right]_\lambda\cos\phi\,d\phi + \int_{\phi_1}^{\phi_2}\left[-\frac{d\theta}{dt}\right]_\lambda\cos\phi\,d\phi \\ & + \frac{1}{a}\left\{\cos\phi_2\,[(v_{\phi_2})_\lambda(\theta)_\lambda]_\lambda - \cos\phi_1[(v_{\phi_1})_\lambda(\theta)_\lambda]_\lambda\right\} \\ & + \frac{1}{a}\left\{\cos\phi_2\,[v_{\phi_2}]_\lambda[\theta]_\lambda - \cos\phi_1[v_{\phi_1}]_\lambda[\theta]_\lambda\right\} \\ & - \frac{1}{a}\,[\theta]_{\lambda,\phi}\left\{\cos\phi_2[v_{\phi_2}]_\lambda - \cos\phi_1[v_{\phi_1}]_\lambda\right\}\end{aligned} \tag{5.11}$$

The last two lines in equation 5.11 are of opposite sign and are nearly, but not quite, equal. With a temperature gradient of 10°K/10° latitude and with θ approximately equal to 200°K, $[\theta]_{\lambda,\phi}$ is different from either θ at ϕ_1 or θ at ϕ_2 only by about 2 or 3%. The last two lines in equation 5.11 will thus tend to cancel and their sum is negligible. Therefore, they are neglected.

The integrals in equation 5.11 are evaluated, for example, by the approximation

$$\int_{\phi_1}^{\phi_2}\left[\frac{\partial\theta}{\partial t}\right]_\lambda\cos\phi\,d\phi = \left[\frac{\partial\theta}{\partial t}\right]_\lambda\cos\left(\frac{\phi_1+\phi_2}{2}\right)(\phi_2-\phi_1), \tag{5.12}$$

where $\left[\frac{\partial\theta}{\partial t}\right]_\lambda$ is evaluated at latitude $\frac{\phi_1 + \phi_2}{2}$. With the approximations exampled by equation 5.12, equation 5.11 becomes

$$\left[-\frac{\partial\theta}{\partial p}\omega\right]_\lambda = \left[\frac{\partial\theta}{\partial t}\right]_\lambda - \left[\frac{d\theta}{dt}\right]_\lambda + \frac{\left\{\cos\phi_2[(v_{\phi_2})_\lambda(\theta)_\lambda]_\lambda - \cos\phi_1[(v_{\phi_1})_\lambda(\theta)_\lambda]_\lambda\right\}}{\left\{a\cos\left(\frac{\phi_1 + \phi_2}{2}\right)(\phi_2 - \phi_1)\right\}} \qquad 5.13$$

The zonally-averaged vertical motion, $[\omega]_\lambda$, is calculated from equation 5.13 assuming that ω and $\left(-\frac{\partial\theta}{\partial p}\right)$ are uncorrelated. The first term on the right side is the local temperature change, and the second term is the diabatic heating. The third term is the temperature change due to the divergence of the horizontal eddy heat flux.

The local change in temperature, the static stability and the horizontal eddy heat fluxes (geostrophic) can be determined from the SIRS-derived atmospheric structure. The diabatic heating, $\frac{d\theta}{dt}$, is due to radiative heating or cooling and cannot be calculated without a knowledge of the vertical distribution of ozone. However, stratospheric, radiative heating rates, calculated from climatological conditions, are available. Rodgers (1967) has calculated radiative heating rates in the troposphere and stratosphere in the Northern Hemisphere up to 70°N, for the months of January, April, July and October. Similar calculations have been carried out by Dopplick (1972) between 80°N and 80°S for each month of the year with the results presented as cross-sections of seasonal-average values. The values of Rodgers for January appear to be almost identical to those of Dopplick for the December-January-February period in the Northern Hemisphere. Table 5.1 gives the values

of $\frac{d\theta}{dt}$ (adapted from Dopplick, 1972) used in this study as a function of latitude and layer. The Northern Hemisphere heating rates are those given by Dopplick for the December through February period, while the June through August values are used for the Southern Hemisphere.

	Latitude				
	80°N	70°N	60°N	50°N	40°N
10-30 mb	-1.2	-1.2	-1.0	-0.8	-0.5
30-50 mb	-0.9	-0.9	-0.8	-0.6	-0.3
50-100 mb	-0.6	-0.6	-0.5	-0.4	-0.2
	80°S	70°S	60°S	50°S	40°S
10-30 mb	-0.6	-0.8	-0.5	-0.3	-0.2
30-50 mb	-0.4	-0.4	-0.3	-0.2	-0.2
50-100 mb	-0.3	-0.3	-0.3	-0.2	-0.2

Table 5.1 Values of $\frac{d\theta}{dt}$ used in vertical motion calculations (Adapted from Dopplick, 1972). Units: °C/day.

The calculations of $[\omega]_\lambda$ are made for each ten degrees of latitude between 40° and 80° latitude using fluxes at the intervening latitudes of 35°, 45°, etc. The computation of ω at 80° uses the flux at 75° and the fact that the flux is zero at 90°. An additional calculation is carried out at 85° using the eddy flux at 80°.

5.2.3 Vertical motion patterns

The local change term in equation 5.13 is of the order of 0.1°K/day, while the heating due to the eddy flux convergence is of the order of 1°K/day in polar latitudes. The term $\frac{d\theta}{dt}$ is negative everywhere during

the polar night in the stratosphere and is of the order of 1°K/day. Because the diabatic heating term varies less with latitude than the flux divergence term, the latter is most important in determining the latitudinal variability of ω. For this reason the enthalpy flux as a function of latitude is examined.

Figure 5.7 shows the poleward heat flux in the 10-30 mb layer averaged over January 1970 for the Northern Hemisphere and over July 1969 for the Southern Hemisphere. Both SIRS and NMC curves are presented for the Northern Hemisphere. The geostrophic approximation is used for these computations. In both hemispheres the peak poleward flux is reached at 60°. It should be remembered that the polar vortex in the Northern Hemisphere broke down in early January that year. Consequently, the Northern Hemisphere curves may not be representative of normal (non-breakdown) conditions. The two SIRS curves peak at almost the same value. The total flux convergence between 60° and the pole is approximately equal in the two hemispheres. However, the shape of the two curves is different. The Southern Hemisphere curve shows the flux decreasing very rapidly just poleward of 60°S and gradually levelling out. The greatest flux convergence is in the area between 60°S and 75°S. The Northern Hemisphere curve has a relatively constant decrease with latitude, indicating that the flux convergence is spread out more uniformly than that in the Southern Hemisphere. This difference in shape of the enthalpy flux curves is also evident in the 30-50 mb and 50-100 mb layers, but it is not so obvious.

The enthalpy flux distributions for all three layers for the Southern Hemisphere July 1969 are given in Figure 5.8. In each layer there is a rapid decrease in the flux poleward of the peak, then a

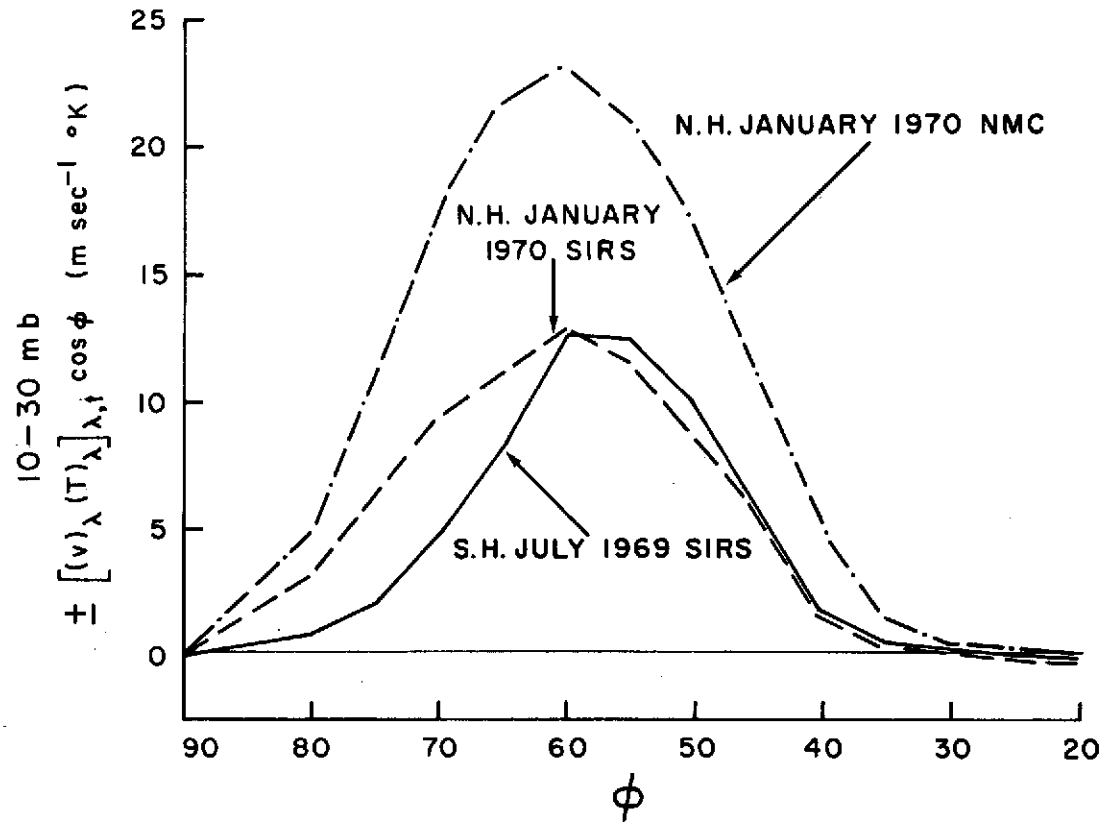

Fig. 5.7 Poleward heat flux in the 10-30 mb layer-January 1970 in the N. H., July 1969 in the S. H.

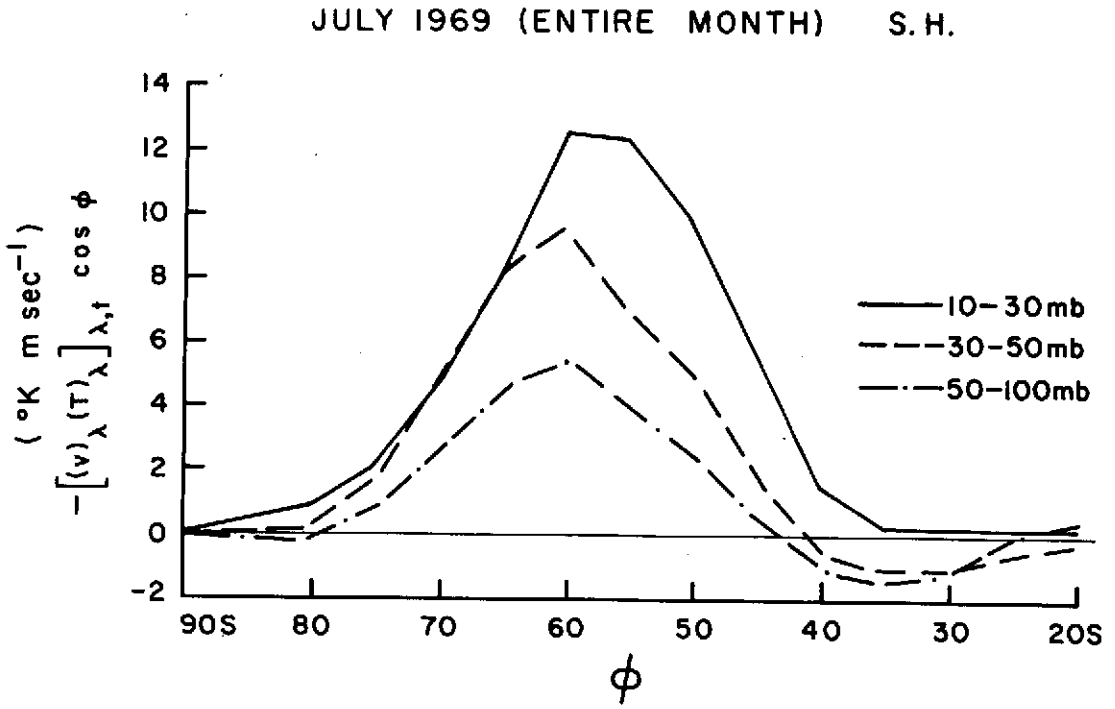

Fig. 5.8 Poleward heat fluxes in the stratosphere of the S. H. for July 1969.

flattening out of the curve in very high latitudes. The value at 80°S in the 50-100 mb layer is slightly negative, meaning that between 80°S and the pole there is a flux divergence. The flux in the 30-50 mb layer at 80°S has a very small positive value so that in this layer the flux convergence between 80°S and 90°S is also very small. In the Northern Hemisphere there is substantial flux convergence between 80°N and the pole (see Figure 5.7). Thus there is a significant difference between the hemispheres in the patterns of heat flux and heat flux convergence in the polar-night stratosphere.

The results of evaluating the terms in equation 5.13 and solving for ω in the Northern Hemisphere for January 1970 with both NMC and SIRS-based structure are shown in Figures 5.9a and b. The NMC-based calculation (Figure 5.9a) shows rising motion in high latitudes and sinking in lower latitudes. The axis of ascent slopes poleward with height and the maximum upward motion is located at 20 mb at the pole. The pattern of rising motion over the pole and sinking in midlatitudes is typical of that found by other authors (e.g., Mahlman, 1966) for the Northern Hemisphere. Mahlman (1966) also showed that this distribution of ascent and descent occurs before, during and after breakdowns. Miller, Brown and Campana (1972) using the quasi-geostrophic, adiabatic omega equation obtain a cross-section of ω for the period 1-15 January 1970, which also indicates the same general pattern of ascent and descent as in Figure 5.9a. Thus the use of equation 5.13 and NMC structure appears to produce a cross-section of vertical motion in the stratosphere, which closely resembles previous estimates made for different years, and also resembles a calculation made for the same year.

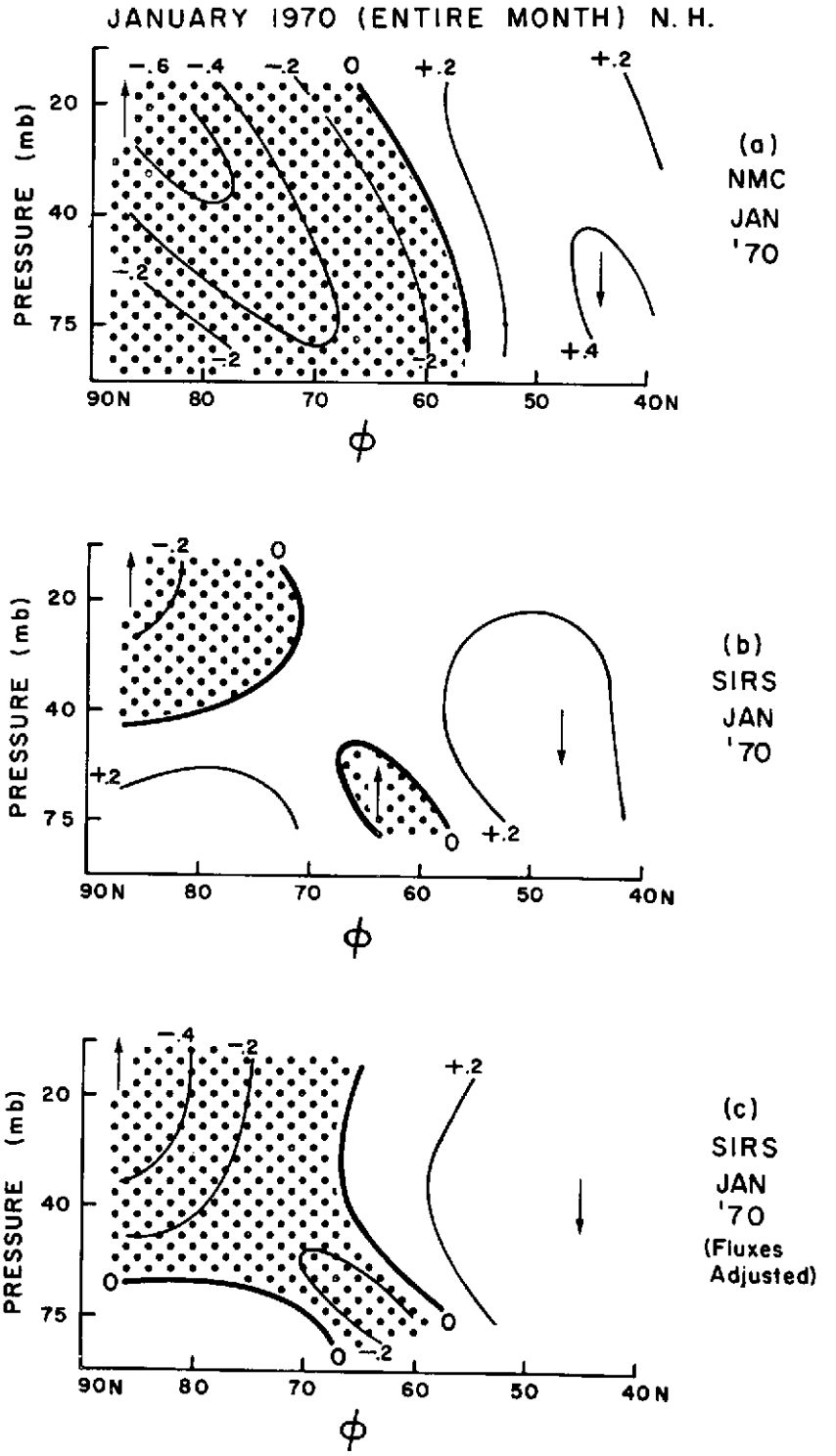

Fig. 5.9 Zonally-averaged vertical motion patterns for the N. H. for January 1970. Units: mb day^{-1}. Stippled area denotes area of ascent.

Figure 5.9b shows the vertical motions for the Northern Hemisphere calculated using the heat fluxes, local temperature changes and static stability derived from the SIRS-based structure. There are some similarities and some differences between Figures 5.9a and b. In Figure 5.9b there is rising motion over the pole in the higher layers and sinking motion in midlatitudes. There is also a small area of ascent at 60°N at 75 mb. The maximum rising motion is found at or near the pole and in the top layer (10-30 mb). However, the volume of upward motion is much less than that shown in Figure 5.9a. Magnitudes of maximum rising and sinking motions are underestimated.

The vertical velocities in this section are presented in terms of ω and in units of mb/day. The conversion from ω to $w = dz/dt$ varies with density. For a temperature of -60°C the conversions are as follows for the various heights:

$$\begin{aligned} &\text{at 20 mb, 1.0 mb/day} = 3.6\text{mm/sec} \\ &\text{at 40 mb, 1.0 mb/day} = 1.8\text{mm/sec} \\ &\text{at 75 mb, 1.0 mb/day} - 1.1\text{mm/sec} . \end{aligned} \qquad 5.14$$

Therefore, the rising motion of 0.6 mb/day at 20 mb in Figure 5.9a is approximately equivalent to 2.2mm/sec.

The main factor in the difference between Figures 5.9a and b is the underestimation of eddy heat fluxes in the SIRS-based calculation, evident in Figure 5.7. Although the SIRS-based calculation undervalues the magnitude of the actual fluxes, it reproduces the shape of the NMC curve and the locations of flux divergence and convergence. This is also true for the two lower layers (30-50 mb and 50-100 mb). The underestimation by the SIRS-based fluxes varies with latitude and between layers, the minimum underestimation between 40°N and 75°N being 56%. To at least

partially correct for this effect a factor of 1.8 (based arbitrarily on the 56% figure) is applied to the SIRS-based flux values and the vertical motion computation is redone. The results are shown in Figure 5.9c. The general rising motion in high latitudes at high levels and the sinking motion in mid-latitudes are still present. The region of rising motion has expanded and indicates the slope with height of the NMC-based cross-section. Magnitudes of maximum rising and sinking motion are also in closer agreement. The adjustment factor 1.8 as based on the minimum underestimation is chosen because the author of this study believes that the larger underestimations present, especially in the lower layers, are due to the low density of satellite radiance data in the Northern Hemisphere for January 1970 relative to the density of observations over the Southern Hemisphere in July 1969, the Southern Hemisphere winter month to be examined.

The results of the vertical motion calculations for the Southern Hemisphere for July 1969 are shown in Figures 5.10a and b. Part a of the figure is based on fluxes calculated directly from the SIRS-based structure, and part b is based on calculations made with the fluxes adjusted by the factor of 1.8. Both parts of Figure 5.10 show an area of descending motion centered at 50°S, an area of ascent centered at about 70°S and a small area of descent over the South Pole, below about 50 mb. With the assumption of ascent in low latitudes (<30°S), Figure 5.10 indicates a possible three-celled meridional circulation in the lowest part of the stratosphere, and a two-celled structure in the middle stratosphere. The Southern Hemisphere pattern is significantly different from that in the other hemisphere, particularly with regard to the location and strength of the upward branch. While in the

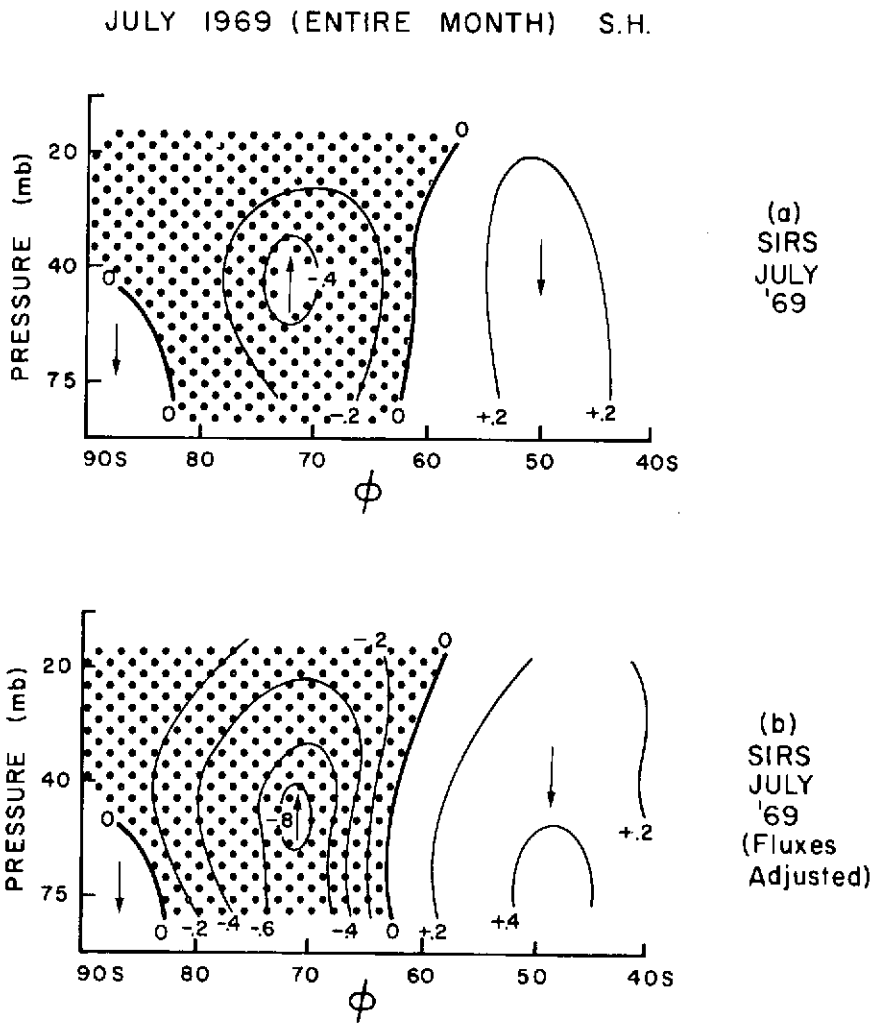

Fig. 5.10 Zonally-averaged vertical motion patterns for the S. H. for July 1969. Units: mb day^{-1}.

Northern Hemisphere the axis of rising motion tilts poleward in the vertical, at southern latitudes the axis is approximately vertical. The maximum rate of ascent is over the pole in the Northern Hemisphere, but is located at 70°S in the other hemisphere. The magnitude of the maximum also seems to be larger in the Southern Hemisphere.

The boundary in Figure 5.10 between the main areas of ascent and descent (60°S) is the approximate latitude of the polar night jet stream. The same is true in the Northern Hemisphere. Because the temperature decreases toward the pole, relatively cold air is ascending and relatively warm air is descending. Therefore, there is a conversion of zonal kinetic energy (KZ) to zonal available potential energy (AZ). It seems apparent then, that the stratospheric polar jet is maintained by a conversion from eddy kinetic energy (KE) to KZ. Therefore, although mean monthly maps show a nearly zonal pattern, the eddies must still be very significant in the maintenance of the Southern Hemisphere polar night jet stream.

From Figure 5.10 there does not appear to be a general sinking motion over the South Pole, except in the lowest part of the stratosphere. However, since Rubin and Weyant (1963) have already noted a general subsidence below 75 mb to the surface over the South Pole, it is plausible that ozone-rich air in the lower stratosphere is transported downward to the surface to produce the midwinter peaks in surface ozone observed over Antarctica (Wisse and Meerburg, 1969).

5.3 Variations in the circulation of the Southern Hemisphere stratosphere in relation to the presence or absence of a minor midwinter warming

5.3.1 Background

During July 1969, there were significant variations in the circulation of the Southern Hemisphere stratosphere. These changes were related to the occurrence, early in the month, of a minor midwinter warming identified by Miller, Finger and Gelman (1970) through the use of satellite radiance data. Specifically, Miller et al. used the mean SIRS channel 8 radiance around the 60°S latitude circle as a gross indicator of variations of stratospheric temperature at that latitude. This is reasonable since the weighting function (see Figure 3.1) for this channel shows nearly all the contribution to the radiance coming from the stratosphere. Large increases in Miller's index are associated with a contracting of the polar vortex related to a warming event. The plot of this indicator versus time for the Southern Hemisphere winter of 1969 shows a sharp rise in mean radiance at the very end of June with a relative maximum being reached about 10 July. A very sharp decrease follows, after which there is a period of low and relatively constant mean radiance. At the very end of July, about the 29th, the mean radiance again increases sharply. The sharp rises early and late in the month are evidence of minor midwinter warmings. The period of low, relatively constant values is what will be referred to here as a quiet period.

In this section the stratospheric circulation is compared between the early July minor midwinter warming period and the following quiet period. Variations of the mean meridional motion, the eddy heat flux

and the wave characteristics are examined. Time-longitude diagrams of the satellite-derived thickness and height fields are used to study the wave activity.

5.3.2 Wave characteristics

Conventional data above 100 mb in the Southern Hemisphere are generally inadequate to determine many important characteristics of wave motions other than those which can be obtained by single-station analysis. An exception is an analysis by Phillpot (1969). A few other studies have been done using satellite information. Lovill (1972) and Reiter and Lovill (1973) show time-longitude diagrams of total ozone as determined from the Nimbus 3 Infrared Interferometer Spectrometer (IRIS) experiment. Their diagrams indicate rapid eastward movement of waves during the Southern Hemisphere winter. Time-longitude diagrams of satellite radiance at 60°S in SIRS channels 7 and 8 are given by Miller, Finger and Gelman (1970) covering the same period to be discussed here, and Fritz (1970) examines the time-longitude distributions of channel 8 in May 1969. These diagrams of the radiance emanating from the stratosphere also indicate eastward-moving waves. The radiances represent a vertical integration of the temperature structure. Because the waves present in the stratosphere probably have a phase shift with height, the vertical integration inherent in the satellite radiances may mask some waves, especially smaller ones, or may misrepresent the actual amplitudes at a particular level. For this reason the thermal structure as obtained from the satellite radiances by the regression technique should better define the wave activity than merely the radiances themselves. In addition, the retrieval technique produces mass distribution information

(geopotential height fields) so that phase relations between temperature and height can be examined.

Time-longitude diagrams of the 30-50 mb thickness and the 30 mb height averaged between 50°S and 70°S are given in Figures 5.11 and 5.12 respectively. The analysis on the thickness chart uses an interval of 50 meters, equivalent in this layer to a temperature interval of about 3.3°C. Most main features are evident on both diagrams; however, a few are clearly discernible only on one diagram. The period covered is 1-31 July 1969. The latitude belt 50°-70°S covers the zone of the Antarctic stratospheric jet stream.

The period 1-10 July is associated with a minor warming. Figures 5.11 and 5.12 show the period dominated by a stationary wave number 1 pattern with a warm ridge centered about 200°E. Superimposed upon the stationary pattern is an approximate wave number 3 pattern moving rapidly toward the east with a phase speed of about 30° longitude/day. Comparing the phases of both the stationary wave number 1 and the transient wave number 3 on both diagrams reveals that the temperature field lags behind the height field. This results in a westward slope with height of the waves. Actually the phase difference between the height and temperature (thickness) fields is underestimated. The height field in Figure 5.12 is at 30 mb; the thickness field (Figure 5.11) is for the layer 30-50 mb, thus representing the temperature distribution slightly below 30 mb. The 30 mb temperature field would be shifted westward slightly from the 30-50 mb thickness field because of the westward phase shift with height. Thus the phase lag between the height and temperature fields is somewhat larger than indicated by the two

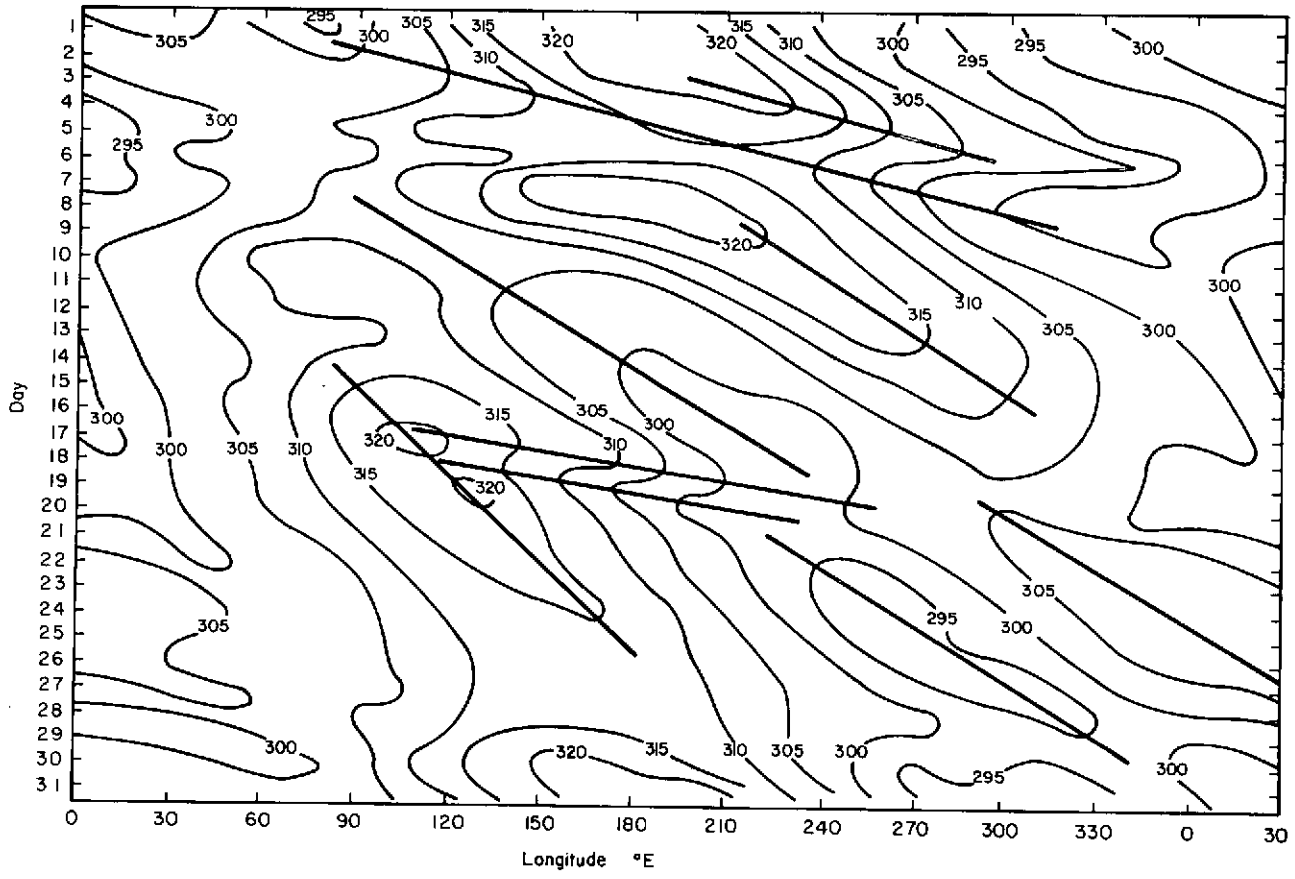

Fig. 5.11 Time-longitude diagram of 30-50 mb thickness averaged from 50°-70°S in July 1969. Slopes of straight lines indicate phase speeds.

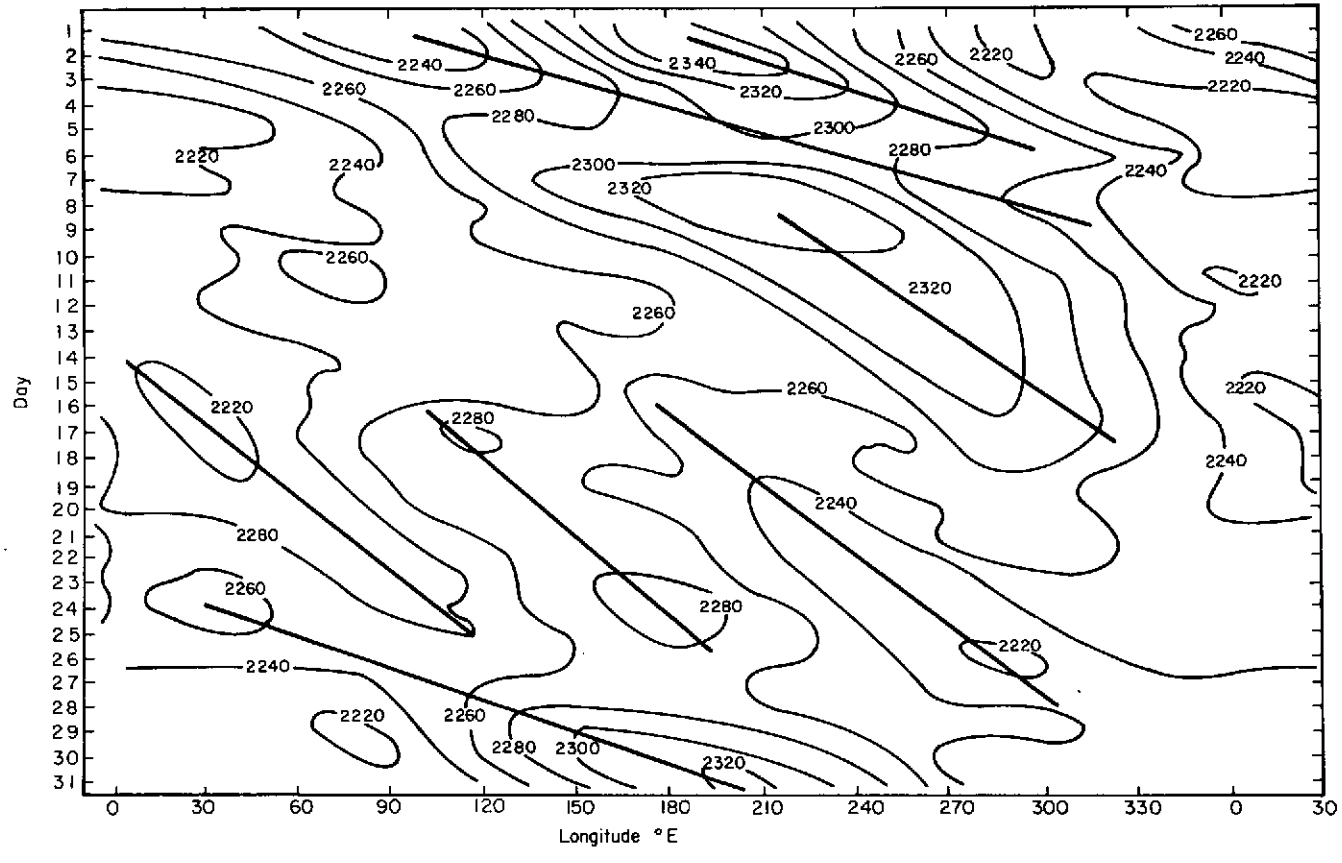

Fig. 5.12 Time-longitude diagram of 30 mb geopotential height averaged from 50°-70°S in July 1969.

diagrams. An eddy heat flux towards the pole is associated with this temperature-height phase relation.

On about 9 July the dominant wave number 1 pattern associated with the warming begins to dissolve. For approximately the next 15-18 days, the time-longitude diagrams are dominated by eastward moving waves, primarily wave number 2. The approximate phase speed of these waves is 10° longitude/day. There is also evidence in the thermal pattern (Figure 5.11) for a shorter wave (wave number = 3) in the period 17-20 July. The phase speed of this wave is about 40° longitude/day. During this time of the month (11th to the 27th), the radiance index of Miller, et al. (1970) is low, which is indicative of a quiet period (i.e., no warming event).

At almost the end of the month Miller's radiance parameter again indicates a warming at 60°S. Accompanying this increase is an apparent change in the wave characteristics with a return to a stationary wave number 1 pattern with a wave ridge at about 180°-200°E. There also appears to be a transient wave, most evident in Figure 5.12, superimposed on the stationary (k = 1) pattern.

Therefore, at both the beginning and end of the month, a stationary wave number 1 pattern is present and is associated with a midwinter minor warming. In the middle of the month, during a quiet period, transient wave number 2 dominates. Whether this relation is common to the entire winter and/or to other winters is unknown. Phillpot (1969) in a time-longitude diagram of 30 mb heights at 65°S for late winter and spring of 1967 indicates a nearly stationary wave number 1 pattern of varying intensity with the ridge at 170°E to 220°E with transient waves (k = 2) superimposed. The location of the wave number 1 ridge is

approximately at the same longitude where it is found in Figure 5.12. Therefore, it seems that when wave number 1 dominates the stratospheric polar vortex, the highest heights in the midstratosphere are located in the Pacific sector.

The waves shown in Figures 5.11 and 5.12 propagate in a medium with large vertical and horizontal shears so that the simple Rossby wave equation cannot be expected to hold. However, the waves do exhibit Rossby-wave-like characteristics. Principally, the phase speed increases with wave number. However, there is difficulty in even attempting to apply the Rossby wave formula. A suitable zonal wind speed is difficult to choose because of large variations in the horizontal and especially in the vertical. The mean zonal geostrophic wind speed at 30 mb for the entire month at 60°S is 66 m sec^{-1}. At 50 mb the speed is lower, less than 50 m sec^{-1}. Using the 30 mb zonal wind speed, the Rossby wave equation gives a $k = 1.3$ for a stationary wave, reasonably close to the $k = 1$ observed. However, the formula gives considerably higher than observed phase speeds for $k = 2$. Obviously there are other effects present other than those incorporated into the Rossby wave formula. Using the Petterssen wave equation (Petterssen, 1956, p. 153), which takes into account the horizontal wind shear, results in a reduction of the calculated phase speed. However, these speeds are still considerably higher than the observed.

5.3.3 Mean meridional motion and eddy heat fluxes

To inspect the variability of the mean meridional circulation in relation to the presence or absence of a midwinter minor warming, calculations of zonally-averaged ω were carried out for two ten-day periods

using the method described in Section 5.2.2. The first interval, 1-10 July, covers the time of the warming event. The quiet period is represented by the time span of 18-27 July. The vertical motion patterns during the minor warming and the quiet period exhibit significant differences. The vertical component of the mean meridional circulation during the minor warming is given in Figures 5.13a and b. The pattern for 18-27 July 1969 (quiet period) is given in Figures 5.14a and b. During 1-10 July, the area of descent over the South Pole below 50 mb disappears, and the ascending and descending branches at about 70°S and 50°S respectively have larger magnitudes than the monthly averages in those locations. The ascending branch is still centered between 70°S and 75°S.

During the quiet period (18-27 July 1969), the vertical motion pattern shows descent over the pole at all levels of this calculation (Figure 5.14a and b). According to Figure 5.14b, the descending motion covered the area poleward of about 80°S with maximum downward velocity occurring in the lowest layer of calculation. Consequently, it appears that during this time period the Southern Hemisphere stratosphere has a three-celled mean meridional circulation pattern, assuming an area of ascent in low latitudes. The ascending branch at 70°S and the descending branch farther equatorward are less intense than the monthly average (Figure 5.10) and much less intense than they are during the minor warming (Figure 5.13).

The difference in vertical motion patterns between the periods 1-10 July and 18-27 July 1969 is closely related to the eddy heat flux distributions for those two periods (see equation 5.13). These distributions are shown in Figures 5.15a and b. The peak fluxes during

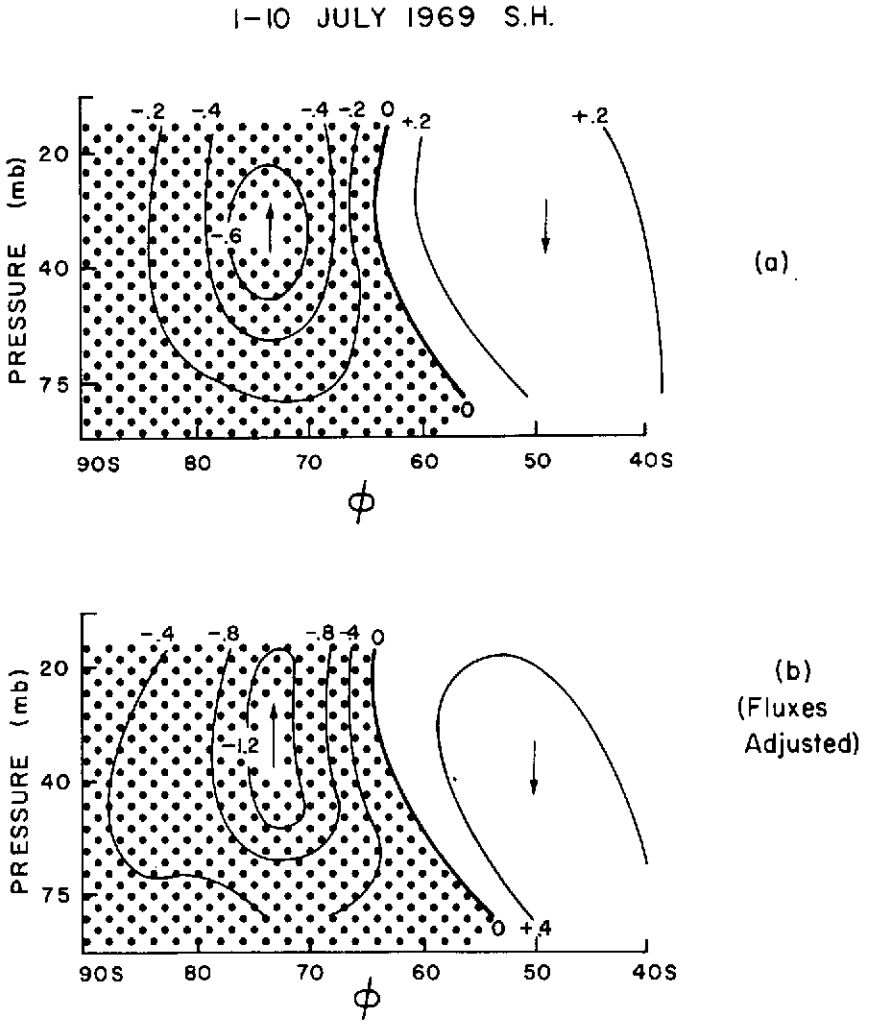

Fig. 5.13 Zonally-averaged vertical motion patterns for the S. H. for the period 1-10 July 1969, during a minor midwinter warming. Units: mb day^{-1}.

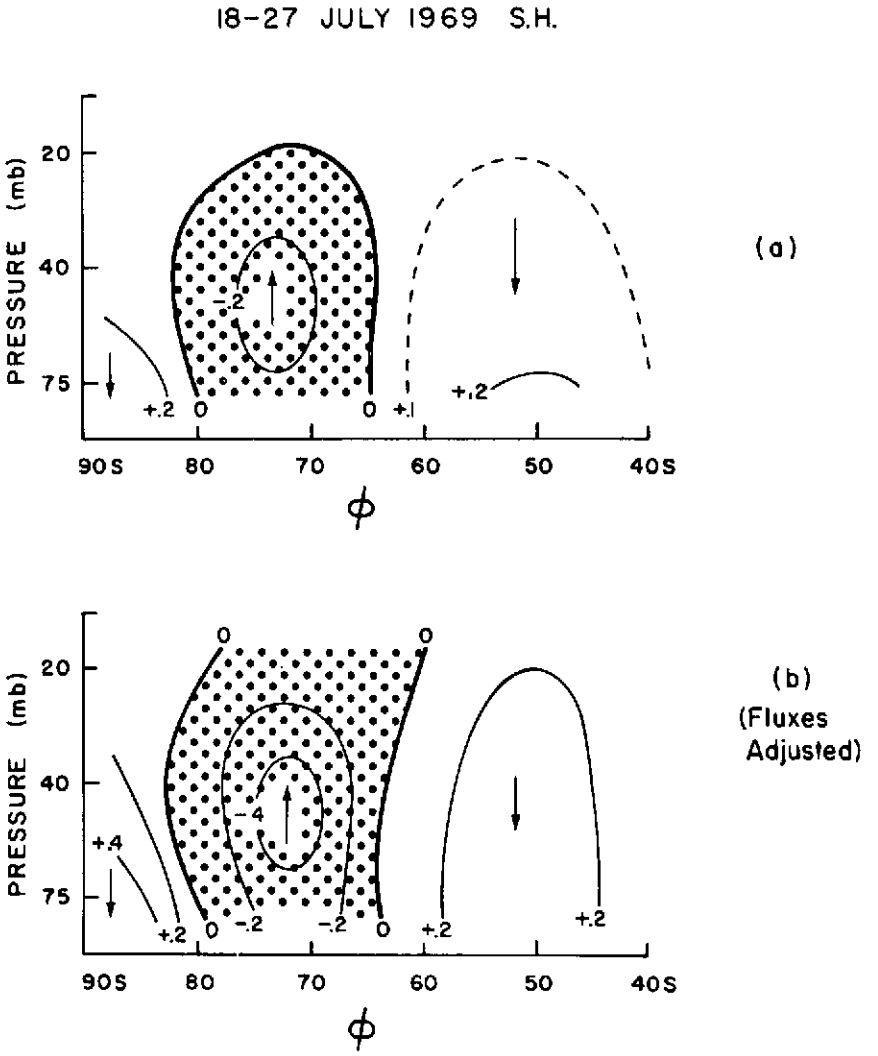

Fig. 5.14 Zonally-averaged vertical motion patterns for the S. H. for the period 18-27 July 1969, a quiet period. Units: mb day^{-1}.

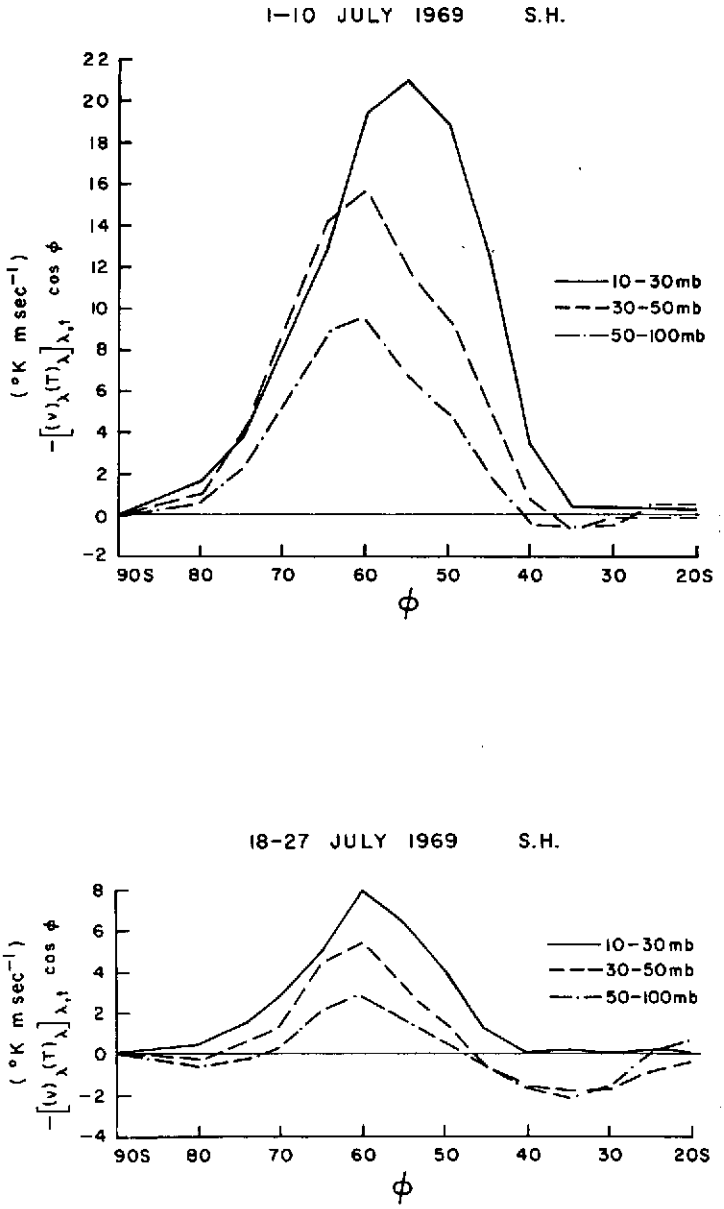

Fig. 5.15 Poleward heat fluxes in the S. H. during the periods (a) 1-10 July and (b) 18-27 July 1969.

1-10 July are approximately three times as great as those for the 18-27 July period. Thus the flux divergences on either side of the peak are also about three times as great. In very high latitudes another important variation is that, although both the 50-100 mb and 30-50 mb layers exhibit eddy flux divergence between 80°S and 90°S during the period 18-27 July, all layers exhibit flux convergence in that location for the 1-10 July period. This is the reason for the existence of the difference in vertical motion patterns over the pole between the two periods.

The variations with time of the heat flux and vertical motion patterns just discussed lead to some speculation concerning stratospheric events leading to the observed mid-winter peaks in surface ozone observed over Antarctica (Wisse and Meerburg, 1969). During a minor mid-winter warming the poleward heat flux is large and there is apparently no descending motion over the South Pole. Assuming that large heat fluxes are coincident with large poleward fluxes of ozone in the stratosphere, one may postulate a build-up of ozone in the lower stratosphere over Antarctica. During an immediately subsequent quiet period the built-up ozone reservoir could be tapped by the descending motion over the South Pole which has been shown to extend through the troposphere to the surface (Rubin and Weyant, 1963).

Fritz and Soules (1970) examine a number of Southern Hemisphere stratospheric temperature fluctuations during the fall, winter and spring of 1969 using SIRS channel 8 data. Between 25 June and 10 July, they indicate a large increase in channel 8 radiance in the southern polar regions. Accompanying the warming (increasing radiance) in the high latitudes of the Southern Hemisphere, they also find decreasing radiance

(cooling) in Southern Hemisphere low latitudes and in the Northern Hemisphere. The early July case is just one of several similar compensating changes noted by Fritz and Soules. Another rapid increase of zonally-averaged radiance occurs between 26 July and 8 August in high southern latitudes. These two periods of radiance increase noted by Fritz and Soules have already been discussed in the previous section with regard to wave characteristics. In this section it has been noted that there are significant differences in the eddy flux of enthalpy patterns and in the derived mean meridional motion patterns between the time of the early July warming (1-10 July) and the quiet period (18-27 July). These observations support the Fritz and Soules postulate that irregular (non-seasonal) fluctuations in stratospheric temperature are related to changes in large-scale eddies and/or changes in the mean meridional circulations.

5.4 Chapter summary

The most significant results of this chapter are those regarding the structure in both hemispheres of the stratospheric polar vortex and the calculation of the mean meridional circulation in the Southern Hemisphere. The temperature structure of the southern vortex is shown to be significantly different than that in the Northern Hemisphere in midwinter so that a previously-derived instability criterion tends not to be met in the Southern Hemisphere. This agrees with the absence of complete, midwinter breakdowns south of the equator. The Southern Hemisphere vortex structure is also shown to vary between midwinter and spring so that the instability criterion tends to be met in spring when the southern vortex breaks down.

The calculation of zonally-averaged vertical motion in the Southern Hemisphere stratosphere presented in Section 5.2.3 is the first realistic (that is, including the effects of eddy transports) estimate of the mean meridional circulation at those heights south of the equator. The results indicate the presence of a two-celled structure for the monthly mean pattern with rising motion centered about 70°S and the axis of sinking motion at approximately 50°S. With temperature decreasing toward the pole in these latitudes of the stratosphere the circulation is indirect. Consequently, the Antarctic stratospheric jet stream at 60°S is not maintained by the mean motions, but by the large-scale eddies.

In Section 5.3 there are shown to be significant variations in the Southern Hemisphere circulation during July 1969 in relation to the presence or absence of a minor midwinter warming. During the warming a stationary wave number 1 pattern dominates and the poleward eddy heat flux is large, while during a quiet period transient waves of wave number 2 are most evident and the heat flux is relatively small. The mean meridional circulation during the warming (Section 5.3.3) is similar to the monthly-mean pattern (Section 5.2.3); but during the quiet period the mean circulation becomes three-celled with the addition cell occurring in very high latitudes with sinking motion over the South Pole. It is possible that the quiet period may be more representative of "normal" conditions in the Southern Hemisphere stratosphere than the monthly-mean calculation. Therefore, the final determination of the normal configuration of the mean meridional circulation will have to await additional study.

CHAPTER 6

SUMMARY AND CONCLUSIONS

The basic purpose of this study is to compare the structure and flow characteristics of the upper troposphere and stratosphere of the Northern and Southern Hemispheres. Atmospheric structure obtained from satellite, multi-channel radiance data has provided the primary basis for the comparisons. The results of this study confirm some previously-made conclusions and assert new conclusions regarding inter-hemispheric comparisons and the Southern Hemisphere circulation.

The satellite, multi-channel radiance data have been shown to be a valuable asset in the study of the general circulation. In this study they have provided information on atmospheric structure with equal, or nearly equal, time and space resolutions in the two hemispheres. This investigation is, therefore, the first comparison of circulations of the Northern and Southern Hemispheres based on a data system having comparable resolution and quality of data above and below the equator. The radiosonde network of the Southern Hemisphere has nearly an order of magnitude fewer stations than the Northern Hemisphere version. Therefore, the comparison between the hemispheres of statistics based on these radiosonde systems may be open to question. This may be especially true of quantities whose estimation requires good horizontal resolution on the time scale of a day.

Most previous observational studies of the atmosphere's general circulation have centered on the Northern Hemisphere, because of the better upper-air network there. However, in order to understand the general circulation on a global basis we must first develop a knowledge of the characteristics of the circulation in both hemispheres. Because there is little hope that the number of Southern Hemisphere radiosonde stations will increase to become comparable to the network in the Northern Hemisphere, there will be continued heavy reliance on satellite data to study the general circulation below the equator. Numerical models of the global general circulation in the troposphere and stratosphere now exist. In the Northern Hemisphere these models can be verified against statistics compiled from the relatively dense radiosonde network; in the Southern Hemisphere this verification will have to depend more heavily on satellite-based studies, especially for eddy terms, and especially for layers above the mid-troposphere. Hopefully, the current investigation has provided a beginning in that direction.

The results of this investigation do show that the satellite radiance data, as used here, have two main limitations in this type of study. First, because of cloud effects in the lower levels, results for the most part are restricted to layers above 500 mb. Even above 500 mb results improve with height into the stratosphere. The second limitation is the tendency of the satellite-derived atmospheric structure to underestimate the amplitude of eddies.

The major results and conclusions of this study are summarized in the following paragraphs.

Zonally-averaged vertical motion fields in the stratosphere calculated in both hemispheres confirm a two-cell structure to the mean

meridional circulation in Northern Hemisphere winter with rising motion over the North Pole. In the Southern Hemisphere winter, the calculations also show a two-cell structure in the mid-stratosphere, but with the main ascending branch located at approximately 70°S. The mean circulation in the vicinity of the Antarctic stratospheric jet stream is indirect, thus the maintenance of the jet stream must depend on the large-scale eddies. The calculation of the mean meridional circulation of the Southern Hemisphere stratosphere presented in this paper is the first realistic estimation of that circulation. That is, it is the first to include the very important influence of large-scale eddies.

There are significant variations during the Southern Hemisphere winter in relation to stratospheric synoptic events. During a minor midwinter warming, the flow is dominated by a stationary wave number 1 pattern, the eddy flux of heat at 60°S is large, and the vertical motion magnitudes are also large. During a "quiet" period, the flow is dominated by a transient wave number 2 pattern, the eddy flux is relatively small, and a descending branch of the mean meridional circulation appears over the South Pole. Consequently, during this quiet period there appears to be three instead of two cells in the mean meridional circulation.

A previous calculation based on IGY data in the Southern Hemisphere concluded that the Southern Hemisphere mid-latitude eddy flux of heat is approximately one half as large as that in the Northern Hemisphere. Another study, based on energy budget considerations, concludes that the two values are about the same. The results of the present study indicate that the eddy flux is much closer to being equal in the two hemispheres than to being different by a factor of two.

The existence of longitudinal variations in the pattern of eddy heat flux in southern mid-latitudes, as there are in northern mid-latitudes, is also shown. These variations are best defined in both hemispheres during winter. The Northern Hemisphere variations are closely tied to standing waves; in the Southern Hemisphere the variations are due more to longitudinal variations of the strength of transient eddies. In winter, at 45°S, three peaks are well defined, seemingly associated with the three land areas, Australia, South America and Africa.

The relative importance of standing eddies in the two hemispheres has been examined closely in this study. The calculations confirm that, on a hemispheric-averaged basis, the Southern Hemisphere has a lower percentage of AE and KE contained in standing eddies. In the Southern Hemisphere the percentage of energy contained in the standing eddies is smaller in summer than in winter; in the Northern Hemisphere, the percentage either remains the same or increases from winter to summer, depending on the layer and parameter under consideration. This difference reflects the dominance of the Asian summer monsoon in the Northern Hemisphere.

The distribution with latitude in the upper troposphere of the ratio of standing eddy temperature variance to the total variance shows large inter-hemispheric differences. This parameter indicates the importance of standing eddies as a function of latitude. In winter, poleward of 30°, the Northern Hemisphere shows one peak at about 50°N; the Southern Hemisphere has two peaks, one at 40°S and one over Antarctica. In mid-latitudes (40-60°), the Southern Hemisphere value is lower than that in the Northern Hemisphere; in high latitudes (>60°),

the reverse is true. In summer, in low latitudes (<35°), both hemispheres show maxima associated with the summer monsoon in each hemisphere. The Northern Hemisphere maximum is much larger than the Southern Hemisphere one. At all latitudes in summer the ratio is larger in the Northern Hemisphere.

In winter, at the latitude of maximum eddy kinetic energy (~30°), the standing eddies contribute substantially to the total. In the Southern Hemisphere, the percentage contribution is about 30%; in the Northern Hemisphere it is about 40%. These percentages are larger than the hemispheric-averaged values. In summer the percentages are less in both hemispheres.

In the Northern Hemisphere during winter, about 50% of the eddy heat transport in mid-latitudes is accomplished by the standing eddies. In the Southern Hemisphere, the percentage contribution is much less. According to calculations in this study, the Southern Hemisphere percentage is about 20%. Other previous studies have indicated a lower percentage.

The satellite-based zonal mean temperature and mass structure confirm the inter-hemispheric differences previously noted from climatological information. The upper tropospheric temperature gradient between 20° and 80° latitude is larger in the Southern Hemisphere in both winter and summer, with the largest disparity occurring in summer. The same difference is evident in the distribution of 200 mb geopotential height. These variations are also reflected in the computed values of zonal available potential energy (AZ) and zonal kinetic energy (KZ). In summer the AZ of the Southern Hemisphere is twice as large as that in the Northern Hemisphere. Because the winter difference is relatively

small, there is an annual cycle of global AZ with peak values occurring during the northern winter.

The contributions from the upper tropospheric and tropopause layers to the eddy available potential energy (AE) and eddy kinetic energy (KE) do not show the large inter-hemispheric differences that are evident in the zonal components, AZ and KZ. Therefore, the ratios of AZ to AE and KZ to KE are larger in the Southern Hemisphere.

The winter stratospheres of the Northern and Southern Hemispheres are also studied in relation to the difference in breakdown climatologies. The temperature structure of the winter stratospheric vortices are shown to vary between the hemispheres in a way that a previously-derived instability criterion tends to be met in the Northern Hemisphere, but not in the Southern Hemisphere, during midwinter. This difference may be related to the dissimilar midwinter breakdown climatologies. In the Southern Hemisphere, the structure varies between midwinter and spring so that the vortex tends to meet the instability criterion in spring when the vortex normally breaks down.

REFERENCES

Charney, J. G. and M. E. Stern, 1962: On the stability of internal baroclinic jets in a rotating atmosphere. J. Atmos. Sci., 19, 159-172.

Craig, R. A., 1965: The Upper Atmosphere: Meteorology and Physics, New York, Academic Press, 509 pp.

Crutcher, H. L. and J. M. Meserve, 1970: Selected-level heights, temperatures, and dew point temperatures for the Northern Hemisphere. NAVAIR 50-1C-52 rev., Chief Naval Operations, Washington, D. C., 17 pp. plus charts.

Dopplick, T. G., 1972: Radiative heating of the global atmosphere. J. Atmos. Sci., 29, 1278-1294.

Dutton, J. A. and D. R. Johnson, 1967: The theory of available potential energy and a variational approach to atmospheric energetics. Advan. Geophys., 12, 333-463.

Ellis, J. S., 1974: Interannual variations in the earth's radiative budget and the general circulation. Atmos. Sci. Paper, Colorado State University.

Fleming, H. E., 1972: A method for calculating atmospheric thicknesses directly from satellite radiation measurements. Preprints Conference on Atmospheric Radiation, Fort Collins, Colorado, Amer. Meteor. Soc., 134-137.

_____ and W. L. Smith, 1972: Inversion techniques for remote sensing of atmospheric temperature profiles. Proceedings of the 5th Symposium on Temperature: Its Measurement and Control in Science and Industry.

Fritz, S., 1970: Earth's radiation to space at 15 microns: Stratospheric temperature variations. J. Appl. Meteor., 9, 815-824.

_____ and S. D. Soules, 1970: Large-scale temperature changes in the stratosphere observed from Nimbus III. J. Atmos. Sci., 27, 1091-1097.

Haines, D. A., and J. S. Winston, 1963: Monthly mean values and spatial distribution of meridional transport of sensible heat. Mon. Wea. Rev., 91, 319-328.

Julian, P. R., 1967: Midwinter stratospheric warmings in the Southern Hemisphere: General remarks and a case study. J. Appl. Meteor., 6, 557-563.

_____ and K. Labitzke, 1965: A study of atmospheric energetics during the January-February 1965 stratospheric warming. J. Atmos. Sci., 22, 597-610.

Kao, S. K., R. L. Jenne and J. F. Sagendorf, 1970: The kinetic energy of large-scale atmospheric motion in wavenumber-frequency Space: II. Mid-troposphere of the Southern Hemisphere. J. Atmos. Sci., 27, 1008-1020.

_____, _____ and _____, 1971a: Spectral characteristics of the meridional transport of angular momentum in the midtroposphere of the Southern Hemisphere. Pure Appl. Geophys., 86, 171-183.

_____, _____ and _____, 1971b: Wavenumber frequency spectra of the meridional transport of sensible heat in the mid-troposphere of the Southern Hemisphere. Pure Appl. Geophys., 86, 159-170.

_____ and J. F. Sagendorf, 1970: The large-scale meridional transport of sensible heat in wavenumber frequency space. Tellus, 22, 172-185.

_____ and L. L. Wendell, 1970: The kinetic energy of the large-scale atmospheric motion in wavenumber-frequency space: I. Northern Hemisphere. J. Atmos. Sci., 27, 359-375.

Labitzke, K. and H. van Loon, 1972: The stratosphere in the Southern Hemisphere. Meteorology of the Southern Hemisphere, Meteor. Monogr., 13, No. 35, 113-138.

Lorenz, E. N., 1955: Available potential energy and the maintenance of the general circulation. Tellus, 7, 157-167.

_____, 1967: The Nature and Theory of the General Circulation of the Atmosphere. WMO No. 218, TP115, 161 pp.

Lovill, J. E., 1972: Characteristics of the general circulation of the atmosphere and the global distribution of total ozone as determined by the Nimbus III Satellite Infrared Interferometer Spectrometer. Atmos. Sci. Paper No. 180, Colorado State University, 72 pp.

Mahlman, J. D., 1966: Atmospheric General Circulation and Transport of Radioactive Debris. Atmospheric Science Paper No. 103, Colorado State University, 184 pp.

Matsuno, T., 1971: A dynamical model of the stratospheric sudden warming. J. Atmos. Sci., 28, 1479-1494.

Miller, A. J., J. A. Brown and K. A. Campana, 1972: A study of the energetics of an upper stratospheric warming (1969-1970). Quart. J. R. Met. Soc., 98, 730-744.

_____, F. G. Finger and M. E. Gelman, 1970: 30 mb Synoptic Analyses for the 1969 Southern Hemisphere Winter Derived with the Aid of Nimbus III(SIRS) Data, NASA TMS-2109, Washington, D. C., 27 pp.

Muench, H. S., 1968: Large-scale disturbances in the summertime stratosphere. J. Atmos. Sci., 25, 1108-1115.

Newell, R. E., D. G. Vincent, T. G. Dopplick, D. Ferruzza and J. W. Kidson, 1970: The energy balance of the global atmosphere. The Global Circulation of the Atmosphere, G. A. Corby, Ed., Roy. Met. Soc., London, 42-90.

Newton, C. W., 1971: Global angular momentum balance: Earth torques and atmospheric fluxes. J. Atmos. Sci., 28, 1329-1341.

_____, 1972: Southern Hemisphere general circulation in relation to global energy and momentum balance requirements. Meteorology of the Southern Hemisphere, Meteor. Monogr., 13, No. 35, 215-246.

Nordberg, W., A. W. McCulloch, L. L. Foshee and W. R. Bandeen, 1966: Preliminary results from Nimbus II. Bull. Amer. Meteor. Soc., 17, 857-872.

Obasi, G. O. P., 1963: Poleward flux of atmospheric angular momentum in the Southern Hemisphere. J. Atmos. Sci., 20, 516-528.

_____, 1965: On the maintenance of kinetic energy of mean zonal flow in the Southern Hemisphere. Tellus, 17, 95-105.

Ohring, G., 1972: Application of step-wise multiple regression techniques to inversion of Nimbus IRIS observations. Mon. Wea. Rev., 100, 336-344.

Oort, A. H., 1964: On estimates of the atmospheric energy cycle. Mon. Wea. Rev., 92, 483-493.

_____, 1971: The observed annual cycle in the meridional transport of atmospheric energy. J. Atmos. Sci., 28, 325-339.

_____ and E. M. Rasmusson, 1971: Atmospheric circulation statistics. NOAA Prof. Paper 5, U. S. Dept. Commerce, 323 pp.

Palmer, C. E. and R. C. Taylor, 1960: The vernal breakdown of the stratospheric cyclone over the South Pole. J. Geophys. Res., 65, 3319-3329.

Pedlosky, J., 1964: The stability of currents in the atmosphere and the ocean, Part I. J. Atmos. Sci., 21, 201-219.

Petterssen, S., 1956: Weather Analysis and Forecasting, Volume I, Motion and Motion Systems, New York, McGraw-Hill, 428 pp.

Phillpot, H. R., 1969: Antarctic stratospheric warming reviewed in the light of 1967 observations. Quart. J. R. Met. Soc., 95, 329-348.

Raschke, E., T. H. Vonder Haar, W. R. Bandeen and M. Pasternak, 1973: The annual radiation balance of the earth-atmosphere system during 1969-70 from Nimbus 3 measurements. J. Atmos. Sci., 30, 341-364.

Reed, R. J., J. Wolfe and H. Nishimoto, 1963: A spectral analysis of the energetics of the stratospheric sudden warming of early 1957. J. Atmos. Sci., 20, 256-275.

Reiter, E. R., 1969a: Atmospheric Transport Processes, Part I: Energy Transfers and Transformations. Atomic Energy Comm., TID-24868, 253 pp.

_____, 1969b: Mean and eddy motions in the atmosphere. Mon. Wea. Rev., 97, 200-204.

_____, 1971: Atmospheric Transport Processes, Part II: Chemical Tracers. Atomic Energy Comm., TID-25314, 382 pp.

_____ and J. E. Lovill, 1974: The longitudinal movement of stratospheric ozone waves as determined by satellite. Arch. Meteorol. Geophys. Bioklimatol., Ser. A, in press.

Robinson, J. B., Jr., 1970: Meridional eddy flux of enthalpy in the Southern Hemisphere during the IGY. Pure Appl. Geophys., 80, 319-334.

Rodgers, C. D., 1967: The radiative heat budget of the troposphere and lower stratosphere. M. I. T. Planetary Circulations Project, Report No. A2, 99 pp.

Rubin, M. J. and W. Weyant, 1963: The mass and heat budget of the Antarctic atmosphere, Mon. Wea. Rev., 91, 487-493.

Saltzman, B. and A. Fleisher, 1960: The modes of release of available potential energy in the atmosphere. J. Geophys. Res., 65, 1215-1222.

Sasamori, T., J. London and D. V. Hoyt, 1972: Radiation budget of the Southern Hemisphere. Meteorology of the Southern Hemisphere, Meteor. Monogr., 13, No. 35, 9-24.

Sellers, W. D., 1965: Physical Climatology, Chicago, University of Chicago Press, 272 pp.

Shen, W. C., G. W. Nicholas and A. D. Belmont, 1968: Antarctic stratospheric warmings during 1963 revealed by 15μ TIROS VII data. J. Appl. Meteor., 7, 268-283.

Smith, W. L., H. M. Woolf and W. J. Jacob, 1970: A regression method for obtaining real time temperature and geopotential height profiles from satellite spectrometer measurements and its application to Nimbus III SIRS observations. Mon. Wea. Rev., 98, 582-603.

Srivatsangam, S., 1973: A contribution to the synoptic climatology of the extratropics. Atmos. Sci. Paper No. 203, Colorado State University, 34 pp.

Taljaard, J. J., 1972a: Physical features of the Southern Hemisphere. Meteorology of the Southern Hemisphere, Meteor. Monogr., 13, No. 35, 1-8.

_____, 1972b: Synoptic meteorology of the Southern Hemisphere. Meteorology of the Southern Hemisphere, Meteor. Monogr., 13, No. 35, 139-214.

_____, H. van Loon, H. L. Crutcher and R. L. Jenne, 1969: Climate of the Upper Air: Southern Hemisphere. Vol. I, Temperatures, Dew Points, and Heights at Selected Pressure Levels. NAVAIR 50-1C-55, Chief Naval Operations, Washington, D. C., 135 pp.

Taylor, R. C., 1961: Upper-air temperatures at U. S. Antarctic stations, 1956-1957. IGY General Report No. 14, National Academy of Sciences, Washington, D. C., 48 pp.

van Loon, H., 1972a: Temperature in the Southern Hemisphere. Meteorology of the Southern Hemisphere, Meteor. Monogr., 13, No. 35, 25-58.

_____, 1972b: Pressure in the Southern Hemisphere. Meteorology of the Southern Hemisphere, Meteor. Monogr., 13, No. 35, 59-86.

_____, 1972c: Wind in the Southern Hemisphere. Meteorology of the Southern Hemisphere, Meteor. Monogr., 13, No. 35, 87-100.

_____, 1972d: Cloudiness and precipitation in the Southern Hemisphere. Meteorology of the Southern Hemisphere, Meteor. Monogr., 13, No. 35, 101-112.

_____ and R. L. Jenne, 1972: The zonal harmonic standing waves in the Southern Hemisphere. J. Geophys. Res., 77, 992-1003.

_____, J. J. Taljaard, R. L. Jenne and H. L. Crutcher, 1971: Climate of the Upper Air: Southern Hemisphere. Vol. II, Zonal Geostrophic winds. NCAR TN/STR-57 and NAVAIR 50-1C-56, National Center for Atmospheric Research, Boulder, Colo., 43 pp.

Vincent, D. G., 1968: Mean meridional circulations in the Northern Hemisphere lower stratosphere during 1964 and 1965. Quart. J. R. Met. Soc., 94, 333-349.

Vonder Haar, T. H., 1972: Natural variation of the radiation budget of the earth-atmosphere system as measured from satellites. Preprints Conference on Atmospheric Radiation, Fort Collins, Colo., Amer. Meteor. Soc., 211-220.

_____ and A. H. Oort, 1973: New estimate of annual poleward energy transport by Northern Hemisphere oceans. J. Phys. Oceanogr., 3, 169-172.

_____ and V. E. Suomi, 1971: Measurements of the earth's radiation budget from satellites during a five year period. Part I: Extended time and space means. J. Atmos. Sci., 28, 305-314.

Wark, D., D. Hilleary, J. Lienesch and P. Clark, 1969: The satellite infrared spectrometer (SIRS) experiment. The Nimbus III User's Guide, The Nimbus Project, Goddard Space Flight Center, Greenbelt, Md., 147-179.

Wisse, J. A. and A. J. Meerburg, 1969: Ozone observations at Base King Baudouin in 1965 and 1966. Arch. Meteorol. Geophys. Bioklimatol., Ser. A., 18, 41-54.

Wooldridge, G. and E. R. Reiter, 1970: Large-scale atmospheric circulation characteristics as evident from Ghost balloon data. J. Atmos. Sci., 27, 183-194.

APPENDIX

REGRESSION COEFFICIENTS

The general form of the regression equations used in this study is

$$D = \alpha_0 + \alpha_1 N_1 + \alpha_2 N_2 + \text{---} + \alpha_8 N_8 \ , \qquad \text{A.1}$$

where D is the geopotential thickness, α_0 is the equation constant, α_1 through α_8 are the regression coefficients and N_1 through N_8 are the radiances in the eight SIRS channels.

In the four tables which follow the coefficients in the thickness-radiance regressions equations are given. Coefficients are presented for each of the eight layers and for each of three latitude bands: I, 20°-40°; II, 40°-60°; III, 60°-80°. The variance explained (V. E.) and the standard error of estimate (S. E. E.) in both meters and °C are also exhibited. No regression equations were determined for the 10-30 mb layer in the Southern Hemisphere, because of a lack of conventional data at that altitude.

Each equation's constant, α_0, is given in the column marked "Constant." The values of α_1 through α_8 are shown in the following eight columns. A blank location means that the α for that channel is zero. The units in the regression equations are: thickness, m; temperature, °C; radiance, ergs cm^{-2} sec^{-1} $steradian^{-1}$ $(cm^{-1})^{-1}$. A typical value for the radiance N is 50 ergs cm^{-2} sec^{-1} $steradian^{-1}$ $(cm^{-1})^{-1}$.

An examination of the coefficients in the tables indicates that layers in the stratosphere have regression equations with large positive coefficients for channels six and seven. This is physically sound, since the weighting functions for those channels have peaks in the lower stratosphere (see Figure 3.1). As one moves from stratospheric layers to those below 100 mb, the major positive coefficient shifts toward channels with weighting functions which peak at lower altitudes. However, in the two lowest layers, especially 700-1000 mb, this physical relationship does not seem to hold. In other words, based on the distribution of weighting functions in Figure 3.1, one would expect a large positive coefficient for channel one, two or three in the last row of each of the tables. This, however, is not the case. Because not all cloud-contaminated data have been eliminated, the selection procedure picks other channels which are not as affected by clouds as are channels one through three. Since there is a significant negative correlation between tropospheric and stratospheric temperature, channel five, six or seven enters the regression equation with the dominant coefficient, a negative one.

		Constant	N_1	N_2	N_3	N_4	N_5	N_6	N_7	N_8	V.E.(%)	S.E.E. (m)	S.E.E. (°C)
10-30 mb	I	6982.0						-112.77	111.88		76.0	25.4	0.8
	II	6207.1							22.52		39.9	62.0	1.9
	III	6457.3					-13.96		73.11	-38.65	51.1	46.5	1.4
30-50 mb	I	2634.5							13.41		38.2	23.4	1.6
	II	2575.5						-11.43	24.93		62.0	23.0	1.5
	III	2695.2					-9.68	15.14	7.18		81.5	14.5	1.0
50-100 mb	I	2821.2					-6.99		53.23	-12.81	66.1	40.5	2.0
	II	2817.2							30.72		82.2	29.2	1.4
	III	3359.5						13.68	8.70		84.7	19.4	1.0
100-200 mb	I	3329.0				-5.52		67.12		-29.85	74.1	30.3	1.5
	II	3842.1				-13.99		85.03	-52.49		75.3	50.5	2.5
	III	3788.0				-14.51	49.06			-14.26	68.4	37.2	1.8
200-300 mb	I	1963.3		-1.33			42.13	-20.43	-4.50		57.2	22.6	1.9
	II	2047.7		-0.83		-0.48	45.24	-31.06			49.1	22.1	1.8
	III	2095.1					34.91		-16.54	-4.72	56.2	25.2	2.1
300-500 mb	I	3045.6					46.51	-56.36		17.63	70.3	24.4	1.6
	II	2952.1		-1.78		28.62		-30.63		12.18	68.5	34.4	2.3
	III	3272.7		-1.97		38.08	-41.35			7.46	59.0	33.6	2.2
500-700 mb	I	2696.6				2.08	13.96	-27.01		7.25	66.1	15.8	1.6
	II	2316.8				12.40		-19.98		9.51	66.1	22.9	2.3
	III	2407.2				20.93	-29.10			7.63	64.6	23.5	2.4
700-1000 mb	I	3240.0	1.15						-30.35	19.47	50.8	30.6	2.9
	II	3056.4	1.27			5.69		-10.91			59.1	30.4	2.9
	III	3528.3		2.44			-22.60			5.37	60.2	32.0	3.1

Table A.1 Regression coefficients for July 1969, Northern Hemisphere.

		Constant	N_1	N_2	N_3	N_4	N_5	N_6	N_7	N_8	V.E.(%)	S.E.E. (m)	S.E.E. (°C)
10-30 mb	I	6449.2								13.29	60.0	24.8	0.8
	II	5918.7					-54.29		86.88	-9.49	76.4	108.1	3.4
	III	7084.6					-53.69		59.06	-5.81	66.5	97.1	3.0
30-50 mb	I	2914.4							25.61	-15.33	64.4	42.0	2.8
	II	2655.6							29.75	-14.91	65.3	54.0	3.6
	III	2540.0							32.69	-15.69	85.4	36.9	2.5
50-100 mb	I	3224.9					-14.61		70.12	-27.81	94.5	37.9	1.9
	II	3519.2						37.25		-14.79	76.3	52.6	2.6
	III	3148.7					30.62		13.20	-13.54	87.7	53.9	2.6
100-200 mb	I	3253.7				-7.27		47.51		-10.36	81.6	38.7	1.9
	II	3554.5				-16.16	55.28		-13.96	-2.67	82.3	40.2	2.0
	III	3483.6				-16.30	58.57		-18.64		89.0	43.7	2.2
200-300 mb	I	1898.9		-1.15		8.80	20.76		-12.15		70.3	26.9	2.3
	II	1969.0				-4.00	28.38		-11.83	1.84	70.7	27.8	2.3
	III	2162.2			-2.80		21.75		-8.55		72.2	32.7	2.7
300-500 mb	I	3677.8		-1.12		22.06		-26.53			79.5	40.7	2.7
	II	2934.3		-4.22		41.45		-27.43			64.0	45.3	3.0
	III	3004.3		-2.56		35.48	-22.04		-3.68		51.6	38.5	2.6
500-700 mb	I	2803.3				10.11		-27.62		7.78	80.0	28.9	2.9
	II	2117.9		-3.32		35.51		-34.75	8.32		62.9	40.8	4.2
	III	2110.0				21.88		-26.04	9.04		58.2	38.6	3.9
700-1000 mb	I	3524.7		2.41				-26.57		5.59	64.1	44.1	4.2
	II	2456.1				23.90		-14.48	-9.29	3.84	49.8	66.0	6.3
	III	2564.4	3.36		4.95			-9.10		1.33	58.2	59.5	5.7

Table A.2 Regression coefficients for January 1970, Northern Hemisphere.

		Constant	N_1	N_2	N_3	N_4	N_5	N_6	N_7	N_8	V.E.(%)	S.E.E. (m)	S.E.E. (°C)
10-30 mb	I												
	II												
	III												
30-50 mb	I	2141.0					16.72		19.93	-10.38	69.3	22.0	1.5
	II	2500.6							33.48	-14.93	83.8	29.6	2.0
	III	2312.3						11.08	25.31	-13.55	79.8	26.5	1.8
50-100 mb	I	3893.9					-45.44	77.05		-16.05	91.8	30.5	1.5
	II	3658.1						16.67	19.11	-16.33	77.4	36.8	1.8
	III	3200.3						46.53		-16.14	77.9	39.0	1.9
100-200 mb	I	3865.0					-56.02	159.44	-89.10		86.3	36.6	1.8
	II	3769.4					-41.91	128.04	-66.74		68.2	44.9	2.2
	III	3275.6					-28.75	121.85	-62.67		89.2	33.6	1.6
200-300 mb	I	1568.2				-11.19	85.15	-50.50			76.5	25.9	2.2
	II	2055.1				-11.78	41.02		-23.42	7.27	47.4	29.8	2.5
	III	2006.5				-11.37	38.10		-11.76		67.2	24.9	2.1
300-500 mb	I	3027.7		-2.09		32.44		-33.82		9.30	85.6	33.8	2.2
	II	2443.3		-5.50		60.50	-43.41			7.37	58.3	37.9	2.5
	III	2256.3		-3.55		44.40		-16.31			69.1	36.0	2.4
500-700 mb	I	2449.8				30.59	-49.13		11.97		80.8	24.3	2.5
	II	1805.6	-1.50		2.78	28.21		-33.05	18.48		47.2	31.6	3.2
	III	1603.2				35.47		-40.96	25.50	-4.30	69.1	30.2	3.1
700-1000 mb	I	3005.4			3.92			-22.16		11.25	63.3	27.6	2.6
	II	2270.6			9.41						25.1	35.8	3.4
	III	2454.2	9.18				-6.03				56.0	45.4	4.4

Table A.3 Regression coefficients for July, 1969, Southern Hemisphere.

		Constant	N_1	N_2	N_3	N_4	N_5	N_6	N_7	N_8	V.E.(%)	S.E.E. (m)	S.E.E. (°C)
10-30 mb	I												
	II												
	III												
30-50 mb	I	3230.5					-11.02		32.60	-17.21	73.4	18.1	1.2
	II	3329.5					-36.09		33.54		42.9	37.5	2.5
	III	3511.8									0.0	30.7	2.0
50-100 mb	I	4116.4					-26.84		107.39	-63.50	85.2	38.5	1.9
	II	4415.6					-89.13	67.86		16.66	49.7	65.7	3.2
	III	4694.4					-22.39		49.58	-25.41	29.3	27.4	1.3
100-200 mb	I	4260.7				-8.07			65.50	-44.78	57.9	43.4	2.1
	II	4443.3				-16.40		60.22		-32.27	56.7	66.5	3.3
	III	4630.0				-20.06		81.04	-56.48		56.0	26.3	1.3
200-300 mb	I	2700.5		-1.88			26.68		-22.91		69.9	19.9	1.7
	II	2657.5		-1.14			34.60			-25.19	44.3	26.0	2.2
	III	2656.9				-29.86	70.45		-58.02	19.72	50.8	24.8	2.1
300-500 mb	I	3725.9		-3.93		27.12		-45.14	17.47		74.4	25.2	1.7
	II	3624.5		-6.53		32.76		-44.79		14.60	65.6	37.9	2.5
	III	3445.3		-4.41		42.05		-77.43	39.28		67.7	26.4	1.8
500-700 mb	I	2669.5				10.79		-37.68	22.15		67.2	16.4	1.7
	II	2615.8		-2.57		17.20		-31.29		12.20	67.4	26.9	2.7
	III	2448.3	-13.69	16.25		14.81		-19.60			63.3	22.0	2.2
700-1000 mb	I	3025.2	1.66				14.26	-47.82		21.38	59.0	33.0	3.2
	II	2924.8	15.20	-26.12		56.14	-43.15				66.4	35.8	3.4
	III	2787.9				12.61		-35.66	21.37		35.3	23.4	2.2

Table A.4 Regression coefficients for January, 1970, Southern Hemisphere.

BIBLIOGRAPHIC DATA SHEET	1. Report No. At. Sci. Paper No. 216	2.	3. Recipient's Accession No.
4. Title and Subtitle A COMPARISON OF THE STRUCTURE AND FLOW CHARACTERISTICS OF THE UPPER TROPOSPHERE AND STRATOSPHERE OF THE NORHTERN AND SOUTHERN HEMISPHERES			5. Report Date April 1974 6.
7. Author(s) Robert F. Adler			8. Performing Organization Rept. No. CSU-ATSP
9. Performing Organization Name and Address Colorado State University Department of Atmospheric Science Foothills Campus Fort Collins, Colorado 80521			10. Project/Task/Work Unit No. 11. Contract/Grant No. NASA NGR 06-002-098 AEC AT(11-1)-1340
12. Sponsoring Organization Name and Address National Aeronautics and Space Administration Greenbelt, Md. 20770 Atomic Energy Commission Washington, D. C. 20545			13. Type of Report & Period Covered 14.

15. Supplementary Notes

16. Abstracts

The general circulations of the Northern and Southern Hemispheres are compared with regard to the upper troposphere and stratosphere using atmospheric structure obtained from satellite, multi-channel radiance data. Specifically, the data are from the Satellite Infrared Spectrometer (SIRS) instrument aboard the Nimbus 3 spacecraft. The inter-hemispheric comparisons are based on two months of data (one summer month and one winter month) in each hemisphere.

Topics studied include: mean meridional circulation in the Southern Hemisphere stratosphere; magnitude and distribution of tropospheric eddy heat flux; relative importance of standing and transient eddies in the two hemispheres; magnitudes of energy cycle components; and the relation of vortex structure to the breakdown climatology of the Antarctic stratospheric polar vortex.

17. Key Words and Document Analysis. 17a. Descriptors

general circulation
Southern Hemisphere
Northern Hemisphere
troposphere
stratosphere
satellite data
multi-channel radiance data

17b. Identifiers/Open-Ended Terms

17c. COSATI Field/Group

18. Availability Statement	19. Security Class (This Report) UNCLASSIFIED	21. No. of Pages 159
	20. Security Class (This Page UNCLASSIFIED	22. Price